

Handbook T-I

Innovative Applications in Sustainable Energy and Environment

Figueroa-Ramírez, Sandra Jazmín

Flores-Chan, José Enrique

Patiño-Carachure, Cristóbal

Abatal, Mohamed

Coordinators



ECORFAN®

Coordinators

Figueroa-Ramírez, Sandra Jazmín
Flores-Chan, José Enrique
Patiño-Carachure, Cristóbal
Abatal, Mohamed

Editor in Chief

Vargas-Delgado, Oscar. PhD

Executive Director

Ramos-Escamilla, María. PhD

Editorial Director

Peralta-Castro, Enrique. MsC

Web Designer

Escamilla-Bouchan, Imelda. PhD

Web Diagrammer

Luna-Soto, Vladimir. PhD

Editorial Assistant

Trejo-Ramos, Iván. BsC

Philologist

Ramos-Arancibia, Alejandra. BsC

ISBN: 978-607-8948-51-2

ECORFAN Publishing Label: 607-8948

HIASE Control Number: 2024-13

HIASE Classification (2024): 311224-0113

©ECORFAN-México, S.C.

Park Pedregal Business 3580 – Adolfo Ruiz Cortines Boulevard, CP-01900. San Jerónimo Aculco Álvaro Obregón - Mexico City.

No part of this writing protected by the Federal Copyright Law may be reproduced, transmitted or used in any form or by any means, graphic, electronic or mechanical, including, but not limited to, the following: Quotations in radio or electronic journalistic data compilation articles and bibliographic commentaries. For the purposes of articles 13, 162, 163 fraction I, 164 fraction I, 168, 169, 209 fraction III and other relative articles of the Federal Copyright Law. Infringements: Being compelled to prosecute under Mexican copyright law. The use of general descriptive names, registered names, trademarks, or trade names in this publication does not imply, even in the absence of a specific statement, that such names are exempt from the relevant protection in laws and regulations of Mexico and therefore free for general use by the international scientific community. HAMTFE is part of ECORFAN Media [www.ecorfan.org]. Published by ECORFAN-Mexico. All Rights Reserved.

Derivative works: Users may reproduce tables of contents or prepare lists of chapters including abstracts for internal circulation within their institutions or companies. Other than for chapters published under the CC BY license.

Storage or usage: Except as outlined above or as set out in the relevant user license, no part of this publication may be reproduced, stored in a retrieval system or transmitted in any form or by any means, electronic, mechanical, photocopying, recording or otherwise, without prior written permission of the publisher.

The Authors. Published by ECORFAN-Mexico, S.C. for its Holding Mexico on behalf of Handbook HESPCU. This is an open access handbook under the CC BY-NC-ND license [<http://creativecommons.org/licenses/by-nc-nd/4.0/>]

Handbooks

Definition of Handbooks

Scientific Objectives

To support the International Scientific Community in its written production of Science, Technology and Innovation in the CONAHCYT and PRODEP research areas.

ECORFAN-Mexico, S.C. is a Scientific and Technological Company in contribution to the formation of Human Resources focused on the continuity in the critical analysis of International Research and is attached to the RENIECYT of CONAHCYT with number 1702902, its commitment is to disseminate research and contributions of the International Scientific Community, academic institutions, agencies and entities of the public and private sectors and contribute to the linkage of researchers who perform scientific activities, technological developments and training of specialized human resources with governments, businesses and social organizations.

To encourage the interlocution of the International Scientific Community with other study centres in Mexico and abroad and to promote a wide incorporation of academics, specialists and researchers to the serial publication in Science Niches of Autonomous Universities - State Public Universities - Federal IES - Polytechnic Universities - Technological Universities - Federal Technological Institutes - Teacher Training Colleges - Decentralised Technological Institutes - Intercultural Universities - S&T Councils - CONAHCYT Research Centres.

Scope, Coverage and Audience

Handbooks is a product edited by ECORFAN-Mexico S.C. in its Holding with repository in Mexico, it is a refereed and indexed scientific publication. It admits a wide range of contents that are evaluated by academic peers by the double-blind method, on topics related to the theory and practice of the CONAHCYT and PRODEP research areas respectively with diverse approaches and perspectives, which contribute to the dissemination of the development of Science, Technology and Innovation that allow arguments related to decision-making and influence the formulation of international policies in the field of Science. The editorial horizon of ECORFAN-Mexico® extends beyond academia and integrates other segments of research and analysis outside that field, as long as they meet the requirements of argumentative and scientific rigour, in addition to addressing issues of general and current interest of the International Scientific Society.

Editorial Board

CASTILLO - TÉLLEZ, Beatriz. PhD
University of La Rochelle

CERCADO - QUEZADA, Bibiana. PhD
Intitut National Polytechnique Toulouse

FERNANDEZ - ZAYAS, José Luis. PhD
University of Bristol

HERNANDEZ - ESCOBEDO, Quetzalcoatl Cruz. PhD
Universidad Central del Ecuador

RIVAS - PEREA, Pablo. PhD
University of Texas

ROCHA - RANGEL, Enrique. PhD
Oak Ridge National Laboratory

RODRÍGUEZ - MORALES, José Alberto. PhD
Universidad Politécnica de Madrid

VAZQUEZ - MARTINEZ, Ernesto. PhD
University of Alberta

VEGA - PINEDA, Javier. PhD
University of Texas

RODRIGUEZ - ROBLEDO, Gricelda. PhD
Universidad Santander

Arbitration Committee

CASTILLO - QUIÑONES, Javier Emmanuel. PhD
Universidad Autónoma de Baja California

CHÁVEZ-LUGO, Pedro. PhD
Universidad Michoacana de San Nicolás de Hidalgo

FLORES - RAMÍREZ, Oscar. PhD
Universidad Politécnica de Amozoc

GÓMEZ - MERCADO, Abdiel
Instituto Tecnológico de Pachuca

HERNÁNDEZ - GÓMEZ, Víctor Hugo. PhD
Universidad Nacional Autónoma de México

HERRERA - ROMERO, José Vidal. PhD
Universidad Nacional Autónoma de México

MEJIAS - BRIZUELA, Nildia Yamileth. PhD
Instituto Nacional de Astrofísica, Óptica y Electrónica

PÉREZ - ROBLES, Juan Francisco. PhD
Instituto Tecnológico de Saltillo

AGUILAR - VIRGEN, Quetzalli. PhD
Universidad Autónoma de Baja California

RAMÍREZ - COUTIÑO, Víctor Ángel. PhD
Centro de Investigación y Desarrollo Tecnológico en Electroquímica

Assignment of Rights

By submitting Scientific Work to ECORFAN Handbooks, the author undertakes not to submit it simultaneously to other scientific publications for consideration. To do so, the author must complete the Originality Form for his or her Scientific Work.

The authors sign the Authorization Form for their Scientific Work to be disseminated by the means that ECORFAN-Mexico, S.C. in its Holding Mexico considers pertinent for the dissemination and diffusion of their Scientific Work, ceding their Scientific Work Rights.

Declaration of Authorship

Indicate the name of 1 Author and a maximum of 3 Co-authors in the participation of the Scientific Work and indicate in full the Institutional Affiliation indicating the Unit.

Identify the name of 1 author and a maximum of 3 co-authors with the CVU number - PNPC or SNI-CONAHCYT - indicating the level of researcher and their Google Scholar profile to verify their citation level and H index.

Identify the Name of 1 Author and 3 Co-authors maximum in the Science and Technology Profiles widely accepted by the International Scientific Community ORC ID - Researcher ID Thomson - arXiv Author ID - PubMed Author ID - Open ID respectively.

Indicate the contact for correspondence to the Author (Mail and Telephone) and indicate the Contributing Researcher as the first Author of the Scientific Work.

Plagiarism Detection

All Scientific Works will be tested by the PLAGSCAN plagiarism software. If a Positive plagiarism level is detected, the Scientific Work will not be sent to arbitration and the receipt of the Scientific Work will be rescinded, notifying the responsible Authors, claiming that academic plagiarism is typified as a crime in the Penal Code.

Refereeing Process

All Scientific Works will be evaluated by academic peers using the Double-Blind method. Approved refereeing is a requirement for the Editorial Board to make a final decision which will be final in all cases. MARVID® is a spin-off brand of ECORFAN® specialized in providing expert reviewers all of them with PhD degree and distinction of International Researchers in the respective Councils of Science and Technology and the counterpart of CONAHCYT for the chapters of America-Europe-Asia-Africa and Oceania. The identification of authorship should only appear on a first page, which can be removed, in order to ensure that the refereeing process is anonymous and covers the following stages: Identification of ECORFAN Handbooks with their author occupancy rate - Identification of Authors and Co-authors - PLAGSCAN Plagiarism Detection - Review of Authorization and Originality Forms-Assignment to the Editorial Board - Assignment of the pair of Expert Referees - Notification of Opinion - Statement of Observations to the Author - Modified Scientific Work Package for Editing - Publication.

ECORFAN Innovative Applications in Sustainable Energy and Environment

Volume I

The Handbook will offer volumes of selected contributions from researchers who contribute to the scientific dissemination activity of the Universidad Autónoma del Carmen in their areas of research in Engineering Sciences. In addition to having a total evaluation, in the hands of the directors of the Universidad Autónoma del Carmen the quality and timeliness of its chapters, each individual contribution was refereed to international standards (V|LEX, RESEARCH GATE, MENDELEY, GOOGLE SCHOLAR and REDIB), the Handbook thus proposes to the academic community, recent reports on new developments in the most interesting and promising areas of research in the Science and Technology.

Innovative Applications in Sustainable Energy and Environment

Handbooks

Coordinators

Figueroa-Ramírez, Sandra Jazmín
Flores-Chan, José Enrique
Patiño-Carachure, Cristóbal
Abatal, Mohamed

Universidad Autónoma del Carmen

December, 2024

DOI: <https://doi.org/10.35429/H.2024.13.1.95>



Preface

The Faculty of Engineering and Architecture of the Universidad Autónoma del Carmen (UNACAR), through the Master's Program in Materials and Energy Engineering, organized the 1st Colloquium of Research in Materials and Energy Engineering, held on October 23-25, 2024, to precede the 5 previous editions of the Master's Student Colloquium. The main purpose of this first colloquium is to open a space for the dissemination and diffusion of research topics developed by students, academics and technologists of the different undergraduate, master's and doctoral programs in the area of sciences and engineering of UNACAR and other graduate programs in the region, the country and abroad. Specifically, the colloquium seeks to promote discussion, debate and feedback on research advances in the areas of materials, energy systems, environmental sciences, hydrogen technologies, electrochemistry, corrosion, control and instrumentation, modeling and numerical simulation, among others. The organizers and most of the participants of this first colloquium, who belong to research groups from different Academic Groups and make up the "Thematic Network of Materials and Energy Engineering" together with members of national and international institutions, presented the progress of their research through oral presentations, posters, lectures and virtual conferences, workshops, as well as the exhibition of some technological prototypes designed and manufactured by students.

This HandBook Entitled "Innovative Applications in Sustainable Energy and Environment" is a compendium of 9 chapters focused on the use of clean technologies and sustainable processes for energy transition and environmental conservation is a product of the first edition of the Research Colloquium 2024, and is a reference that highlights the fundamental guideline of the Universidad Autónoma del Carmen and its commitment to quality education.

Coordinators

*Figueroa-Ramírez, Sandra Jazmín
Flores-Chan, José Enrique
Patiño-Carachure, Cristobal
Abatal, Mohamed*

Content

Page

1 Implementation of solar thermal and photovoltaic energy for the production process of corn tortillas Rayón-Alcudia, Cesar, Meza-Cruz, Onésimo and Mandujano-Ramírez, Humberto J.	1-10
2 Use of natural and treated zeolite for soften drinking water in the municipality of Carmen Gutiérrez-Laffon, Yazmin Michelle, Anguebes-Franceschi, Francisco, Abatal, Mohamed and Aguilar-Ucán, Claudia Alejandra	11-20
3 Evaluation of the potential for bioenergy production from coyol fruit by anaerobic digestion Aguilar-Aguilar, Fidel A., Mena-Cervantes, Violeta Y., Ramírez-Estrada, Alejandro and Hernández-Altamirano, Raúl	21-33
4 Exhaust gas characterization of biofuel blends in an open cycle gas turbine Morales-Sánchez, Leticia Isabel, Andrade-Duran, Juan Edgar, Sánchez-Quintal, Ricardo de Jesús and May-Tzuc, Oscar de Jesús	34-45
5 Causes of cracking in the turbine housings of a turbocharger Duffus-Scott, A. B., Machado-Rodríguez, L. A., Álvarez-García, E. A. and Patiño-Carachure, C.	46-55
6 Structural modeling of steel profiles to infer preventive maintenance in educational infrastructure Gutiérrez-Can, Yuriko, Palemón-Arcos, Leonardo, Naal-Pech, José Wilber and Álvarez-Arellano Juan Antonio	56-66
7 Thermal analysis of a single-cell PEM-type fuel cell with a coil as flow field architecture and its impact on cathode water formation Ceballos-Pérez, José, Ordóñez-López, Luis and Sierra-Grajeda, Juan	67-75
8 Comparison of the effect on electricity production in benthic microbial fuel cells using plasma-treated anodes Flores-Martínez, Jordy Alexis, Fuentes-Albarrán, María del Carmen, Alarcón-Hernández, Fidel Benjamín and Gadea-Pacheco, José Luis	76-84
9 Evaluation of an aqueous solution degradation of textile dye Permalon Rhodamine B by non-thermal plasma treatments Gómez-Anzures, Uriel Yosimar, Alarcón-Hernández, Fidel Benjamín, Fuentes-Albarrán, María del Carmen and Gadea-Pacheco, José Luis	85-95

Implementation of solar thermal and photovoltaic energy for the production process of corn tortillas

Implementación de energía solar térmica y fotovoltaica para el proceso de producción de tortillas de maíz

Rayón-Alcudia, Cesar^a, Meza-Cruz, Onésimo*^b and Mandujano-Ramírez, Humberto J.^c

^a  Universidad Autónoma del Carmen •  LYO-1293-2024 •  0009-0002-1841-0430

^b  Universidad Autónoma del Carmen •  LTD-0198-2024 •  0000-0002-0875-6852 •  488085

^c  Universidad Autónoma del Carmen •  LTC-9972-2024 •  0000-0003-3714-5564 •  266189

CONAHCYT classification:

DOI: <https://doi.org/10.35429/H.2024.13.1.10>

Area: Engineering

Field: Engineering

Discipline: Energy Engineering

Sub-discipline: Solar Energy

Key Handbooks

This paper offers a method of implementing solar thermal and photovoltaic energy to reduce the consumption of gas and electricity from the network that a common business dedicated to the production of tortillas, thereby it is intended to contribute to the vector aimed at the implementation of clean energy, and also serve as a guide for these facilities become common not only in the field of tortilla if not in other small and medium enterprises. One of the key aspects of this research is to understand the import culture of the corn tortilla as a staple food in Mexican society as well as the process and cost of manufacture and thus be able to design alternatives to reduce costs through the implementation of new technologies. The implementation of a hybrid solar thermal - photovoltaic system is undoubtedly an excellent proposal for cost reduction in the production process of corn tortillas, it is also a responsible proposal that helps to reduce greenhouse gas emissions.

Citation: Rayón-Alcudia, Cesar, Meza-Cruz, Onésimo and Mandujano-Ramírez, Humberto J. 2024. Implementation of solar thermal and photovoltaic energy for the production process of corn tortillas. 1-10. ECORFAN.

*  [omeza@pampano.unacar.mx]

Handbook shelf URL: <https://www.ecorfan.org/handbooks.php>



ISBN 978-607-8948-51-2 ©2009 The Authors. Published by ECORFAN-Mexico, S.C. for its Holding Mexico on behalf of Handbook HRPG. This is an open access chapter under the CC BY-NC-ND license [<http://creativecommons.org/licenses/by-nc-nd/4.0/>]

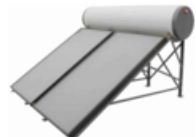
Peer Review under the responsibility of the Scientific Committee MARVID®- in contribution to the scientific, technological and innovation Peer Review Process by training Human Resources for the continuity in the Critical Analysis of International Research.



1702902 CONAHCYT

Abstract

A methodology was developed for the implementation of solar thermal and photovoltaic energy in an establishment dedicated to the production of tortillas with an electrical consumption between 491 kWh and 572 kWh per year, with a consumption of 2,235 liters of LP gas weekly. The available solar resource was determined at an angle of 22 ° using the Liu & Jordan method, and the F-Chart method was also used for thermal sizing. For photovoltaic sizing, the critical month was selected, and the peak power that the photovoltaic system must have to generate the energy consumed by the electrical loads was also determined. It was calculated that 511.4 kg of LP gas and 2,984.76 kWh of electrical energy will be saved per year.

Implementation of solar thermal and photovoltaic energy for the production process of corn tortillas		
Objectives	Metodología	Contribución
Conduct energy consumption studies in a tortilla factory  Sizing the solar thermal and thermal installation for a tortilla factory	Thermal sizing, Liu & Jordan method and F-Chart  Photovoltaic sizing, based on peak power 	Efficiency and sustainability in traditional food production  Decrease in LP gas and electricity consumption

Photothermal, Photovoltaic, Implementation

Resumen

Se desarrolló una metodología para la implementación de la energía solar térmica y fotovoltaica en un establecimiento dedicado a la producción de tortillas con un consumo eléctrico entre los 491 kWh y los 572 kWh bimestrales, con un consumo de 2,235 litros de gas LP semanalmente. Se determinó el recurso solar disponible a un ángulo de 22° utilizando el método de Liu & Jordan, así también para el dimensionamiento térmico se utilizó el método F-Chart. Para el dimensionamiento fotovoltaico se seleccionó el mes mes crítico, también se determinó la potencia pico que el sistema fotovoltaico debe tener para generar la energía consumida por las cargas eléctricas. Se calculó que al año se ahorrarán 511.4 kg de gas LP y 2,984.76 kWh de energía eléctrica.

Implementación de energía solar térmica y fotovoltaica para el proceso de producción de tortillas de maíz		
Objetivos	Objetivos	Contribución
Realizar los estudios de consumo energético en una tortillería  Dimensionar la instalación solar térmica y térmica para una tortillería	Dimensionamiento térmico, Método Liu & Jordan y F-Chart  Dimensionamiento fotovoltaico, con base a la potencia pico 	Eficiencia y sostenibilidad en la producción de alimentos tradicionales  Disminución del consumo de gas LP y electricidad

Fototérmico, Fotovoltaico, Implementación

Introduction

The corn tortilla represents a fundamental basis in the diet of Mexicans and South Americans, and being such a versatile element in the kitchen, it has been marketed in North America under the concept of fast food ‘Tex-Mex food’ and in Europe in the eighties, to later become popular around the world. However, it is in Mexico where we could say that this industry is fully developed, both in the production of corn tortillas and in the elaboration of nixtamal. ‘The term nixtamal comes from the Nahuatl: nixté (ashes) and tomalli (cooked dough), as in ancient times the ashes of the cooker were used as a source of alkalis to achieve the cooking in an alkaline medium, necessary to give the desired texture to the dough and allow the starch to mix with the protein or gluten’.

The industry dedicated to the production of corn tortillas is large abroad, but even more so in our country, it is so important in the diet that it is included in the food basket where it is estimated that around 217.9 grams of tortillas are consumed per person per day, generating a monthly expenditure of approximately \$147.04 mxn, representing 11% of the total estimated at \$1,344.94 mxn per person. Taking this into account, we can say that the energy demand for its production is very important. For this reason, studies have been carried out to evaluate various alternatives not only to supply, but also to reduce this energy demand. Some studies are aimed at optimising the processes that are carried out either by making modifications to the mills, the maintenance that is given to them or the type of raw material that is used, testing different quantities of maize, maize flour, water and/or lime, and others are aimed at obtaining energy by other means to reduce costs caused by the same energy demand; examples of this are the attempts to implement clean energy in the production process or reusing heat that is normally wasted during the process (CONEVAL, 2021) (Juárez Hernández & Sheinbaum Pardo, 2019).

Box 1

Food basket 2021

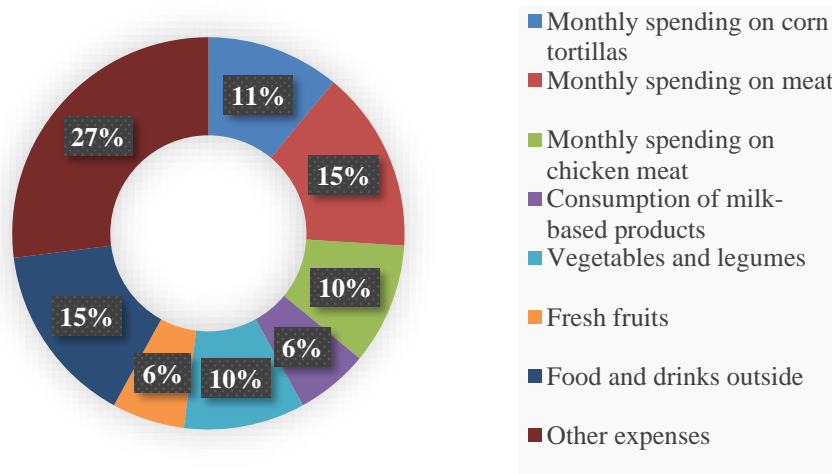


Figure 1

Percentage of expenditure on food basket 2021

Source: Own elaboration with information from CONEVAL

Solar thermal heaters are an option to inject thermal energy into the process without generating an expense in the production, this type of technology has already been implemented in the mills with satisfactory results. It is worth mentioning that the objective of these heaters is not to replace the burning of natural gas to satisfy the thermal demand of the process, but to implement them as a source of energy for pre-heating the water used to cook the corn. We could say that, with the exception of some rural mills in the country, absolutely all the mills work with electric motors in the process during the cooking of the corn to obtain the nixtamal, but in the same way we can say that the great majority of tortilla factories in the country use them during the cooking of the dough, where attempts have been made to increase their efficiency and that of the mechanical components present in the machines used.

On the other hand, we have the need to satisfy the electrical energy demanded by the electric motors, and it is here where photovoltaic solar energy and photovoltaic cells could have a significant impact on the nixtamalisation and production of tortillas, because apart from being a clean and inexhaustible energy, their main advantage is that, like solar thermal collectors, they do not generate a constant expense in production.

However, despite the fact that a large number of projects have been carried out implementing all the aforementioned alternatives, the truth is that within the tortilla production sector the implementation of these technologies is still seen as an option with many unknowns, as a result of the lack of knowledge of the high profitability that these technologies provide to the tortilla production process. Not to mention that the results of projects carried out have not been properly disseminated, which is why this project aims to evaluate the energy demand of a common tortilla factory in the city of Ciudad del Carmen, Campeche, and make an estimate of the economic profitability that a project using these energy technologies could present compared to the current market.

Methodology

The activities in the tortilla factory under study begin at 05:00 hrs, the first grinding of nixtamal is carried out and then the tortilla machine is turned on and tortilla production begins. Tortilla production takes place on two occasions during the day, the first starts at 05:00 hrs and ends at approximately 08:30 hrs in the morning, the second starts at approximately 11:00 hrs and ends at 13:00 hrs of the day.

The maize is cooked the day before, so that in the morning the maize is ready to be ground, during the first grinding the volume of maize is around 80 kilograms and during the second grinding around another 120 kilograms. The nixtamal is mixed with nixtamalised maize flour in a ratio of 1 kilogram of nixtamal to 3 kilograms of nixtamalised maize flour, so that around 600 kilograms of nixtamalised maize flour are used daily. The mixer is in charge of this process and does it intermittently with loads of 40 to 50 kilograms, which are stirred for around 5 minutes. Once the nixtamal has been mixed with the nixtamalised corn flour, the result is the dough used to make tortillas, which is delivered to the tortilla hopper in 50-kilogram portions. The tortilla machine works constantly during most of the production hours. During the afternoon from 14:00 to 15:00 hours, the maize to be used the following day is cooked; this quantity varies on some days between 200 and 250 kilograms. The maize is cooked in water at a ratio of 1 litre per kilogram of maize for approximately 5 minutes until it reaches 70° and is left to stand for the rest of the day and night until the early hours of the morning, when it is used for the first milling of the day.

Water consumption

The water used in maize cooking is 1 litre per kilogram of maize used, using about 200 litres of water per cooking per day, and for each kilogram of nixtamalised maize flour, about 1.4 litres of water are used, using about 840 litres of water per day. So the total water demand for the production of corn tortillas is the sum of the water used in these two processes, so that about 1040 litres of water are used per day.

Electricity consumption

The tortilla factory has 4 electric motors to perform different functions within the tortilla production process:

Milling: The motor used for milling the corn grain is the one with the largest capacity, it has a power of 5 horsepower and operates at 220 Volts with a consumption at full load of 12 amperes. This mill takes about 1 minute to grind 2 kilograms of maize, so that throughout the day it keeps operating for approximately 2 hours net throughout the day, on average, the mill consumes about 5.2 kWh per day.

Mixer: The motor used by the mixer has a power of 2 horsepower and operates at 110 Volts with a full load consumption of 3.5 amperes, the mixer takes on average 5 minutes to do its job, mixing around 50 kilograms per load, in total around 33 loads are mixed per day. The daily usage time is about 3 hours net over the course of the day and on average, the mixer consumes about 1.1 kWh per day.

Tortilla machine: The motor used in the tortilla machine is a 1 horsepower motor which operates at 110 Volts with a full load consumption of 5 amps. The tortilla machine is kept in operation for approximately 2 hours in the morning and 1.5 hours in the afternoon working for 3.5 net hours per day, so on average the tortilla machine consumes about 1.9 kWh per day.

Agitator: The last motor is the agitator, not all threshing machines have this last process, the purpose of the agitator is to arrange the tortillas and arrange them once they come out of the burner, the motor used is 1/4 horsepower, it operates at 110V with a consumption of 2 Amperes. This motor runs for the same amount of time that the tortilla shaker is in operation, approximately 3.5 hours a day. On average the shaker consumes about 0.8 kWh per day.

At the end of the day the electric motors used in the tortilla production consume a total of 9 kWh per day, 270 kWh per month, giving a total of 540 kWh per two-month billing period.

The service number of the premises was requested from the Federal Electricity Commission (CFE) in order to compare the billed consumption with the consumption measured in Figure 2, which shows that the consumption ranges between 491 kWh and 572 kWh billed throughout the year. This means that the energy demanded by the electric motors actually amounts to around 540 kWh.

Box 2

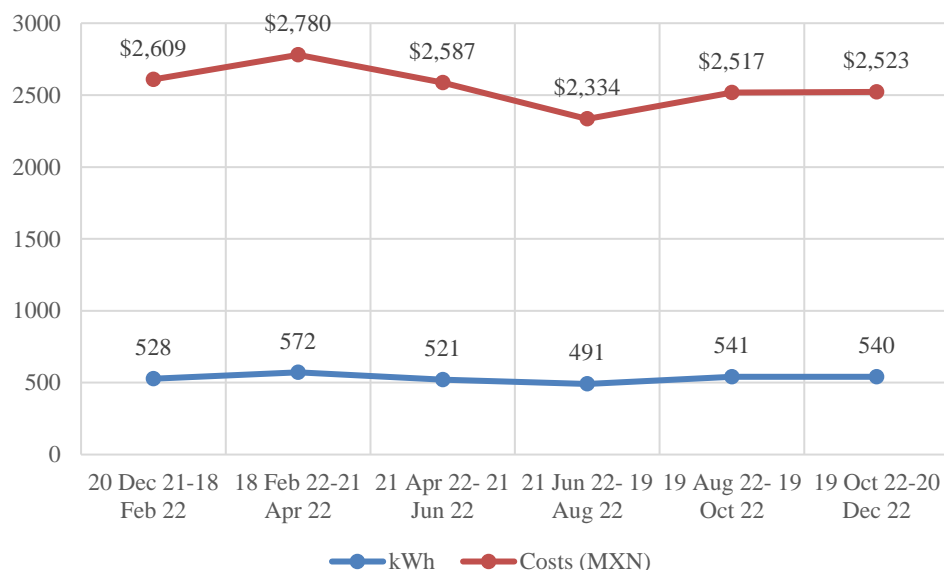


Figure 2

Graph of energy consumption and costs per period

Source: Own elaboration with CFE receipts

The same graph shows the economic amounts for energy consumption determined by the CFE, where the highest amount coincides with the highest consumption recorded, so that the amount for electricity consumption is around \$2,500 pesos per billing period. It is important to mention that the tariff applied is Low Voltage Small Demand.

Calorific consumption

The amount of heat energy used can be estimated by the equation [1].

$$Q = m * C_p * \Delta T \quad [1]$$

Where:

Q: Heat energy (J)

m: Mass of material (kg)

C_p: Specific heat (J/kg * K)

ΔT: Temperature change experienced by the material (K)

The amount of energy demanded must be calculated according to the quantities of ingredients used, cooking requires a total of 200 litres of water per cooking, 200 kg of corn is cooked daily and 2 kg of lime is added. Nixtamal cooking at the Insurgentes tortillería consists of injecting heat into the mixture for 5 to 10 minutes to reach a temperature of 70°C and then leaving it to rest for the rest of the day.

Liu & Jordan method

The Liu & Jordan method (Duffie & Beckman, 2013) allows the calculation of incident solar radiation on an inclined plane, providing an approximation using few variables for estimation and maintaining a margin of error compared to field measurements. This method is useful for finding the optimal angle of inclination for solar collectors, as it is possible to obtain approximate values of collection depending on the angles of incidence and inclination; in this project, latitude was used as the angle of inclination for the solar collectors and the generation potential at this angle is estimated using the following equation [2].

$$H_{t,i} = H_t \left(1 - \frac{H_d}{H_t} \right) R_b + H_d \left(\frac{1+\cos\beta}{2} \right) + H_t \rho_g \left(\frac{1-\cos\beta}{2} \right) \quad [2]$$

Where:

$H_{t,i}$: Total insolation incident on a sloping surface ($\text{kW} * \text{h/m}^2$)

H_t : Total global desolation of the site ($\text{kW} * \text{h/m}^2$)

H_d : Horizontal diffuse insolation ($\text{kW} * \text{h/m}^2$)

R_b : Ratio of direct insolation to total insolation

β : Solar collector inclination

ρ_g : Terrain reflectance

The f -Chart Method

The f -Chart curves method is commonly used for the sizing of solar thermal installations, it allows the calculation of the contribution that a solar thermal collection system would have to the total heat demand of a process, as well as its average performance over a long period of time. This method is efficient for calculations and estimations over long periods of time, i.e. it should not be used for short term (daily-weekly) estimations. It is important to mention that this method is only applicable in heating systems where the minimum temperature for the energy supply is approximately 20 °C. Monthly meteorological data on solar radiation, water temperature and ambient temperature are used for its development (De la cruz Figueroa, et al., 2021). The method for liquid systems is performed using the equation [3].

$$f = 1.029X - 0.065Y - 0.245X^2 - 0.0018Y^2 + 0.0215X^3 \quad [3]$$

Its application consists of identifying the dimensionless variables of the heating system and performing operational simulations to determine the correlations between the variables and the performance of the system for a given period of time. The resulting correlations determine the variable f (fraction of the monthly load supplied by solar energy as a function of the dimensionless parameters). The method comprises 2 dimensionless parameters "X" and "Y", where the former represents the ratio between the absorbed solar radiation and the demanded heat load and the latter is a ratio between the collector losses and the heat loads. (Duffie & Beckman, 2013)

Photovoltaic sizing

The sizing of the PV system is done based on the peak power that the PV system must have to generate the energy consumed by the ECL electrical loads, which is calculated according to the equation [4].

$$P_P(AFV) = \frac{E_{CL}}{H_P * \eta_{ET} * R_T} \quad [4]$$

Where:

E_{CL} : Energy consumed by electrical loads (kWh).

H_P : Local solar resource (h).

η_{ET} : Overall total system electrical efficiency.

R_T : Thermal efficiency of the module (Typically taken as 85% for systems without batteries).

The overall total electrical efficiency of the system “ η_{ET} ” is determined by multiplying the efficiency of the lines or losses set in the wiring “ η_{L} ”, efficiency of the charge controller “ η_{CC} ”, efficiency of the electrochemical storage system “ η_{ESS} ”, efficiency of the inverter “ η_{INV} ” and the efficiency of any other electronic devices that use and handle or drive the generated power. The commonly used default values are: $\eta_{L} = 0.95$, $\eta_{CC} = 0.9$, $\eta_{ESS} = 0.9$, $\eta_{INV} = 0.95$. It is important to mention that the peak power of an existing PV array can be calculated based on the total number of PV modules and the peak power of the PV module in question, as shown in equation 3.26 (Sánchez Juárez, Martínez Escobar, Santos Magdaleno, Ortega Cruz, & Sánchez Pérez, 2017).

$$P_P(AFV) = N_T * P_P(MFV) \quad [5]$$

Where:

N_T : Total number of photovoltaic modules which results from the multiplication of the number of modules connected in series. “ N_S ” by the number of modules connected in parallel “ N_P ”.

Results

The calculated thermal demand was 3,586.05 kWh, energy required to raise the temperature of the water from room temperature to the reference temperature (70 °C). Table 1 shows that the amount of energy demanded is similar throughout the year, with a slight increase between the months of November and March.

Box 3

Table 1

Thermal demand				
Month	ΔT (°C)	N (day/month)	DQ (MJ)	DQ(kWh)
January	45.3	31	1175.68	326.58
February	44.7	28	1047.84	291.07
March	43.7	31	1134.15	315.04
April	42.1	30	1057.38	293.72
May	40.9	31	1061.49	294.86
June	40.4	30	1014.69	281.86
July	40.7	31	1056.3	293.42
August	40.5	31	1051.1	291.97
September	40.4	30	1014.69	281.86
October	41.1	31	1066.68	296.3
November	43	30	1079.99	300

Source: own elaboration.

The tortilla factory uses three-phase electric motors operating at 220 VAC, and that the local electrical distribution network (RELD) provides electrical energy at a voltage of 220 VAC, three-phase at 60 Hz, we can deduce that the system requires a two-phase 220VAC, 60 Hz DC/AC inverter to be able to feed our installation and interconnect with the RELD. The first step is to calculate the electrical demand of the system, this with 4 motors in the production process; table 2 shows the daily electrical consumption of each one of them.

Box 4

Table 2

Daily electricity consumption					
Loads	Volts	Amper	Power (kW)	Time of use (h)	Consumption (kWh)
Mill	220	12	2.64	2	5.28
Mixer	110	3.5	0.39	3	1.17
Tortilla machine	110	5	0.55	3.5	1.93
Agitator	110	2	0.22	3.5	0.77
Total	220	22.5	3.8	12	9.15

Source: own elaboration

Once the thermal demands were calculated with equation 1, the calculation of the incident solar radiation at the angle of the latitude of the place was carried out, and the Liu & Jordan Method was also applied, where own meteorological data was used, as well as the real data of commercial flat plate solar collectors, the model chosen was the AXOL 240 LITRES MS 2.5 BLUE of the commercial brand Modulo Solar. Finally, it was possible to compare the results obtained between the monthly heat demand, the thermal energy of the proposed collectors and the consumption of LP gas, as shown in figure 3. In this figure it can be seen that for the latitude of the place under study in the months of November, December and January are the months with the lowest contribution of thermal energy with the proposed system.

Box 5

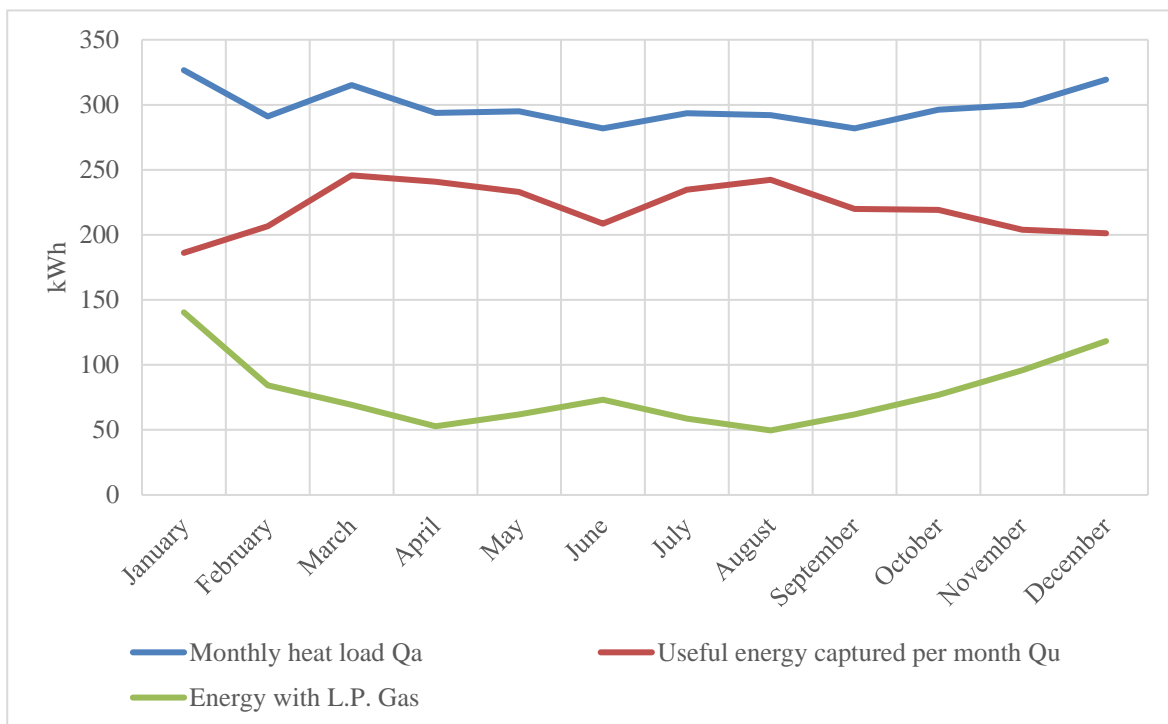


Figure 3

Comparison of thermal energy

Source: Own elaboration

Based on the estimates of the available area for the installation of the equipment, it was determined that high efficiency photovoltaic modules were needed, and that they should be panels with a monocrystalline structure. The solar photovoltaic module selected was the LR5-72HTH 585~600 M model from LONGi. Once the calculations had been made, comparisons were obtained between the electrical energy demanded and the electrical energy coming from the proposed system, as shown in figure 3. It should be noted that in the months of July and August the photovoltaic electrical energy is exceeded, so the system interconnected to the grid will supply this surplus to the national electrical grid.

Box 6

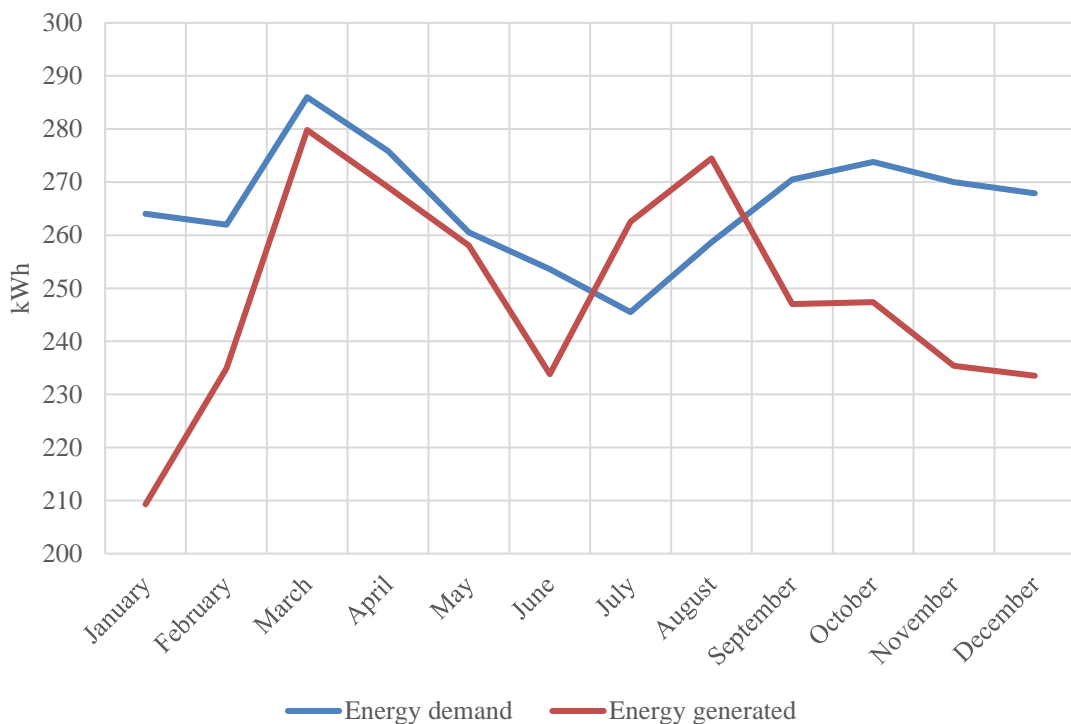


Figure 3

Comparison of electricity

Source: Own elaboration

In the case of the results with respect to the payback time of the investment, calculations were made and it was determined that the present project would recover the investment in 5.04 years. In a study from Spain and Ecuador, a minimum payback time of 8.75 years was estimated for photothermal installations, noting that only the photothermal installation without photovoltaic was considered, although it is not a comparison of similar projects, it gives us an overview of the results obtained in the present study.

Conclusions

The system will have an annual solar fraction of 0.7368, in other words, the solar thermal system will provide 73.68% of the thermal energy demanded. In the case of the solar photovoltaic system, throughout the year, the installation will produce 94% of the electrical energy demanded, so it is concluded that the use of solar thermal and photovoltaic energy is profitable for businesses similar to the one in the study, and if extrapolated to the whole country, it would contribute to the medium-term goals set for the use of clean technologies, improving efficiency and sustainability in traditional food production, concluding that the use of these mature technologies would economically benefit Small and Medium Enterprises in Mexico, as well as their consequent support to the environment by decreasing the consumption of LP gas and electricity.

Statements

Conflict of interest

The authors declare that they have no conflicts of interest. They have no financial interests or personal relationships that could have influenced this book.

Authors' contribution

Rayón-Alcudia, Cesar: contributed to the calculations for the entire project.

Meza-Cruz, Onésimo: Contributed to the project idea, and advised on the photothermal part.

Mandujano-Ramírez, Humberto J: Advised on the photovoltaic part.

Availability of data and materials

Data are available on request at: omeza@pampano.unacar.mx

Acknowledgements

To the tortillería ‘Insurgentes’, in Cd del Carmen Campeche, and to the Universidad Autónoma del Carmen for providing the meteorological data through the LENERSE project.

Abbreviations

AFV	Photovoltaic Array
MFV	Photovoltaic Module

References

Background

De la Rosa Armijo, D., & Moreno Alarcón, C. R. (2008). [Uso de la energía en molinos de Nixtamal](#). Tesis de Pregrado, Universidad Autónoma Metropolitana Unidad Iztapalapa, México. Retrieved 20 August 2022.

Juárez Hernández, S., & Sheinbaum Pardo, C. (2019). Water and energy use and greenhouse gas emissions for nixtamalised. *Journal of Cleaner Production*.

Basics

Calleja Pinedo, M., & Basilia Valenzuela, M. (2016). [La tortilla como identidad culinaria](#). Región y sociedad. Recuperado el 20 de 08 de 2022, de

Carreño King, P. (2017). [La industria solar fotovoltaica y fototérmica en México](#). Ciudad de México: ProMexico. Retrieved 10 September 2022.

CONEVAL. (2021). [Evolución de las líneas de pobreza por ingresos](#) (Enero 1992 - Diciembre 2021). Ciudad de México. Retrieved 23 May 2023.

Duffie, J. A., & Beckman, W. A. (2013). [Solar Engineering of Thermal Processes](#). Hoboken, New Jersey: John Wiley & Sons, Inc.

Sánchez Juárez, A., Martínez Escobar, D., Santos Magdaleno, R. d., Ortega Cruz, J., & Sánchez Pérez, P. A. (2017). [Aplicaciones fotovoltaicas de la energía solar \(Primera ed.\)](#). Ciudad de México: Instituto de Energías Renovables, UNAM. Retrieved 20 May 2023.

Support

De la cruz Figueroa, O., Meza-Cruz, O., Mandujano-Ramírez, H., Sierra-Grajeda, J., Figueroa-Ramírez, S., & Santis-Espinosa, L. (2021). [Calentamiento de agua solar para el proceso de escaldado de cerdo en el rastro municipal de Cd del Carmen, Campeche](#). En ANES (Ed.), XLV Semana de Energía Solar (pág. 318). CDMX: ANES.

Difference

Noritz Molina, E. M. (2024). [Análisis energético y económico de un proyecto de instalación solar térmica para proveer agua caliente sanitaria en una misma edificación residencial en cuatro zonas geográficas diferentes dentro de España y Ecuador](#). Tesis de Maestría, Universidad Politécnica de Valencia, Valencia.

Use of natural and treated zeolite for soften drinking water in the municipality of Carmen

Uso de zeolita natural y tratada para ablandar el agua potable del municipio del Carmen

Gutiérrez-Laffon, Yazmin Michelle^a, Anguebes-Franceschi, Francisco^b, Abatal, Mohamed^c and Aguilar-Ucán, Claudia Alejandra^d

^a  Universidad Autónoma del Carmen •  0009-0005-3607-6992 •  1320888

^b  Universidad Autónoma del Carmen •  0000-0003-0489-7110 •  217824

^c  Universidad Autónoma del Carmen •  6047-2018 •  0000-0003-2479-8769 •  203026

^d  Universidad Autónoma del Carmen •  7723-2021 •  0000-0002-1733-2867 •  93717

CONAHCYT classification:

DOI: <https://doi.org/10.35429/H.2024.13.11.20>

Area: Engineering

Field: Engineering

Discipline: Chemical engineering

Sub-discipline: Materials science

Key Handbooks

The main contribution of this research lies in the evaluation of clinoptilolite zeolite, both in its natural and modified form, as a sustainable and economic solution for the softening of drinking water in the municipality of El Carmen. This study not only structurally characterizes the properties of the zeolite using advanced techniques such as XRD and IR, but also delves into its chemical behavior by determining the point zero charge (PZC) and evaluating adsorption isotherms. In addition, the effects of pH on the adsorption process were identified. These results contribute to the development of alternative materials for water treatment, reducing the dependence on conventional technologies of higher cost and energy consumption, and promote the use of local resources with low environmental impact. The relationship between pH and adsorption: pH control is essential to avoid precipitate formation and maximize the effectiveness of the material in practical applications. The structural stability of the treated zeolite: This ensures its viability for long-term implementation in water treatment systems. The flexibility and scalability of the method: The results allow extrapolating this approach to other global contexts where water hardness represents a problem, promoting the application of economical and environmentally friendly solutions. Structural analyses confirmed that the chemical modification does not significantly affect zeolite stability, but does increase its ion exchange capacity. However, it was identified that pH plays a crucial role in the adsorption process, since under basic conditions it can promote the precipitation of hardness ions, which affects the accuracy of the measurements. This work highlights the importance of optimizing the experimental conditions, in particular pH control, to improve the efficiency of the process.

Citation: Gutiérrez-Laffon, Yazmin Michelle, Anguebes-Franceschi, Francisco, Abatal, Mohamed and Aguilar-Ucán, Claudia Alejandra. 2024. Use of natural and treated zeolite for soften drinking water in the municipality of Carmen. 11-20. ECORFAN.

Handbook shelf URL: <https://www.ecorfan.org/handbooks.php>



ISBN 978-607-8948-51-2 ©2009 The Authors. Published by ECORFAN-Mexico, S.C. for its Holding Mexico on behalf of Handbook HPGC. This is an open access chapter under the CC BY-NC-ND license [<http://creativecommons.org/licenses/by-nc-nd/4.0/>]

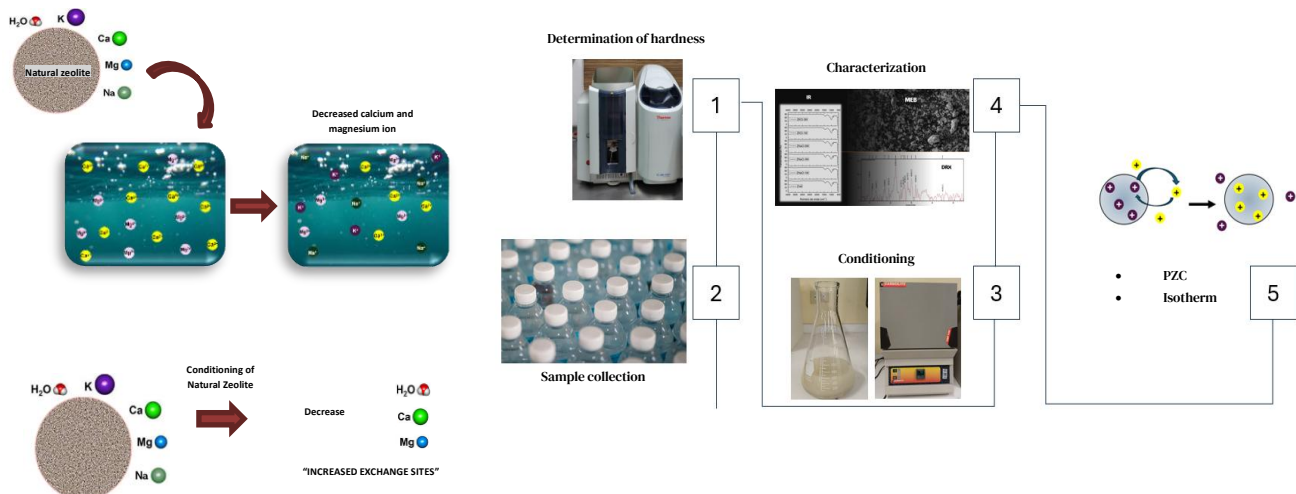
Peer Review under the responsibility of the Scientific Committee MARVID®- in contribution to the scientific, technological and innovation Peer Review Process by training Human Resources for the continuity in the Critical Analysis of International Research.



1702902 CONAHCYT

Abstract

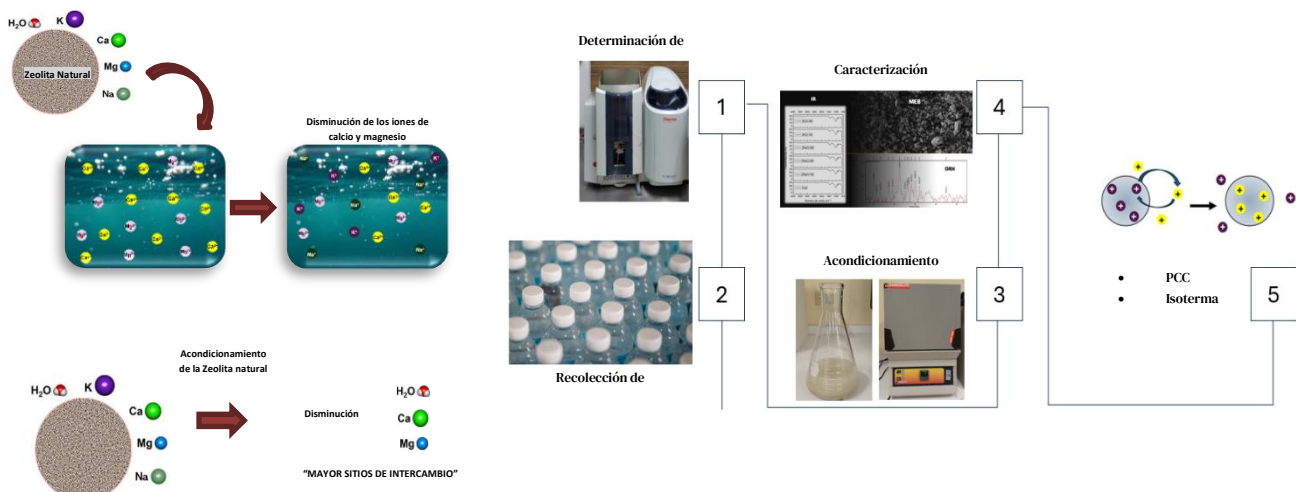
This study addresses the use of Clinoptilolite-type zeolite, natural and modified with sodium chloride (1M, 3M y 5M) and potassium chloride (1 M y 3 M), to reduce water hardness by adsorbing calcium and magnesium ions. Clinoptilolite is structurally characterized by X-ray diffraction (XRD) and infrared spectroscopy (FTIR) to evaluate changes in its structure and functional groups after modification, and its point of zero charge (PZC) is determined to understand the effect of pH on adsorption. Adsorption experiments, performed under controlled conditions, show that modified zeolite increases its efficiency compared to natural zeolite, although it is observed that pH can induce precipitation of hardness ions, affecting the accuracy of the measurements.



Hardness, Ion exchange, Zeolite

Resumen

Este estudio aborda el uso de zeolita tipo Clinoptilolita, natural y modificada con cloruro de sodio (1 M, 3 M y 5 M) y cloruro de potasio (1 M y 3 M), para reducir la dureza del agua mediante la adsorción de iones de calcio y magnesio. La Clinoptilolita se caracteriza estructuralmente mediante difracción de rayos X (DRX) y espectroscopía infrarroja (FTIR) para evaluar cambios en su estructura y grupos funcionales tras la modificación, y se determina su punto cero de carga (PZC) para entender el efecto del pH en la adsorción. Los experimentos de adsorción, realizados en condiciones controladas, muestran que la zeolita modificada incrementa su eficacia en comparación con la zeolita natural, aunque se observa que el pH puede inducir la precipitación de los iones de dureza, afectando la precisión de las mediciones.



Dureza, intercambio iónico, zeolita

Introduction

Water hardness is a widely studied phenomenon of significant relevance, as it affects both the efficiency of distribution systems and the lifetime of household appliances and other water-dependent equipment. Hardness is mainly due to high concentrations of calcium (Ca^{2+}) and magnesium (Mg^{2+}) ions, which react with cleaning agents, forming insoluble compounds that reduce their effectiveness, and the accumulation of scale that affects water conveyance systems. In the Municipality of Carmen, Mexico, where water hardness levels represent a challenge for residents, there is an urgent need to implement affordable and sustainable solutions to improve drinking water quality.

There are several techniques for water softening, including the use of membrane technologies and reverse osmosis, which are the most common, but have certain limitations such as high energy consumption and high operational costs. In the face of these limitations, the use of natural and treated zeolites emerges as a promising alternative due to their ion exchange capacity, low cost and availability in various regions. Zeolites are porous minerals with a crystalline structure that allows the adsorption and exchange of specific ions; in the context of this project, their ability to remove calcium and magnesium, responsible for water hardness, is investigated.

This study focuses on Clinoptilolite zeolite, a type of natural zeolite, whose effectiveness is analysed after a modification process with sodium and potassium. These elements are selected because of their ability to increase the zeolite's affinity for calcium and magnesium ions, thus improving its ion exchange capacity compared to untreated zeolite. In addition to evaluating the efficiency of treated zeolite in water softening, this study investigates the structural stability of the material during the adsorption process, an essential feature for its possible implementation in domestic filtration systems.

Methodology

Water sample collection

Water samples were collected at various locations in the Municipality of Carmen, Campeche, and nearby areas, including Chicbul, Checubul, Sabancuy, Isla Aguada, Frontera, Hecelchakán and Mérida. In each of these localities, samples were taken from representative water bodies, while in the case of the Municipality of Carmen, samples were taken directly from the household drinking water intake at the point of domestic supply.

The samples were collected in polystyrene bottles of approximately 1 L, previously cleaned and rinsed to avoid external contamination. They were then transported to the laboratory under appropriate conditions. The pH of each sample was measured and the concentration of calcium and magnesium was calculated by flame atomic absorption spectrophotometry using a Thermo Scientific ^{iCETM} 3000 spectrophotometer. For the determination of calcium, acetylene gas was used, and for magnesium, nitrous oxide, using ultra-dry air as an auxiliary gas in both cases.

Conditioning of Clinoptilolite-type natural zeolite

Clinoptilolite-type natural zeolite was initially washed with 500 mL of deionised water, immersing 100 g of the material. It was left in agitation at 190 rpm for 30 minutes. This procedure was repeated three times, followed by additional rinses with deionised water until the rinse water was clear. The zeolite was allowed to dry at room temperature and subsequently heat treated at 250 °C for two hours.

Subsequently, the washed zeolite was conditioned in sodium chloride (NaCl) solutions at 1 M, 3 M and 5 M concentrations, and in potassium chloride (KCl) solutions at 1 M and 3 M concentrations. For the NaCl treatment, 50 g of zeolite were immersed in 500 mL of the solution and left in constant agitation at 190 rpm for 3 hours; this procedure was repeated twice for each concentration. In the case of the KCl treatment, 50 g of zeolite were immersed in 500 mL of the solution for 2 hours with agitation at 190 rpm, repeating the procedure three times for each concentration.

Once the treatments with NaCl and KCl at different concentrations were completed, the zeolite was rinsed with deionised water, then filtered and dried at room temperature. Finally, the conditioned zeolite was sieved using a #10 sieve to ensure uniform particle size.

Characterisation

The crystalline structure of the natural and conditioned zeolite was analysed by X-ray diffraction (XRD) using a GNR APD 2000 PRO diffractometer. The analysis was performed with Cu-K α radiation (1.5406 Å) in a 2 θ range from 10° to 60° and a step size of 0.02°.

Characterisation of the zeolite functional groups was performed by Fourier Transform Infrared Spectroscopy (FTIR) in the range of 4000 to 500 cm $^{-1}$. The spectra were obtained in terms of % transmittance, allowing the identification of the characteristic vibrational modes of the functional groups present in the zeolite structure.

Determination of the point zero charge (PZC)

The point zero charge (PZC) of natural and conditioned zeolite is calculated using the pH derivative method. For this purpose, a series of 0.01 M calcium chloride (CaCl₂) solutions were prepared with pH adjusted to values of 2, 4, 6, 8, 8, 10 and 12, using HCl or NaOH as required. To each 50 ml of the pH-adjusted solution, 0.1 ± 0.0005 g of zeolite was added.

The suspensions were allowed to stand for 24 hours to reach equilibrium. Subsequently, they were filtered to obtain only the resulting solution, and the final pH of each solution was measured using a Hanna Instruments edge® pH meter, which allows accurate pH and temperature measurement with automatic temperature compensation (ATC).

To determine the PZC, the final pH is plotted against the initial pH of each solution. The zero loading point was identified at the pH value where the curve shows that the initial pH and final pH are equal, indicating the absence of net loading on the zeolite surface.

Evaluation of adsorption isotherms

The adsorption capacity of zeolite for calcium and magnesium ions was evaluated by means of adsorption isotherms. For this purpose, solutions of calcium and magnesium ions were prepared at different concentrations (10, 20, 50, 100, 250, 500, 500, 700, 800, 900 and 1000 ppm). In each adjusted solution, 0.1 ± 0.0005 g of natural or conditioned zeolite was dispersed and left in contact for 24 hours under constant stirring at 190 rpm to ensure adsorption equilibrium.

, the samples were centrifuged for 3 minutes at 1680 RCF to separate the zeolite from the solution. The final concentration of ions in the solution was determined by flame atomic absorption spectrophotometry using a Thermo Scientific iCE 3000 spectrophotometer. The data obtained allowed the evaluation of the adsorption capacity of the zeolite as a function of the initial concentration of ions in solution.

Results

X-ray diffraction (XRD)

The structural characterisation of the natural zeolite and its modified versions was performed by X-ray diffraction (XRD) as shown in figure 1, evaluating the effects of treatment with sodium chloride (NaCl) at 1 M, 3 M and 5 M concentrations, and with potassium chloride (KCl) at 1 M and 3 M concentrations on the crystalline structure of the Clinoptilolite type zeolite. The XRD pattern of the natural zeolite shows characteristic peaks of Clinoptilolite at 2 θ at approximately 22.5°, 27.5° and 32.2°, indicating a well-defined crystal structure. Samples treated with NaCl at different concentrations maintain the main peaks of natural zeolite, although a gradual decrease in the intensity of these peaks is observed with increasing NaCl concentration. This effect suggests a progressive ion exchange that slightly affects the crystallinity without significantly altering the structure of the clinoptilolite. On the other hand, samples treated with KCl at 1 M and 3 M also retain the main peaks, with a slight decrease in intensity that becomes more pronounced at higher concentrations. The reduction in the intensity of the peaks in these samples may be related to the larger size of the K $^{+}$ ion in comparison to Na $^{+}$.

Box 1

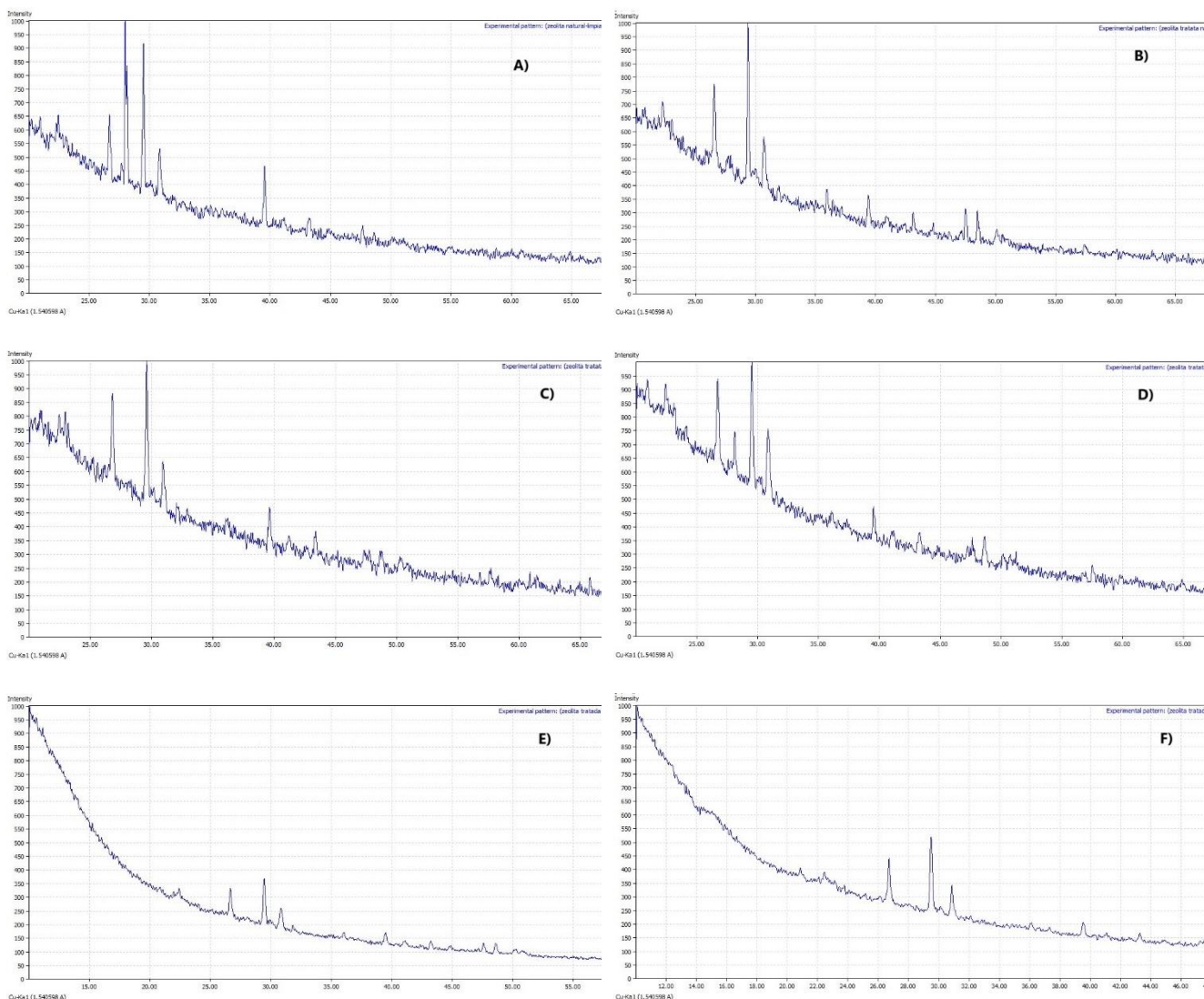


Figure 1

XRD patterns corresponding to Clinoptilolite type zeolite: A) clean natural zeolite, B) zeolite treated with 1M NaCl, C) zeolite treated with 3M NaCl, D) zeolite treated with 5M NaCl, E) zeolite treated with 1M KCl, F) zeolite treated with 3M KCl.

Source: [Own elaboration]

In conclusion, XRD patterns indicate that the structure of Clinoptilolite in zeolite remains stable after NaCl and KCl treatments, although a slight decrease in crystallinity is observed with increasing cation concentration. These results demonstrate the ability of clinoptilolite to withstand ion exchange modifications without losing its basic crystalline structure, which supports its use in water treatment applications.

Infrared (IR) spectroscopy

Infrared (IR) spectra of both natural and modified Clinoptilolite zeolite samples were obtained to evaluate structural changes and the presence of key functional groups. In the range 4000-3000 cm⁻¹, a broad band is observed in all samples, corresponding to the stretching vibrations of the -OH groups, which is characteristic of the presence of water in the zeolitic structure, an inherent feature of zeolitic materials due to their hydrated structure. The bands around 1650 cm⁻¹ are associated with the bending vibrations of adsorbed water, evidencing the ability of clinoptilolite to retain water even after modifications.

In the case of the NaCl and KCl treated samples, slight variations in the band intensities will be observed in the 1000-450 cm⁻¹ range, especially in the peaks around 1020 cm⁻¹, which correspond to the asymmetric stretching vibrations of the Si-O and Al-O bonds in the Clinoptilolite structure. This suggests that, although the basic crystal structure of the zeolite is maintained, the ion exchange process generates slight modifications in the chemical environment of the Si-O-Al groups due to cation substitution at the exchange sites.

The bands between 600 and 450 cm⁻¹, related to the bending vibrations of SiO₄ and AlO₄ tetrahedra, show subtle changes in the treated samples, which could indicate modifications in the cation exchange sites due to the introduction of Na⁺ and K⁺ ions. According to previous studies, these changes in the intensities of the IR bands may be associated with an increased affinity of the modified clinoptilolite for the adsorption of certain metal ions, due to alterations in the electric field generated by the exchanged cations (Hao et al., 2018; Mamba, 2010).

Box 2

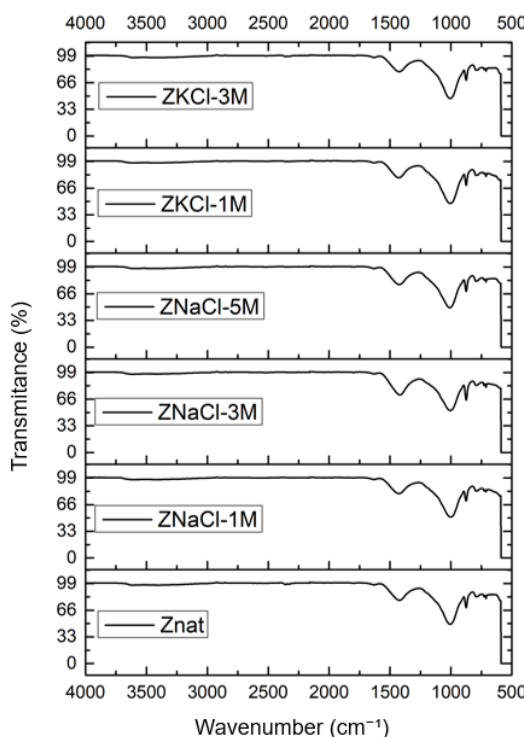


Figure 2

FTIR spectra of zeolite type Clinoptilolite, natural and treated with NaCl (1M, 3M and 5M) and KCl (1 and 3M.).

Source [Prepared by the author]

These results confirm the structural stability of clinoptilolite after treatment with NaCl and KCl and suggest that these modifications may optimise its ion exchange capacity for water treatment applications by increasing the accessibility of active sites without compromising the integrity of the zeolitic structure.

Point of zero charge (PZC)

The determination of the point zero charge (PZC) was performed for natural and modified zeolite with sodium chloride (NaCl) and potassium chloride (KCl) at different concentrations. Figure 3 shows the results of initial pH vs. final pH for each sample, which allows the PZC of each sample to be identified. The PZC of the natural zeolite is found at pH 7.8, indicating that at this pH the net surface charge of the zeolite is neutral, an important characteristic for its ion exchange efficiency. In the case of zeolite modified with sodium chloride at a concentration of 1 M, the PZC decreases slightly to 7.4, suggesting that this modification may enhance the zeolite's ability to attract positive ions, such as calcium and magnesium, in a slightly lower pH range. This behaviour is consistent with the idea that ion exchange with Na⁺ can adjust the surface charge of zeolite, making it more receptive to specific cations in solution. By increasing the sodium chloride concentration to 3 M, the PZC increases slightly to 7.6. This change suggests that the higher NaCl concentration can partially compensate for the decrease in PZC observed at lower concentration, maintaining the effectiveness of the material for ion exchange applications. On the other hand, the zeolite modified with potassium chloride at a concentration of 1 M shows a PZC of 7.8, a value similar to that of the natural zeolite, indicating that modification with K⁺ does not significantly alter the surface charge of the zeolite compared to the natural zeolite.

Box 3

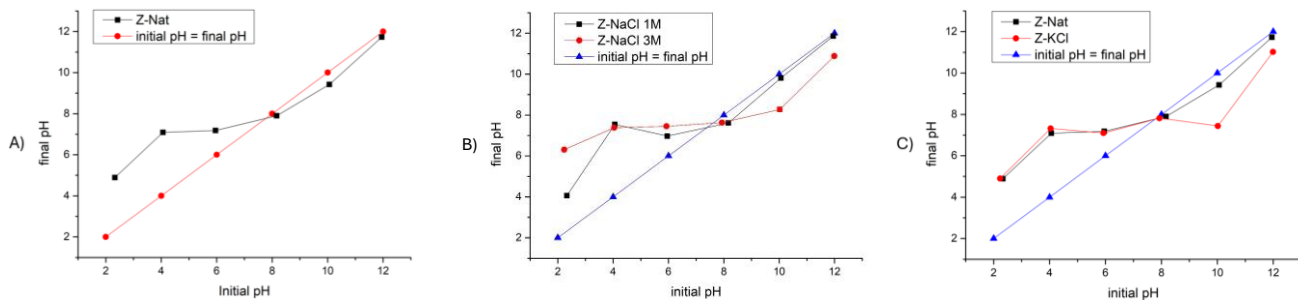


Figure 3

pHpzc of Clinoptilolite type zeolite: A) clean natural zeolite, B) zeolite treated with NaCl at 1M and 3M, C) zeolite treated with KCl at 1M and 3M compared to clean natural zeolite

Source [Own elaboration]

Evaluation of adsorption isotherms

Calcium and magnesium adsorption isotherms on natural zeolite show inconsistent results in terms of concentration variation between initial (C_i) and final (C_f) values after 24 hours of contact. At some concentrations, the final concentration of calcium and magnesium ions in solution is higher than the initial concentration, which is not an expected behaviour in an adsorption process. Additionally, it is observed that the initial concentrations of the solutions decrease after the waiting period, suggesting that the concentration values of the prepared solutions were altered during the adsorption time. This phenomenon could be related to the interaction of the zeolite with the solution, which could have caused an ionic exchange releasing calcium and magnesium from the zeolite matrix into the solution (Kordala & Wyszkowski, 2024). Alternatively, the high pH may have favoured processes of partial dissolution of impurities present in the zeolite or the formation of colloidal species that did not completely precipitate, thus contributing to an increase in the concentrations of these ions detected by atomic absorption spectroscopy (Kordala & Wyszkowski, 2024).

Box 4

Table 1

Concentration (ppm)	Isotherm of magnesium for natural zeolite	
	C_i (mg/L)	C_f (mg/L)
10	0.73	4.54
20	5.78	5.46
50	12.025	13.05
100	45.5	44.1
250	56.3	68.7
500	157.5	177.5
700	120.4	100.8
800	598.4	446
900	568.4	546
1000	714	433

Source [Own elaboration]

Box 5

Table 2

Concentration (ppm)	Isotherm de calcio para zeolita natural	
	C_i (mg/L)	C_f (mg/L)
10	5.19	4.22
20	12.79	16.36
50	26.32	30.05
100	59.94	74.66
250	126	163.5
500	284.2	344.9
700	405	376.8
800	500.2	512.3
900	567.1	579
1000	681.5	752

Source [Own elaboration]

Calcium and magnesium concentrations in the collected water samples show relatively low hardness values (Table 3). This low concentration could be related to the influence of pH in the samples, as they present pH values around 7 and 8, which could be promoting the sedimentation of calcium and magnesium ions in the form of precipitates, thus reducing the measurable concentrations of these ions in the water (Neal & Stanger, 1984; Yan et al., 2020). This phenomenon suggests that the atomic absorption equipment is not capturing the total hardness of the samples due to the sedimentation of the hardness ions under basic pH conditions (Neal & Stanger, 1984; Yan et al., 2020).

Box 6

Table 3

Place	Calcium and magnesium concentration in water samples	
	Conc. De Ca (mg/L)	Conc. De Mg (mg/L)
Champotón	39.15	26.1
Chekubul	15.18	13.02
Aguada Island	14.16	4.71
Merida City	16.5	7.65
Frontera	31.53	22.29
Hecelchakán	35.94	18.42

Source [Own elaboration]

Conclusions

In this study, the adsorption capacity of Clinoptilolite zeolite, both in its natural and modified form, was evaluated for the removal of calcium and magnesium ions under specific concentration and pH conditions. The results indicate that natural and modified zeolite with sodium chloride and potassium chloride show a tendency to reduce the concentration of these ions in solution, although with some inconsistencies attributed to the effect of pH on the adsorption process. The relationship between the point zero charge (PZC) of the zeolite and the pH of the solution was decisive: when the pH of the solution exceeds the PZC of the zeolite (approximately pH 7.8), the surface of the zeolite acquires a negative charge that favours the adsorption of the hardness ions. However, at higher pH, precipitation of the ions in the form of insoluble compounds becomes a relevant factor, affecting the accuracy of concentration measurements by atomic absorption spectroscopy.

The sedimentation of calcium and magnesium ions, both in the solutions prepared for the isotherms and in the water samples collected, represents a challenge for obtaining reliable hardness measurements. These results suggest that pH control is a critical factor in future studies of hardness ion adsorption on zeolites. Adjusting the pH of solutions or implementing complementary techniques to quantify total hardness in the presence of precipitates could improve the accuracy and reliability of measurements. In conclusion, although clinoptilolite presents considerable potential for the treatment of hardness in water, the results of this study highlight the need to optimise the experimental conditions, especially with regard to pH control and knowledge of the zeolite PZC, to ensure effective adsorption and accurate measurement of hardness ions in solution. Future studies should focus on optimising these variables and evaluating the zeolite's efficacy under varying environmental conditions in order to maximise its applicability in water treatment systems.

Declarations

Conflict of interest

The authors declare that they have no conflicts of interest. They have no financial interests or personal relationships that could have influenced this book.

Authors' contribution

Gutiérrez-Laffon, Yazmin Michelle: Drafting, data analysis, figure development
Anguebes-Franceschi, Francisco: General revision
Abatal, Mohamed: Editorial revision, review of results and proofreading.
Aguilar-Ucán, Claudia Alejandra: General revision.

Availability of data and materials

The information contained in this document is not available, as data are still being worked on.

Funding

National Grants for Postgraduate Studies 2023-2.

Acknowledgements

G. L. Yazmín Michelle extends her sincere thanks to co-authors Dr. Francisco Anguebes Franseschi and Dr. Claudia Alejandra Aguilar Ucán for their invaluable support during the development of the project. He also expresses his deep appreciation to Dr. Mohamed Abatal, not only for his guidance in the development of this research, but also for providing access to the materials, reagents and equipment of the ‘Advanced Materials Research Laboratory’.

Special thanks to Dr. Juan Gabriel Flores Trujillo for providing the sieves necessary to establish the zeolite size, and to Dr. Sandra Jazmín Figueroa Ramírez for the loan of the pH measurement equipment, essential tools for the success of the project.

Finally, thanks are due to the National Council of Science and Technology (CONACYT) for the national scholarship granted, without which it would not have been possible to study the Master's Degree in Materials and Energy Engineering (MIME) at the Faculty of Engineering of the Autonomous University of Carmen (UNACAR). The MIME committee is also acknowledged for their constant support and guidance during the development of this research.

Abbreviations

DRX	X-ray diffraction
FTIR	Infrared spectroscopy
PZC	Zero point charge
RCF	Relative centrifugal force

References

Background

Strathmann, H. (2012). *Membrane Separation Processes*, 3. *Membrane Preparation and Membrane Module Constructions*. In *Ullmann's Encyclopedia of Industrial Chemistry* (Vol. 22, pp. 483–512). Wiley-VCH Verlag GmbH & Co. KGaA.

Wang, Z. (2024). *Reverse osmosis*. In *Fundamentals of Membrane Separation Technology* (pp. 241–412). Elsevier.

World Health Organization. (2022). *Guidelines for drinking-water quality: Fourth edition incorporating the first and second addendaquality*.

Basics

Krstić, V. (2021). *Papel del adsorbente de zeolita en el tratamiento de aguas*. En *Handbook of Nanomaterials for Wastewater Treatment: Fundamentals and Scale up Issues* (pp. 417-481). Elsevier.

Support

Doula, M. K. (2006). *Removal of Mn²⁺ ions from drinking water by using Clinoptilolite and a Clinoptilolite–Fe oxide system*. *Water Research*, 40(17), 3167–3176.

- Hao, X., Hu, H., Li, Z., Wu, L., Liu, X., & Zhang, Y. (2018). Adsorption properties of modified clinoptilolite for methane and nitrogen. *Materials*, 11(10).
- Kordala, N., & Wyszkowski, M. (2024). *Zeolite Properties, Methods of Synthesis, and Selected Applications*. In *Molecules* (Vol. 29, Issue 5). Multidisciplinary Digital Publishing Institute (MDPI).
- Mamba, B. & N. D. & M.-B. A. (2010). The effect of conditioning with NaCl, KCl and HCl on the performance of natural clinoptilolite's removal efficiency of Cu²⁺ and Co²⁺ from Co/Cu synthetic solutions. *Water SA*, 36(4).
- Neal, C., & Stanger, G. (1984). Calcium and magnesium hydroxide precipitation from alkaline groundwaters in Oman, and their significance to the process of serpentinization. In *MINERALOGICAL MAGAZINE* (Vol. 48).
- Restiawaty, E., Gozali, V. A., Wibisono, T. A. S. E., & Budhi, Y. W. (2024). Utilizing modified clinoptilolite for the adsorption of heavy metal ions in acid mine drainage. *Case Studies in Chemical and Environmental Engineering*, 9.
- Yan, H., Han, Z., Zhao, H., Pan, J., Zhao, Y., Tucker, M. E., Zhou, J., Yan, X., Yang, H., & Fan, D. (2020). The bio-precipitation of calcium and magnesium ions by free and immobilized *Lysinibacillus fusiformis* DB1-3 in the wastewater. *Journal of Cleaner Production*, 252.

Evaluation of the potential for bioenergy production from coyol fruit by anaerobic digestion

Evaluación del potencial de producción de bioenergía a partir del fruto de coyol por digestión anaerobia

Aguilar-Aguilar, Fidel A.*^a, Mena-Cervantes, Violeta Y.^b, Ramírez-Estrada, Alejandro^c and Hernández-Altamirano, Raúl^d

^a Instituto Politécnico Nacional • LSL-8901-2024 • 0000-0003-3021-1186 • 402762

^b Instituto Politécnico Nacional • AFN-6089-2022 • 0000-0002-4403-8671 • 170728

^c Instituto Politécnico Nacional • 0000-0001-6570-9203 • 563734

^d Instituto Politécnico Nacional • JGR-7510-2023 • 0000-0001-6685-2335 • 131289

CONAHCYT classification:

DOI: <https://doi.org/10.35429/H.2024.13.21.33>

Area: Biotechnology and Agricultural Sciences

Field: Agricultural biotechnology

Discipline: Agricultural biotechnology

Subdiscipline: Others

Key Handbooks

This research contributes to the field of renewable bioenergy by demonstrating the potential of coyol fruit (*Acrocomia aculeata*) as a feedstock for biogas production by anaerobic digestion. It provides data on the efficiency of different components (peel, pulp and seed) and their combinations, highlighting the importance of C/N ratio and volatile solids (VS) content in optimising methane production. This study suggests co-digestion strategies and the use of pre-treatments to improve the biodegradability of lignocellulosic components. The research highlights the importance of characterising biomass components, understanding their C/N ratios and the need for pre-treatments to maximise biogas production. These findings can be applied to other agricultural residues and promote the diversification of sustainable energy sources.

Citation: Aguilar-Aguilar, Fidel A., Mena-Cervantes, Violeta Y., Ramírez-Estrada, Alejandro and Hernández-Altamirano, Raúl. 2024. Evaluation of the potential for bioenergy production from coyol fruit by anaerobic digestion. 21-33. ECORFAN.

*✉ [rhaltamirano@gmail.com]

Handbook shelf URL: <https://www.ecorfan.org/handbooks.php>



ISBN 978-607-8948-51-2 ©2009 The Authors. Published by ECORFAN-Mexico, S.C. for its Holding Mexico on behalf of Handbook HRPG. This is an open access chapter under the CC BY-NC-ND license [<http://creativecommons.org/licenses/by-nc-nd/4.0/>]

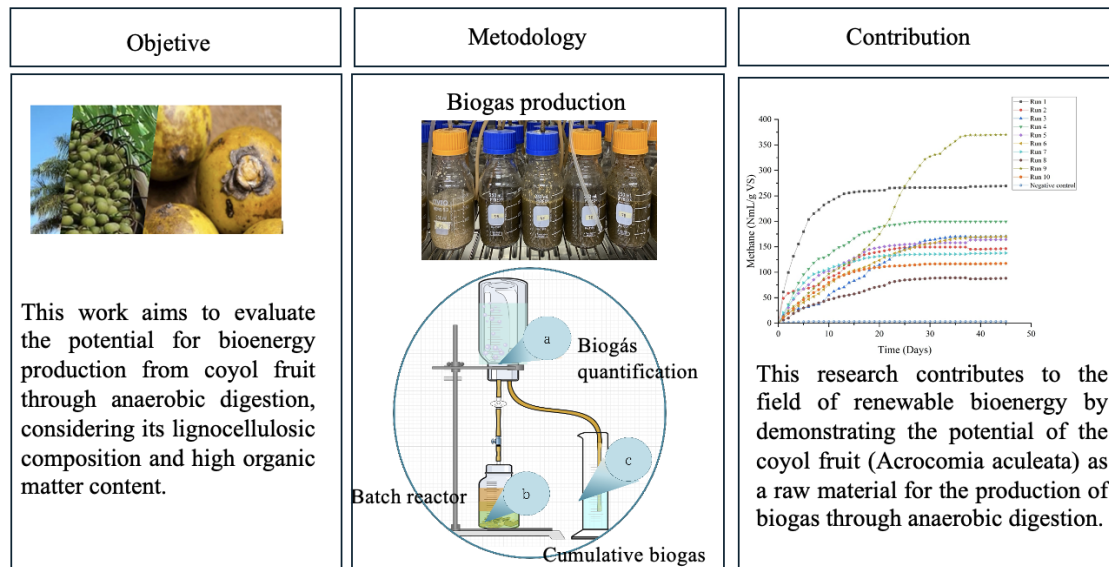
Peer Review under the responsibility of the Scientific Committee MARVID®- in contribution to the scientific, technological and innovation Peer Review Process by training Human Resources for the continuity in the Critical Analysis of International Research.



1702902 CONAHCYT

Abstract

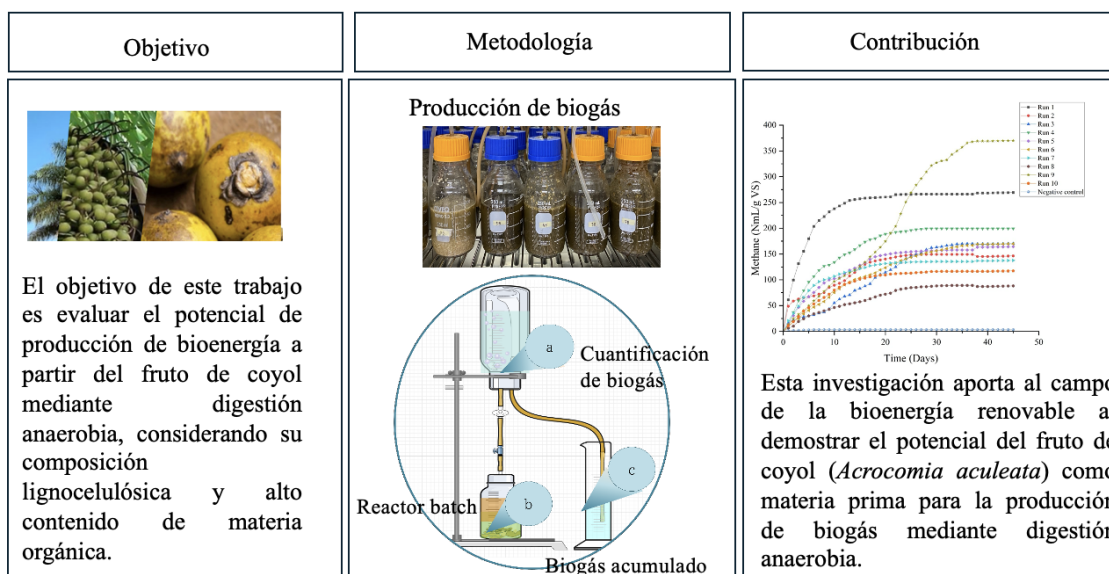
This study aimed to evaluate the biogas production potential from coyol fruit (*Acrocomia aculeata*) through anaerobic digestion. Combinations of peel, pulp and seed were used, processed in batch reactors with a constant mass of 5 g of volatile solids (SV). The tests were carried out at 37°C for 50 days, evaluating biomethane production. The results showed that run 9, composed of 66.67% peel, 16.67% pulp and 16.67% seed, achieved the highest methane production with 350 NmL/g VS, with the seed standing out as the most efficient component due to its high SV/ST ratio and a C/N of 24.40. Therefore, adequate proportions of the components maximize biogas production, and the use of pretreatments to improve peel degradation is suggested. These findings underscore the viability of coyol as a sustainable bioenergy source.



Anaerobic digestion, Bioenergy, Methane production, Lignocellulosic components, Sustainable energy

Resumen

El objetivo de este estudio fue evaluar el potencial de producción de biogás a partir del fruto de coyol (*Acrocomia aculeata*) mediante digestión anaerobia. Se utilizaron combinaciones de cáscara, pulpa y semilla, procesadas en reactores batch con una masa constante de 5 g de sólidos volátiles (SV). Las pruebas se realizaron a 37°C durante 50 días, evaluando la producción de biometano. Los resultados mostraron que la corrida 9, compuesta por 66.67% de cáscara, 16.67% de pulpa y 16.67% de semilla, alcanzó la mayor producción de metano con 350 NmL/g VS, destacando la semilla como el componente más eficiente por su alta relación SV/ST y una C/N de 24.40. Por lo tanto, proporciones adecuadas de los componentes maximizan la producción de biogás, y se sugiere el uso de pretratamientos para mejorar la degradación de la cáscara. Estos hallazgos subrayan la viabilidad del coyol como fuente de bioenergía sostenible.



Digestión anaerobia, Bioenergía, Producción de metano, Componentes lignocelulósicos, Energía sostenible

Introduction

Global dependence on fossil fuels has had significant impacts on both the environment and the global economy (Drosg et al., 2013; Patinvoh et al., 2017). In particular, the combustion of these resources has significantly increased greenhouse gas emissions, directly contributing to climate change, ocean acidification and air pollution (Abatzoglou & Boivin, 2009). Consequently, the search for sustainable and renewable alternatives has emerged as a key priority within global energy policies. In this context, bioenergy is positioned as a viable solution that not only promotes carbon footprint reduction, but also allows harnessing renewable resources efficiently (Horváth et al., 2016; Parsaee et al., 2019, Fang et al. 2024).

Among the various forms of bioenergy, biogas has gained prominence due to its ability to mitigate pollution while providing energy in a cost-effective and sustainable manner. This gas, derived from the anaerobic digestion of organic matter, is mainly composed of methane (CH_4) and carbon dioxide (CO_2), and is widely used to generate heat, electricity or as a vehicle fuel (Abatzoglou & Boivin, 2009; Castellanos-Sánchez et al., 2023; Hung et al., 2017). In contrast to fossil fuels, biogas production promotes a circular economy model by valorising organic waste, which reduces environmental impact and favours sustainable waste management (Hijazi et al., 2016; Sarker et al., 2019, Kwakye et al., 2024).

Furthermore, one of the main advantages of biogas is its low cost compared to other renewable energy sources. Anaerobic digestion plants can be designed to suit various scales, from domestic systems to large capacity industrial facilities. On the other hand, the use of agro-industrial waste as feedstock not only contributes to sustainability, but also fosters the development of rural communities by decreasing their dependence on non-renewable resources (Horváth et al., 2016; Matheri et al., 2017; Parsaee et al., 2019; Sarker et al., 2019).

In this framework, the coyol (*Acrocomia aculeata*) presents itself as a promising option for biogas production. This fruit, native to tropical and subtropical regions, is abundant in Mexico, where currently only a small fraction is used in the production of sweets and artisanal products, while a significant part remains underutilised (F. A. Aguilar-Aguilar et al., 2024; Balick, 1990, César et al., 2015, Magne et al. 2024)). Therefore, anaerobic digestion of coyol not only offers an avenue to harness this underutilised resource, but also contributes to efficient waste management and the development of sustainable circular economy models (Plath et al., 2016). These factors highlight the potential of coyol as an efficient and sustainable feedstock for bioenergy generation.

Objective

The present study aims to evaluate the potential of coyol fruit (*Acrocomia aculeata*) as a feedstock for bioenergy production through anaerobic digestion. This analysis focuses on its lignocellulosic composition and high organic matter content, characteristics that position it as a resource with high energy viability. In particular, the study seeks to demonstrate that coyol can become an efficient source for biogas production, highlighting its comparative advantage over other techniques and substrates used in this process. The central hypothesis postulates that anaerobic digestion of coyol will offer a competitive methane yield against other agricultural residues, thanks to its richness in carbohydrates and lipids, which promotes an efficient conversion of biomass into biogas.

Hypothesis

The main problem identified in this study is the wasteful use of underutilised plant resources with high energy potential. In this context, the transformation of coyol fruit (*Acrocomia aculeata*) into biogas represents a sustainable solution, as it allows the valorisation of a widely available resource while reducing the accumulation of organic waste in local communities. By addressing this challenge, the present work contributes significantly to the diversification of bioenergy sources, promoting an energy model based on sustainability. This approach aims to minimise dependence on fossil fuels and promote cleaner and more environmentally friendly energy development.

Methodology

Obtaining raw material

The coyol fruit (*Acrocomia aculeata*) used in this study was collected in the region of Copainalá, Chiapas. For the experiments, 5 kg of raw material was prepared and separated into its three main components: peel, pulp and seed. Each of these fractions was crushed using a hammer mill to reduce the particle size, which facilitated subsequent analyses and ensured the homogeneity of the material. Subsequently, the shredded material was stored at a controlled temperature of 4°C to preserve its physico-chemical properties before being used in the biochemical potential methane (PBM) tests.

The inoculum used in the anaerobic digestion experiments was obtained from an 8 m³ capacity biodigester, regularly fed with bovine manure. This biodigester generates approximately 3.5 m³ of biogas per day, with an average methane content of 60.5%. These conditions ensure the presence of an active and adequate microbial community to carry out the anaerobic digestion processes efficiently.

TS and TSS analysis

The analysis of total solids (TS) and volatile solids (VS) in coyol pulp, peel and seed was performed following the methodology described in the Standard Methods for the Examination of Water and Wastewater (2540 Solids), 22nd Edition, 2012, published by the American Public Health Association (APHA).

For each sample, approximately 2 grams of material were dried at 105°C to constant weight in order to determine the STs. Subsequently, the dried samples were incinerated at 550°C in a muffle furnace to measure the SVs, which represent the fraction of organic material present in the samples.

Total solids (TS) were calculated using the following equation [1]:

$$ST (\%) = \frac{\text{Weight of dry sample at } 105^\circ\text{C (g)}}{\text{Weight of wet sample (g)}} \times 100 \quad [1]$$

Volatile solids (VS) were calculated using the following equation [2]:

$$SV (\%) = \frac{\text{Weight of the sample after } 550^\circ\text{C (g)}}{\text{Weight of dry sample at } 105^\circ\text{C (g)}} \times 100 \quad [2]$$

These formulae allow the quantification of total and volatile solids in each sample. The SVs provide an estimate of the organic fraction of the biomass that is available for biodegradation during the anaerobic digestion process.

TGA and DTG analysis

The characterisation of coyol (*Acrocomia aculeata*) fruit components - peel, pulp and seed - was performed by thermogravimetric analysis (TGA) and thermogravimetric derivative analysis (TGA) to evaluate their thermal stability and decomposition behaviour. The samples, previously crushed and dried, were pulverised and sieved to obtain a uniform particle size between 100 and 200 µm, ensuring the necessary homogeneity for the analyses (Ramírez-Estrada et al., 2022).

The experiments were carried out using thermogravimetric analysis equipment coupled to a thermogravimetric derivatization system, which allowed obtaining accurate data on mass loss and the different stages of thermal decomposition of each component. The temperature range used was from 25°C to 800°C, with a constant heating rate of 10°C/min, thus ensuring a uniform and controlled decomposition process. To prevent oxidation of the samples during the analysis, a nitrogen atmosphere with a constant flow rate of 50 mL/min was used. The results obtained were fundamental to identify the decomposition onset temperatures, thermal degradation stages and respective mass losses of the lignocellulosic components of the coyol. This information is key to understanding the thermal stability of the husk, pulp and seed, and contributes significantly to the assessment of their potential for energy applications. Furthermore, the findings support the optimisation of techniques for the use of coyol fruit in the production of bioproducts and biofuels, highlighting its versatility in energy conversion processes.

Elemental analysis

Elemental analysis was carried out to determine the carbon (C), hydrogen (H), nitrogen (N) and sulphur (S) contents of the coyol fruit components: pulp, peel and seed. The main objective was to quantify the elemental composition of each fraction and to evaluate their suitability as substrates in anaerobic digestion processes. For this analysis, a CHNS/O elemental analyser (Thermos) was used, which guarantees accurate and reproducible measurements.

Approximately 2 mg of each sample were weighed and placed in tin capsules, which were combusted at 925°C in a pure oxygen environment, thus ensuring complete combustion of the materials. During this process, the elements present in the samples were transformed into gases: CO₂ (carbon), H₂O (hydrogen), NO_x (nitrogen) and SO₂ (sulphur). These gases were transported by a continuous flow of helium through specific chemical traps, and their concentrations were measured with a thermal conductivity detector.

To ensure the accuracy of the analysis, the instrument was calibrated using methionine as a standard reference material. The results obtained were reported as percentages based on the total mass of each sample, providing detailed information on the chemical characteristics of the pulp, peel and seed. This analysis is key to understand the behaviour of each component in the anaerobic digestion process and to optimise methane production by identifying suitable mixtures and treatments to maximise their bioenergy yield.

Batch reactors

To evaluate the impact of different proportions of coyol pulp, seed and peel on biogas production, a mixture-based experimental design was used. This approach allowed to analyse the behaviour of anaerobic digestion by varying the proportions of the three components, maintaining a constant total mass of 5 g volatile solids (VS) per reactor in batch trials ([F. Aguilar-Aguilar et al., 2023a](#)).

Ten different combinations of pulp, seed and peel were designed and carried out, as detailed in Table 1. In each experiment, the sum of the percentages of the components was always equal to 100%, ensuring consistency in the tests and validity of the results obtained. This experimental design made it possible to identify the optimal proportions of coyol components to maximise biogas production and to understand their influence on the efficiency of the anaerobic digestion process.

Box 1

Table 1

Experimental tests of biogas production using different combinations of coyol components

Trials	pulp (%)	Seed (%)	Mask (%)
1	1	0	0
2	0	100	0
3	0	0	100
4	50	50	0
5	50	0	50
6	0	50	50
7	66.67	16.67	16.67
8	16.67	66.67	16.67
9	16.67	16.67	66.67
10	33.33	33.33	33.33

Source: Own elaboration

The experiments were carried out in 250 mL glass bottles sealed with rubber stoppers, thus ensuring fully anaerobic conditions. These bottles were selected for their ability to maintain the experimental conditions and to facilitate both collection and quantification of the biogas produced. A total of 10 reactors were set up in batches, each containing a specific combination of coyol peel, pulp and seed, following the proportions set out in Table 1. The substrate-to-inoculum (S/I) ratio used was 1:1, with 5 g volatile solids (VS) of substrate or mixture and an equivalent amount of inoculum ([F. Aguilar-Aguilar et al., 2023a](#)).

Each reactor was inoculated with 18 mL of inoculum, equivalent to 5 g of SV, and substrates were added according to the defined proportions. To ensure adequate nutrient supply to the microbial consortia, a specific macro- and micronutrient solution was added to each reactor. Macronutrients added included NH₄Cl (1112.0 mg/L), (NH₄)H₂PO₄ (132.5 mg/L), (NH₄)₂HPO₄ (44.5 mg/L), MgCl₂-6H₂O (250.0 mg/L), CaCl₂-2H₂O (189.0 mg/L) and NaHCO₃ (2500.0 mg/L). Micronutrients added were FeCl₃-6H₂O (5.0 mg/L), ZnCl₂ (0.13 mg/L), MnCl₂-4H₂O (1.25 mg/L), (NH₄)₆Mo₇O₂₄-4H₂O (1.6 mg/L), AlCl₃-6H₂O (0.13 mg/L), CoCl₂-6H₂O (5.0 mg/L), NiCl₂-6H₂O (13.0 mg/L), H₃BO₃ (3.0 mg/L), CuCl₂-2H₂O (8.0 mg/L) and HCl (1.0 mg/L) (F. Aguilar-Aguilar et al., 2023b).

To ensure a fully anaerobic environment, air was removed from the headspace of the reactors using a 60 mL syringe. The reactors were maintained at a controlled temperature of 37 ± 3°C in a Memmert oven (model D91126) and incubated for a period of 50 days, or until biogas production stopped. The initial pH of the reactors was adjusted to 7.5 using a 40 g/L buffer solution, ensuring that it remained within the optimal range of 6.5 to 7.5 for anaerobic digestion processes.

Biogas quantification

The biogas volume measurement system used in this study was an adaptation of the method described by Aguilar-Aguilar et al. (F. Aguilar-Aguilar et al., 2023a). This system consisted of an inverted 1000 mL flask (a), containing a 5% HCl solution. The function of this solution was to facilitate the quantification of the total biogas produced in each anaerobic reactor. The flask was modified with a lid that included two orifices: one for the inlet of the gas coming from the anaerobic reactor (b) and one for the outlet of the liquid displaced by the gas, which was collected in a graduated cylinder (c).

Measurements were carried out every 24 hours, starting from the first day of incubation, using the liquid displacement method. The volume of liquid displaced by the biogas was collected in a graduated cylinder, and this volume was converted to standard conditions of pressure and temperature (NmL) - 1 atm and 0°C - by applying the Ideal Gas Law. This approach allowed to obtain accurate and consistent measurements of the volume of biogas produced in the experimental trials.

Box 2

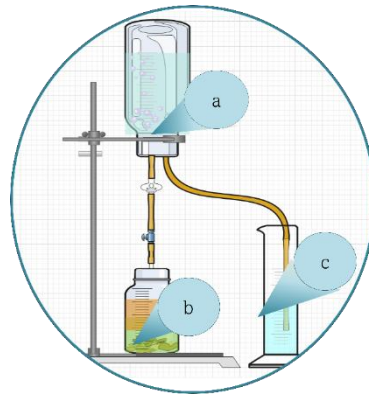


Figure 1

Schematic of the liquid displacement biogas measurement system. (a) 1000 mL inverted flask with 5% HCl solution, (b) anaerobic reactor where biogas is produced, (c) graduated cylinder for collection of the displaced liquid, used to calculate the volume of biogas produced

Source: Own elaboration

Results

Physicochemical characterisation of coyol

Anaerobic digestion occurs in four main stages: hydrolysis, acidogenesis, acetogenesis and methanogenesis. Understanding the composition of the substrate is essential, as it significantly influences microbial metabolism and, consequently, the efficiency of biogas production. Physicochemical characterisation of coyol fruit peel, pulp and seed allows the assessment of critical parameters such as dry matter (DM), volatile solids (VS), VS/TS ratio, chemical oxygen demand (COD) and pH (Aworanti et al., 2023; Browne & Murphy, 2013; Codignole Luz et al., 2018).

Table 2 presents the physicochemical composition of coyol fruit components. All of them show a VS content higher than 85% with respect to TS, indicating a good potential for biogas production. Previous studies suggest that a VS/TS content above 50% in organic substrates is a positive indicator of high biodegradability, which favours their utilisation in anaerobic digestion (Labatut et al., 2011).

Of the three components, seed stands out with the highest VS/TS ratio (93.44%) and a COD of 233.1 g/kg, which makes it an excellent substrate for biogas production. However, its high protein and oil content may pose a risk of inhibition due to ammonia accumulation and excess oils. The pulp, with a VS/TS ratio of 91.85% and a COD of 183.4 g/kg, presents an adequate balance, with a high availability of sugars that facilitates conversion to methane during anaerobic digestion. On the other hand, the husk, although it has a lower VS/TS content (88.508%) and a COD of 147.2 g/kg, is rich in lignocellulosic material. This characteristic may limit its biodegradability under natural conditions; however, specific pre-treatments can enhance the release of fermentable sugars and increase its potential for biogas production (Sarker et al., 2019).

The carbon-to-nitrogen (C/N) ratio, presented in Table 3, is another key factor for anaerobic digestion, as it affects the nutritional balance necessary for efficient microbial activity. Coyol components show significant variability in this ratio. The shell has a very high C/N ratio (241.47), reflecting a high carbon and low nitrogen content, which could limit its biodegradability without the addition of complementary nitrogen sources. Pulp, with a C/N ratio of 62.67, presents a better balance, although it may require additional nutrient adjustments. Seed, on the other hand, has a C/N ratio of 24.40, which is within the optimal range of 20-30 for anaerobic digestion, positioning it as a promising main substrate for biogas production. These differences underline the need to employ appropriate blends or co-digestion with other materials to maximise the efficiency of the process (Drosg et al., 2013; Kafle et al., 2013; Obata et al., 2020).

Box 3

Table 2

Physicochemical composition of coyol fruit components

Components	ST (g/kg)	SS (g/kg)	SV/ST	DQO (g/kg)	Relation C/N
Peel	963.3	852.6	88.508	147.2	241.47
Pulp	957.0	879.0	91.85	183.4	62.67
Seed	981.5	917.1	93.439	233.1	24.40

ST: Total Solids, SV: Volatile Solids, COD: Chemical Oxygen Demand

Source: Own elaboration

Thermogravimetric Analysis

Thermogravimetric analysis (TGA) and thermogravimetric derivative (TGD) of the coyol fruit components - peel, pulp and seed - together with the inoculum, allowed to evaluate their thermal behaviour and stability during decomposition (Figure 2). The TGA plots show how the mass loss of the different components occurs in well-defined stages as the temperature increases up to 800°C.

The shell, depicted in Figure 2, exhibits a significant mass loss in the temperature range of 200°C to 350°C, mainly attributed to the decomposition of hemicellulose and cellulose. A second stage of loss, at temperatures above 500°C, is related to the degradation of more recalcitrant lignocellulosic compounds (Apaydin Varol & Mutlu, 2023; Burhenne et al., 2013).

Pulp, on the other hand, exhibits similar behaviour, although its initial mass loss occurs at slightly lower temperatures, indicating a higher proportion of volatile compounds and easily degradable sugars. This is consistent with its composition rich in simple carbohydrates and its lower lignin content compared to the husk (Coura et al., 2023; Del Río et al., 2016).

In the case of the seed, the highest mass loss is observed in the initial stage (200°C to 350°C), reflecting a significant content of organic compounds such as oils and proteins, which are thermally more labile. A second stage of decomposition, between 450°C and 600°C, is attributed to the degradation of more resistant lipids and proteins (Alpandi et al., 2022; Berton et al., 2013).

On the other hand, the inoculum exhibits a more moderate and stable degradation curve, suggesting a complex composition of organic and microbial material that gradually decomposes over a wide temperature range. The DTG plots (Figure 2B) highlight more pronounced maximum degradation peaks for the seed compared to the shell and pulp, confirming its higher content of readily degradable organic compounds.

Comparatively, TGA and DTG results indicate that the seed has the highest energy potential due to its high organic matter content and its rapid decomposition in the early stages of heating. The shell, with high thermal stability and higher resistance to decomposition, may require pre-treatments to improve its biodegradability. Pulp, on the other hand, shows a balance between thermal stability and decomposition, which makes it suitable for anaerobic digestion processes without significant modifications.

Box 4

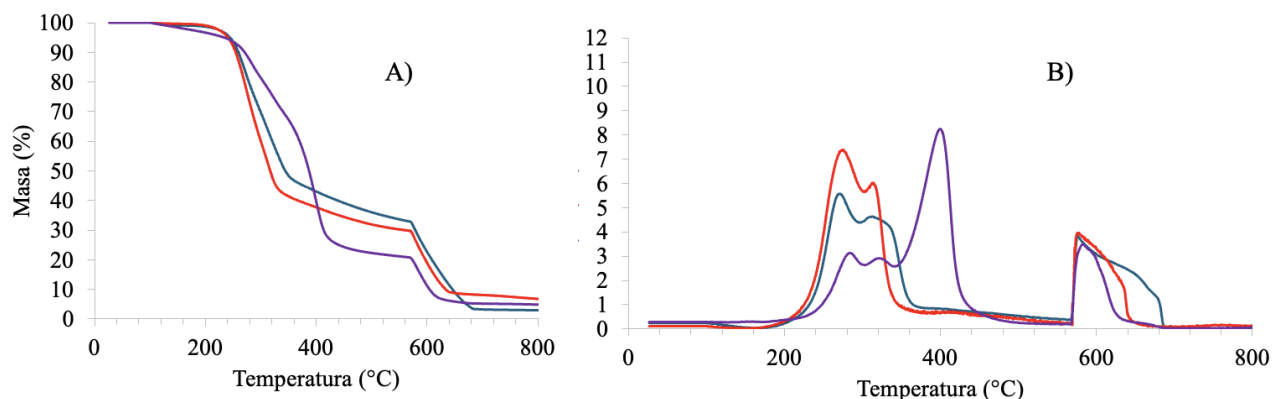


Figure 2

Analysis of A) TGA and B) DTG of coyol and inoculum components used as feedstock for biogas production

Source: *Own elaboration*

Biomethane production kinetics

The kinetics of biomethane production observed in the different experimental trials reveals a significant variation in methane yield, influenced by the proportions of the coyol fruit components (peel, pulp and seed). According to the graph presented, the trial corresponding to run 9, consisting of a mixture of 16.66% pulp, 16.66% seed and 66.66% peel, achieved the highest cumulative methane yield, approximately 350 NmL/g VS (Figure 3). This result indicates that the specific combination of these components favours an optimal environment for methanogenic microbial activity, possibly due to a proper nutrient balance and a favourable C/N ratio ([Cazaudehore et al., 2022](#); [Obata et al., 2020](#)).

In contrast, run 1 (Figure 3), composed of 100% mesocarp (pulp), showed a rapid initial behaviour in biomethane production, stabilising at around 250 NmL/g VS. This suggests that, although the pulp contains readily biodegradable sugars, it may lack other essential nutrients to sustain prolonged methane production without the addition of complementary components.

The trials corresponding to runs 3, 5 and 7 showed more moderate yields of around 150-200 NmL/g VS. This yield can be attributed to the predominant lignocellulosic content in the epicarp (peel), which requires more time and, in some cases, pre-treatment to achieve complete biodegradation. These results are consistent with the high lignocellulosic composition and high C/N ratio of the peel, factors that limit its direct conversion to biomethane ([Brayan Alexis et al., 2015](#); [Morais et al., 2021](#)).

Co-digestion with other nitrogen-rich waste sources could balance the C/N ratio in mixtures with high peel content, further enhancing methane production and avoiding possible inhibitions ([Su et al., 2024](#)). The negative control showed no methane production, confirming the absence of significant biological activity under substrate-free conditions. These findings highlight the importance of specific ratios of coyol components to optimise biomethane production, as well as the potential benefit of combining nutrient-rich components with those of high biodegradability.

Box 5

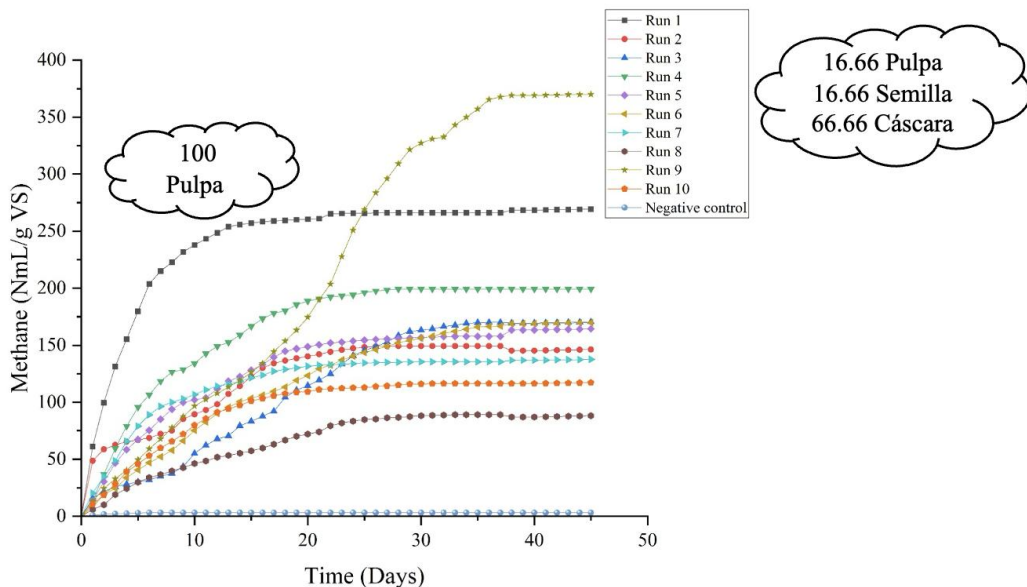


Figure 3

Kinetics of biomethane production from the mixture of coyol components

Source: Own elaboration

Energy recovered

The energy recovered from the different experimental runs showed significant variations, directly related to the proportions of pulp, seed and husk used in each mixture (Table 3). The values of total energy and energy in the form of methane (measured in megajoules, MJ) show the potential of each substrate for biogas production and its application as a renewable energy source.

Among the most outstanding results, run 9 presented the highest energy yield, with a total energy of 32,449.08 MJ, of which 18,637.46 MJ were recovered as methane. This run used a mixture composed mostly of husk (66.67%) and smaller proportions of pulp and seed (16.67% each) (Table 3). This result is particularly relevant from an industrial point of view, where maximising energy yield is a priority (Castellanos-Sánchez et al., 2023; Patinvoh et al., 2017).

In contrast, run 1, which used 100% pulp, managed to recover 25,108.42 MJ of total energy, of which 13,558.55 MJ corresponded to energy in the form of methane (Table 3). Although its yield was lower compared to run 9, the results highlight the contribution of readily biodegradable carbohydrates from the pulp in the anaerobic digestion process.

In practical terms, the energy recovered in these runs has great potential for applications such as heating, electricity generation or as fuel for gas-fuelled internal combustion engines (Abatzoglou & Boivin, 2009; Baena-Moreno et al., 2019; Castellanos-Sánchez et al., 2023). For example, the 18,637.46 MJ of methane generated in run 9 is equivalent to approximately 517 litres of gasoline, considering that 1 litre of gasoline produces about 36 MJ of energy. Similarly, this amount of energy could substitute the use of firewood in rural communities; given that 1 kilogram of firewood produces about 15 MJ of energy, the 18,637.46 MJ would be equivalent to about 1,242 kg of firewood (Abatzoglou & Boivin, 2009; Patinvoh et al., 2017; Torrijos, 2016).

These results highlight the potential of coyol fruit as a feedstock for renewable energy production, contributing to both energy transition and sustainable development in rural and industrial areas. For future research, it is recommended to explore multi-criteria analysis strategies to optimise biogas production and improve the sustainability of the processes (Liu et al., 2024).

Box 6

Table 3

Substrate composition and energy recovered in the different experimental runs

Race	pulp (%)	Seed (%)	Mask (%)	Biogas (MJ/ton)	Biomethane (MJ/Ton)
1	1	0	0	25108.42	13558.55
2	0	1	0	12838.58	7335.97
3	0	0	1	14560.00	8556.91
4	0.5	0.5	0	18988.67	10065.89
5	0.5	0	0.5	13907.83	8248.74
6	0	0.5	0.5	14355.25	8525.58
7	0.67	0.17	0.17	15341.08	6911.16
8	0.17	0.67	0.17	6552.00	4396.39
9	0.17	0.17	0.67	32449.08	18637.46
10	0.33	0.33	0.33	13111.58	5877.92

Source: Own elaboration

Conclusions

The present study confirmed that coyol fruit (*Acrocomia aculeata*) has significant potential for biogas production by anaerobic digestion. In particular, run 9 stood out as the highest yielding run, reaching approximately 350 NmL/g VS of accumulated methane. This mixture, composed of 66.67% husk, 16.67% pulp and 16.67% seed, showed that a proper balance between components with different C/N ratios and volatile solids (VS) contents is essential to optimise biomethane production. Seed, with its high SV/TS ratio (93.44%) and a C/N ratio close to the optimal range (24.40), proved to be a promising main substrate.

This work contributes to the knowledge on renewable bioenergy by validating the use of coyol as a feedstock for biogas production, positioning it as a viable alternative to diversify sustainable energy sources. Furthermore, the results underline the importance of selecting specific combinations of coyol components to maximise bioenergy yield and improve the efficiency of anaerobic digestion processes. For future research, it is recommended to explore the use of pre-treatments aimed at improving the biodegradability of the peel, due to its high lignocellulosic content. In addition, co-digestion with nitrogen-rich residues could balance the C/N ratio in mixtures with high husk content, enhancing methane production and minimising inhibition risks. The implementation of these adjustments will allow process optimisation and broaden the industrial applications of anaerobic digestion using coyol feedstock.

Declarations

Conflict of interest

The authors declare that they have no conflicts of interest. They have no financial interests or personal relationships that could have influenced this book.

Authors' contribution

Fidel A. Aguilar-Aguilar: Contributed to the conceptualisation and design of the study, development of the methodology, analysis of the data and drafting of the manuscript.

Violeta Y. Mena-Cervantes: Participated in the supervision of the project, critical analysis of the results and revision of the manuscript.

Alejandro Ramírez-Estrada: Collaborated in the performance of the laboratory experiments and in the collection and processing of experimental data.

Raúl Hernández-Altamirano: Contributed to the technical analysis of the results, validation of the data and technical and academic review of the final document.

Availability of data and materials

The data and materials used in this study are available.

Funding

No funding

Acknowledgements

We extend our sincere thanks to the National Laboratory for Biofuels Development and Quality Assurance (LaNDACBio) for providing access to their laboratory facilities, and to the National Council of Humanities, Sciences and Technologies (CONAHCyT) for their support.

Abbreviations

SV: Volatile Solids

ST: Total Solids

C/N: Carbon/Nitrogen Ratio

COD: Chemical Oxygen Demand

TGA: Thermogravimetric Analysis

DTG: Thermogravimetric Derivative

PBM: Biochemical Potential Methane

VS/ST: Ratio of Volatile Solids to Total Solids

NmL: Normalised Millilitres

References

Antecedents

- Abatzoglou, N., & Boivin, S. (2009). [A review of biogas purification processes](#). In Biofuels, Bioproducts and Biorefining (Vol. 3, Issue 1, pp. 42-71).
- Aguilar-Aguilar, F. A., Mena Cervantes, V. Y., García-Solares, S. M., & Hernández Altamirano, R. (2024). [Exploring the Biorefinery Potential of Acrocomia aculeata: A Native Mexican Palm for Sustainable Resource Valorization](#). Waste and Biomass Valorization.
- Aguilar-Aguilar, F., Adaya, L., Godoy-Lozano, E. E., Pantoja, L. A., dos Santos, A. S., Eapen, D., & Sebastian, P. J. (2023a). [Anaerobic co-digestion of raw glycerol and swine manure: microbial communities](#). Biomass Conversion and Biorefinery, 13(8), 7127-7138.
- Aguilar-Aguilar, F., Adaya, L., Godoy-Lozano, E. E., Pantoja, L. A., dos Santos, A. S., Eapen, D., & Sebastian, P. J. (2023b). [Anaerobic co-digestion of raw glycerol and swine manure: microbial communities](#). Biomass Conversion and Biorefinery, 13(8), 7127-7138.
- Alpandi, A. H., Husin, H., Sidek, A., & Abdurrahman, M. (2022). [Characterization of Malaysian Jatropha Seed Oil and Discovering the Process of Powdered Jatropha Leaves](#). Processes, 10(12).
- Apaydın Varol, E., & Mutlu, Ü. (2023). [TGA-FTIR Analysis of Biomass Samples Based on the Thermal Decomposition Behavior of Hemicellulose, Cellulose, and Lignin](#). Energies, 16(9).
- Aworanti, O. A., Ajani, A. O., Agbede, O. O., Agarry, S. E., Ogunkunle, O., Laseinde, O. T., Kalam, M. A., & Fattah, I. M. R. (2023). [Enhancing and upgrading biogas and biomethane production in anaerobic digestion: a comprehensive review](#). In Frontiers in Energy Research (Vol. 11). Frontiers Media SA.
- Baena-Moreno, F. M., Rodríguez-Galán, M., Vega, F., Vilches, L. F., & Navarrete, B. (2019). [Review: recent advances in biogas purifying technologies](#). In International Journal of Green Energy (Vol. 16, Issue 5, pp. 401-412). Taylor and Francis Inc.
- Balick, M.J. [Production of coyol wine from *Acrocomiamexicana* \(Arecaceae\) in Honduras](#). *Econ Bot* **44**, 84-93 (1990).

Berton, L. H. C., de Azevedo Filho, J. A., Siqueira, W. J., & Colombo, C. A. (2013). **Seed germination and estimates of genetic parameters of promising macaw palm (*Acrocomia aculeata*) progenies for biofuel production.** Industrial Crops and Products, 51, 258-266.

Brayan Alexis, P.-O., Patricia, T.-L., Luis Fernando, M.-R., Lina Marcela, C.-C., Carlos, V.-F., Wilmar Alexander, T.-L., & José Abdón, O.-A. (2015). Effect of Substrate-Inoculum Ratio on the Biochemical Methane Potential of Municipal Biowastes. Engineering Research and Technology, 1(4), 515-526.

César, A. D. S. S., Almeida, F. D. A., De Souza, R. P., Silva, G. C., & Atabani, A. E. (2015). **The prospects of using *Acrocomia aculeata* (macaúba) a non-edible biodiesel feedstock in Brazil.** In Renewable and Sustainable Energy Reviews (Vol. 49, pp. 1213-1220). Elsevier Ltd.

Drosg, B., Braun, R., Bochmann, G., & Al Saedi, T. (2013). **Analysis and characterization of biogas feedstocks.** The Biogas Handbook: Science, Production and Applications, 52-84.

Horváth, I. S., Tabatabaei, M., Karimi, K., & Kumar, R. (2016). **Recent updates on biogas production - A review.** In Biofuel Research Journal (Vol. 3, Issue 2, pp. 394-402). Green Wave Publishing of Canada.

Matheri, A. N., Ndiweni, S. N., Belaid, M., Muzenda, E., & Hubert, R. (2017). Optimising biogas production from anaerobic co-digestion of chicken manure and organic fraction of municipal solid waste. Renewable and Sustainable Energy Reviews, 80, 756-764.

Parsaee, M., Kiani Deh Kiani, M., & Karimi, K. (2019). **A review of biogas production from sugarcane vinasse.** In Biomass and Bioenergy (Vol. 122, pp. 117-125). Elsevier Ltd.

Patinvooh, R. J., Osadolor, O. A., Chandolias, K., Sárvári Horváth, I., & Taherzadeh, M. J. (2017). **Innovative pretreatment strategies for biogas production.** In Bioresource Technology (Vol. 224, pp. 13-24). Elsevier Ltd.

Plath, M., Moser, C., Bailis, R., Brandt, P., Hirsch, H., Klein, A. M., Walmsley, D., & von Wehrden, H. (2016). **A novel bioenergy feedstock in Latin America? Cultivation potential of *Acrocomia aculeata* under current and future climate conditions.** Biomass and Bioenergy, 91, 186-195.

Sarker, S., Lamb, J. J., Hjelme, D. R., & Lien, K. M. (2019). **A review of the role of critical parameters in the design and operation of biogas production plants.** In Applied Sciences (Switzerland) (Vol. 9, Issue 9). MDPI AG.

Kwakye, J. M., Ekechukwu, D. E., & Ogundipe, O. B. (2024). **Systematic review of the economic impacts of bioenergy on agricultural markets.** International Journal of Advanced Economics, 6(7), 306-318.

Fang, Y. R., Hossain, M. S., Peng, S., Han, L., & Yang, P. (2024). **Sustainable energy development of crop straw in five southern provinces of China: Bioenergy production, land, and water saving potential.** Renewable Energy, 224, 120134.

Magne, A., Khatiwada, D., & Cardozo, E. (2024). **Assessing the bioenergy potential in South America: Projections for 2050.** Energy for Sustainable Development, 82, 101535.

Basic

Aguilar-Aguilar, F. A., Mena Cervantes, V. Y., García-Solares, S. M., & Hernández Altamirano, R. (2024). **Exploring the Biorefinery Potential of *Acrocomia aculeata*: A Native Mexican Palm for Sustainable Resource Valorization.** Waste and Biomass Valorization.

Aguilar-Aguilar, F., Adaya, L., Godoy-Lozano, E. E., Pantoja, L. A., dos Santos, A. S., Eapen, D., & Sebastian, P. J. (2023a). **Anaerobic co-digestion of raw glycerol and swine manure: microbial communities.** Biomass Conversion and Biorefinery, 13(8), 7127-7138.

Aguilar-Aguilar, F., Adaya, L., Godoy-Lozano, E. E., Pantoja, L. A., dos Santos, A. S., Eapen, D., & Sebastian, P. J. (2023b). [Anaerobic co-digestion of raw glycerol and swine manure: microbial communities](#). Biomass Conversion and Biorefinery, 13(8), 7127-7138.

Ramírez-Estrada, A., Mena-Cervantes, V. Y., Mederos-Nieto, F. S., Pineda-Flores, G., & Hernández-Altamirano, R. (2022). [Assessment and classification of lignocellulosic biomass recalcitrance by principal components analysis based on thermogravimetry and infrared spectroscopy](#). International Journal of Environmental Science and Technology, 19(4), 2529-2544.

Exhaust gas characterization of biofuel blends in an open cycle gas turbine

Caracterización de gases de escape de mezclas de biocombustibles en una turbina de gas de ciclo abierto

Morales-Sánchez, Leticia Isabel^a, Andrade-Duran, Juan Edgar*^b, Sanchez-Quintal, Ricardo de Jesús^c and May-Tzuc, Oscar de Jesús^d

^a  Universidad Autónoma de Campeche •  0009-0001-0697-0011 •  1235709

^b  Universidad Autónoma de Campeche •  0000-0002-7370-1209 •  732279

^c  Universidad Autónoma de Campeche •  0009-0003-8437-931X •  786068

^d  Universidad Autónoma de Campeche •  0000-0001-7681-8210 •  627799

CONAHCYT classification:

DOI: <https://doi.org/10.35429/H.2024.13.34.45>

Area: Engineering

Field: Engineering

Discipline: Energy engineering

Sub-discipline: Bioenergy

Key Handbooks

This research offers a sustainable alternative solution to a global problem of environmental pollution produced by the aviation sector, by proposing specific fuel-biofuel mixtures. The methodology in the design of the applied experiment, for the characterization of gases in the reaction turbine and the proper functioning of the Brayton cycle. Among the main conclusions of the research, the best environmentally friendly blend (lower production of CO₂ and NO₂), with adequate lubrication and acceptable propulsion was obtained: BK20 (20% biodiesel and 80% paraffin).

Citation: Morales-Sánchez, Leticia Isabel, Andrade-Duran, Juan Edgar, Sanchez-Quintal, Ricardo de Jesús and May-Tzuc, Oscar de Jesús. 2024. Exhaust gas characterization of biofuel blends in an open cycle gas turbine. 34-45. ECORFAN.

*✉ [jeandrad@uacam.mx]

Handbook shelf URL: <https://www.ecorfand.org/handbooks.php>



ISBN 978-607-8948-51-2 ©2009 The Authors. Published by ECORFAN-Mexico, S.C. for its Holding Mexico on behalf of Handbook HESPCU. This is an open access chapter under the CC BY-NC-ND license [<http://creativecommons.org/licenses/by-nc-nd/4.0/>]

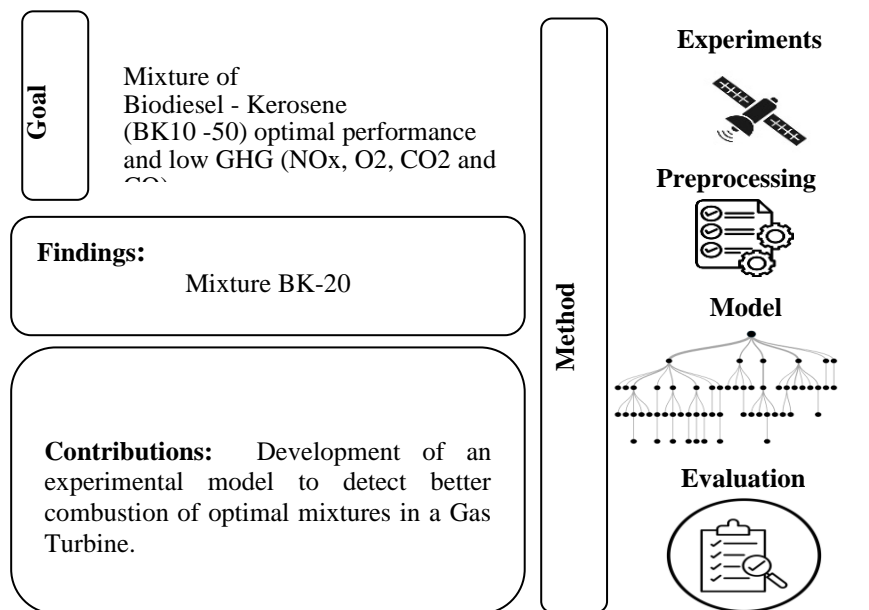
Peer Review under the responsibility of the Scientific Committee MARVID®- in contribution to the scientific, technological and innovation Peer Review Process by training Human Resources for the continuity in the Critical Analysis of International Research.



I702902 CONAHCYT

Abstract

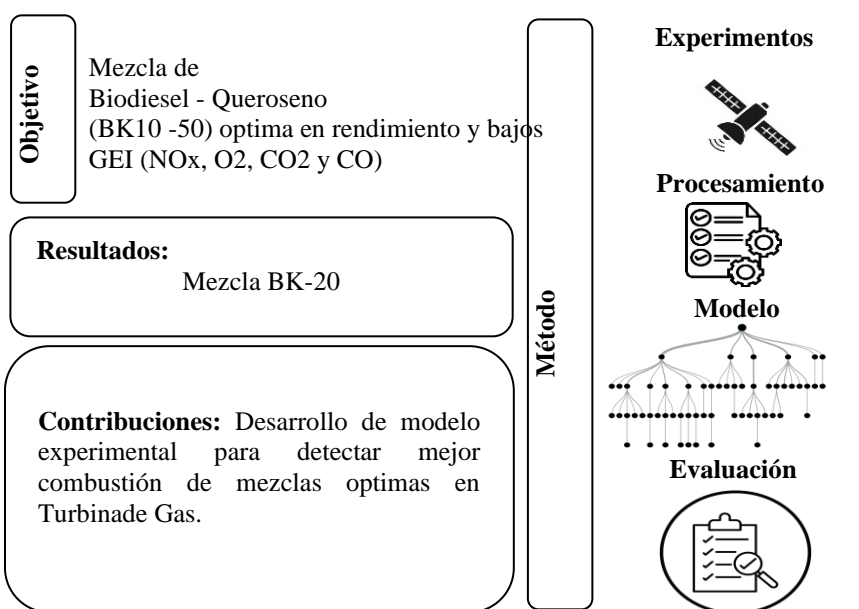
This work seeks to analyze and reduce the percentage in gram/gram of exhaust gases that cause the greenhouse effect using an aeronautical miniturbine. For this research, mixtures of biodiesel (own) and commercial aviation kerosene are used in a BEE-80 model miniturbine. A test bench was implemented which has the microturbine installed, it is monitored telemetrically using an Arduino system and a combustion gas analyzer (CO_2 , CH_4 , SO_x), the turbine parameters allow experimenting with the different mixtures to find the optimal one. It is operated with mixtures varying the percentage of biodiesel from 10%, 20%, 30%, 40% to 50% (B10-B50), to observe the changes in power, consumption, lubricity and mainly the emissions released to the atmosphere. The mixture that showed the best efficiency, an acceptable reduction in greenhouse gases and better lubrication, was B20, in addition to acceptable consumption compared to the other mixtures.



Biodiesel, Transesterification, pollution

Resumen

En este trabajo se busca analizar y disminuir el porcentaje en gramo/gramo de gases de escape causantes del efecto invernadero empleando una miniturbina aeronáutica. Para esta investigación se utilizan mezclas de biodiesel (propio) y queroseno de aviación comercial, en una miniturbina modelo BEE-80. Se implementó un banco de pruebas el cual tiene instalada la microturbina, se monitorea telemétricamente mediante un sistema Arduino y un analizador de gases de combustión (CO_2 , CH_4 , SO_x) los parámetros de la turbina permiten experimentar las diferentes mezclas para encontrar la óptima. Se hace funcionar con mezclas variando el porcentaje de biodiesel desde 10%, 20%, 30%, 40% hasta 50% (B10-B50), para observar los cambios en la potencia, consumo, lubricidad y principalmente las emisiones que libera a la atmósfera. La mezcla que mostró mejor eficiencia, una disminución aceptable de gases de efecto invernadero y mejor lubricación, fue B20, además de un consumo aceptable respecto a las otras mezclas.



Biodiesel, Transesterificación, Contaminación

Introduction

One of humanity's greatest problems is its dependence on fossil fuels, which are not only a non-renewable resource, but are also limited and cause a strong environmental impact with a constant variation in their prices.

One fifth of greenhouse gas emissions are produced by the transport sector, which is the main generator of pollutants worldwide; it is known that these emissions contain polluting compounds such as: carbon dioxide (CO_2), methane (CH_4), nitrous oxide (N_2O), hydrofluorocarbons (HFCs), perfluorocarbons (PFCs) and sulphur hexafluoride (SF_6), generated by the transport sector. Air transport is the second most polluting sector with a global consumption of 800 million litres of turbofuel per day and rising, accounting for about 10% of global energy used for transport.

The challenge is to ensure that renewable energy sources gradually replace these fuels; one alternative could be liquid biomass, especially that which can be converted into biofuel-producing sources. Biofuels currently represent a potential source of renewable energy and could also generate large new markets for agricultural producers.

This work shows how by experimenting with different Biodiesel-Turbosine blends an ideal blend can be found that maintains the ideal power and fuel consumption, while providing the lowest greenhouse gas emissions to the atmosphere, biofuels can offer savings in greenhouse gas emissions of at least 50% compared to fossil fuels such as diesel or gasoline.

Objective

To find the biodiesel-kerosene blend that generates the lowest percentage of greenhouse gases and maintains the best efficiency in terms of power, consumption and lubricity (noise and vibration).

- To produce biodiesel through the transesterification process, ensuring a high degree of purity and yield.
- Examine the properties of biodiesel (density, viscosity, volatility and calorific value) in accordance with ASTM 6761-A, for use in a scale Brayton cycle turbine.
- Determine the best biodiesel-kerosene blends that optimise power, fuel consumption and lubricity in the turbine.
- Determine the positive impact on the environment in terms of greenhouse gas reduction percentages (NO_x , O_2 , CO_2 and CO) by implementing a percentage of biodiesel in the aeronautical fuel (paraffin).

Open Brayton cycle

The Brayton cycle describes the operation of a constant pressure heat engine. Most gas turbines are based on the open Brayton cycle with internal combustion. In this cycle, air from the atmosphere is compressed to the higher pressure and temperature of the compressor. In the combustion chamber, the air is further heated by burning the fuel-air mixture in the air flow. The products and gases of combustion are expanded in the turbine to near atmospheric pressure (engines producing mechanical power or electrical power) or to the pressure required by jet engines. The open Brayton cycle means that the gases are discharged directly into the atmosphere.

Figure 1 shows the P-V (pressure-volume) and T-S (temperature-entropy) diagrams of the Brayton cycle, showing the effect of thermal and pressure levels on the four Brayton cycle processes:

- 1-2 Isentropic compression (in a compressor).
- 2-3 Heat addition at constant pressure.
- 3-4 Isentropic expansion (in a turbine).

- 4-1 Heat rejection at constant pressure.

Box 1

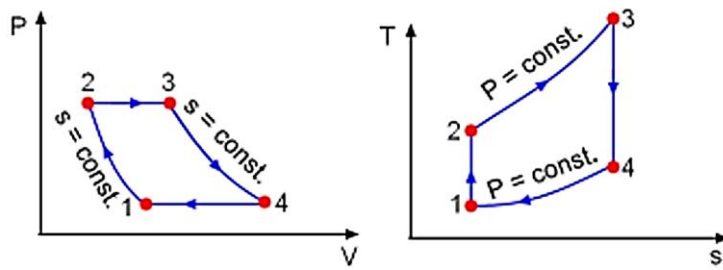


Figure 1

P-V and T-S diagram of the Brayton cycle

Source [*Nuclear power, 2022*]

Gas turbines

Gas turbines generally operate in an open cycle, as shown in Figure 2. In step 1, fresh air at ambient conditions is introduced into the compressor where its temperature and pressure rises, then at point 2, the high-pressure air goes into the combustion chamber where the fuel is burned at constant pressure. At point 3, the resulting high-temperature gases enter the reaction turbine, where they expand to atmospheric pressure, thereby producing power. Finally, at point 4, the exhaust gases leaving the turbine are expelled to the outside (not recirculated), thus the cycle is classified as an open cycle ([Emilio Rivera Chávez, 2020](#)).

Box 2

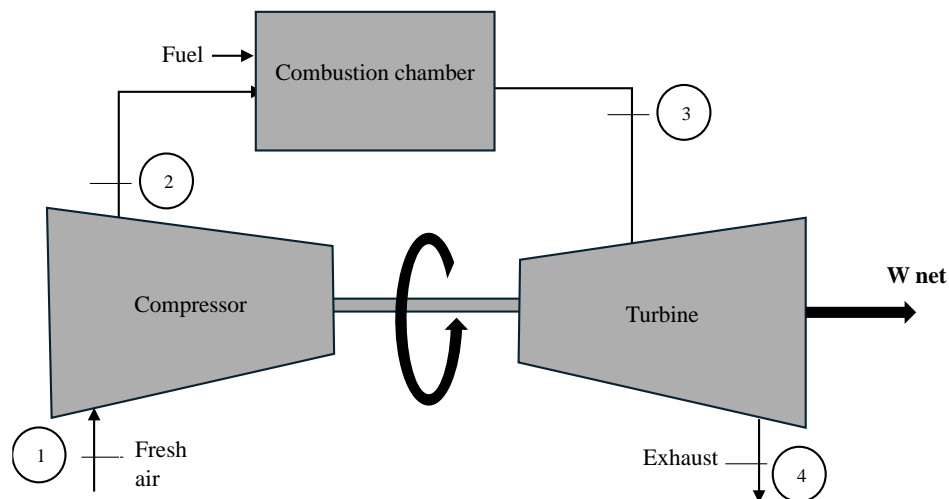


Figure 2

Open cycle gas turbine engine

Source [[Emilio Rivera Chávez, 2020](#)]

Basic components of the gas turbine:

- Compressor (also called action turbine): draws in external air and compresses it.
- Combustion chamber: fuel is added to the pressurised air and ignited.
- Reaction turbine: converts high-speed gas energy into rotational energy through expansion.
- Output shaft and gearbox: delivers rotational energy to the driven equipment.
- Exhaust: extracts the low-emission gas used from the turbine section.

Biofuels

Biofuels are fuels obtained from biomass. The term biomass, in the broad sense, refers to any type of organic matter that has had its immediate origin in the biological process of recently living organisms, such as plants, or their metabolic waste (manure); the concept of biomass includes products of both plant and animal origin. In order to better understand the concept of biomass, we can see in Table 1 the different types of biomass into which it is divided.

Box 3

Table 1

Classification of biomass

Type of biomass	Definition
Primary biomass	Organic matter formed directly from photosynthetic organisms. This group includes plant biomass, including agricultural and forestry residues.
Secondary biomass	It is produced by heterotrophic organisms using primary biomass in their nutrition. It is the faecal matter or meat of animals.
Tertiary biomass	It is produced by organisms that feed on secondary biomass, e.g. the remains and excrements of carnivorous animals that feed on herbivores.
Natural biomass	It is produced by wild ecosystems; 40% of the biomass produced on land comes from the oceans.
Residual biomass	It can be extracted from agricultural and forestry residues, and from human activities.
Energy crops	Any agricultural crop whose purpose is to supply biomass for biofuel production.

Source: [Salinas Edmar & Gasca Víctor, 2009]

Biofuels are considered clean energy because they release only 20% of carbon emissions during combustion compared to fossil fuels. The use of biofuels as an alternative source of energy to hydrocarbons and the reduction of environmental impact is new work, but their use has been done for a long time. For example, in underdeveloped countries (especially in rural areas), and in developed countries, wood is used to generate electricity. Various types of biofuels are currently being developed, but the best known are classified into three groups: first, second and third generation, each of which is described below.

ASTM D6751A Standard

The ASTM D6751A biodiesel standard covers B100 biodiesel for use as a component of a blend with middle distillate fuels. The standard takes into consideration important minimum properties that biodiesel must have: flash point, methanol, kinematic viscosity, sulphated ash, oxidation stability, sulphur, copper strip corrosion, cetane number, cloud point, acid number, carbon residue, total and free glycerol, phosphorus, and water sediment; these depend on the refining practices employed and the nature of the renewable lipids from which they are produced as they can generate similar characteristic volatilities and combustion emissions with different cold flow properties.

Methodology

Fifty samples of residual vegetable oil (150 ml each) are subjected to a transesterification process, i.e. the oil is mixed with methanol in the presence of a basic catalyst and sodium methoxide at 65 °C, yielding quantitatively a methyl ester and glycerol. After this process, an average of 30 ml of glycerine and 150 ml of residual oil biodiesel was obtained (ASTM D 6751 standard is reached), whose density is 0.867 g/ml, therefore: 150 ml x 0.867 g/ml = 130.05 g of residual oil biodiesel.

Mixtures made

1. Ten samples of B10 + aviation paraffin: 10% biodiesel + 90% aviation paraffin.
2. Ten samples of B20 + aviation paraffin: 20% Biodiesel + 80% aviation paraffin.
3. Ten samples of B30 + aviation paraffin: 30% Biodiesel + 70% aviation paraffin.
4. Ten samples of B40 + aviation paraffin: 40% Biodiesel + 60% aviation paraffin.
5. Ten samples of B50 + aviation paraffin: 50% Biodiesel + 50% aviation paraffin.

Characterisation with gas chromatography

To characterise the methyl esters (biodiesel) obtained, they were determined by gas chromatography-mass spectrometry according to the technique used by the researcher Warawut in order to observe the whole range of elements.

Calibration standards supplied by Supelco, Sigma - Aldrich, Glycerine, 1 ml, 500 mg / ml in pyridine, Monoolein, 3 ml, 5,000 g / ml in pyridine, Dolein solution, 2 ml, 5,000 g / mL in pyridine, Triolein, 2 ml, 5,000 g / ml in pyridine, Butanotriol internal standard no. 1, 5 ml, 1,000 g / ml in pyridine, Butanotriol internal standard no. 1, 5 ml, 1,000 g/mL in pyridine, Tricaprin internal standard #2, 5 ml, 8,000 g/mL in pyridine, ASTM D6584 Standard Solution 1,2,3,4 and 5, 1 ml, in pyridine (varied), 1000 ml anhydrous tetrahydrofuran (the standard standards were used exclusively for curve comparison). The technique consisted in extracting 100 µl of biodiesel (from the chosen sample) and diluting it in 0.8 ml of tetrahydrofuran (THF). The syringe was rinsed three times with the solution and 1 µl of diluted biodiesel was injected into the chromatograph with a 10 µl hypodermic syringe.

The gas chromatograph used is a Trace CG ultra from Thermo Finigan Corporation with a capillary column (30 m × 0.25 mm ID × 0.25 µm) and a mass spectrometry detector, which can be seen in Figure 3. The equipment conditions are as follows: injection temperature 280 °C (injector) and detector temperature 200 °C (MS). The oven temperature programme was 140 °C for 4 min, followed by a ramp of 15°C/min to reach 280°C in 7 min, and a second ramp of 10°C/min to reach 340°C, maintaining this temperature for 6 min until the end of the programme. The carrier gas was 99.998% chromatographic grade helium at a constant flow rate of 1 ml/min. These analyses were carried out in the Hydrogen and Biofuels Laboratory of the Institute of Renewable Energies of the Universidad Autónoma de México.

Test bench system

A test bench previously developed by M.I Carlos Gallardo Martínez for his thesis work was used, which has been modified for this new project, whose design is presented in Figure 4. This test bench is equipped with a JetCentral Bee 80 Se microturbine that is telemetrically monitored by an Arduino system and a flue gas analyser that measures parameters such as O₂, CO₂, CH₄, SO_x, among others. This comprehensive approach allows the analysis and comparison of various aspects of performance, such as power output, fuel consumption, greenhouse gas emissions, lubricity (related to mechanical noise and vibration), and thermal stability during operation. The test bench facilitates the evaluation of the microturbine with different fuel blends, in this case biodiesel and paraffin, with the aim of identifying the combination that offers the best overall performance.

Box 4

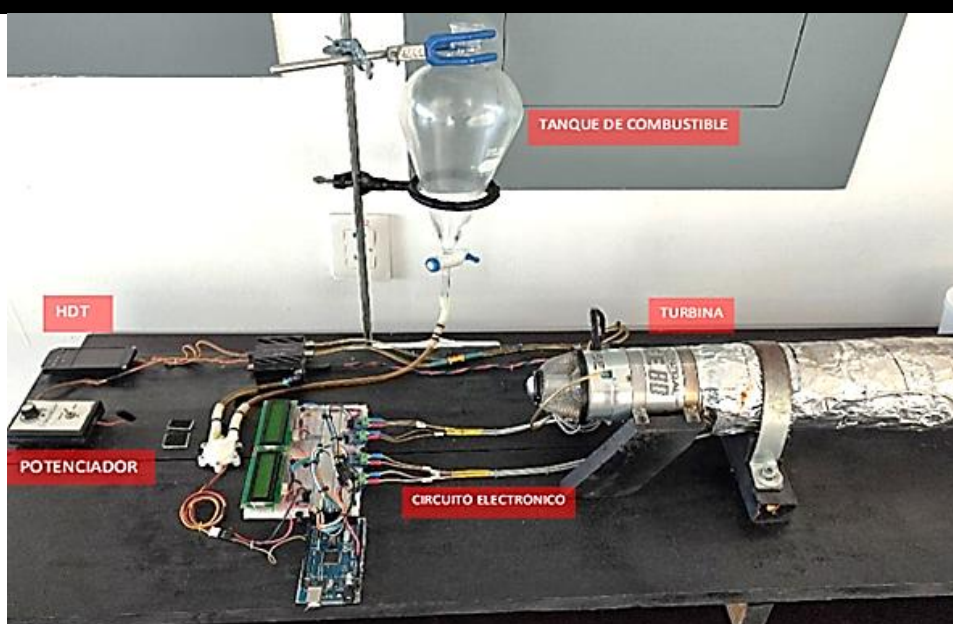


Figure 3

Test bench

Source: [Own elaboration]

The mini-turbine used is an open Brayton cycle gas turbine, with all the characteristics of a large turbine, but on a much smaller scale (250-1), reducing the logistics of operation, consumption, safety, unit cost and testing.

Programming

This project uses an Arduino embedded system, which is an open source platform with easily accessible hardware and software. Two programs were made for the test bench, one in Arduino and one in LabVIEW.

Turbine exhaust gas measurement process

To carry out the process of measuring exhaust gases at the turbine outlet, the combustion gas analyser (E Instruments E4500) is used, which is a practical tool for its rapid analysis and with a minimum error of 5% in the data obtained on site, or for graphing with the interface to the computer, which can be seen in Figure 4.

Box 5



Figure 4

Gas analyser

Source: [[CICSA, 2023](#)]

Results

Gas chromatography

Box 6

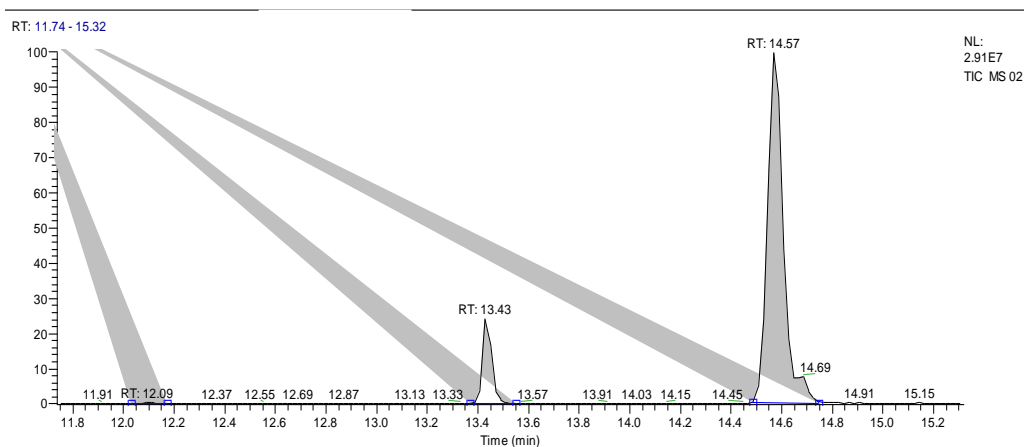


Figure 5

Chromatography of the elements detected in sample 1

Source: [[Own elaboration](#)]

Box 7

Table 2

Name of elements and percentage of sample 1

01.RAW								
RT: 11.74 - 15.32								
Number of detected peaks: 3								
Apex RT	Start RT	End RT	Area	%Area	Height	%Height	Name	Formula
12.09	12.03	12.17	276685.9	0.19	134119	0.37	Glycerine propanetriol	C ₃ H ₈ O ₃
13.43	13.37	13.55	16994521	11.66	6951370	19.28	Pentadecanoic acid, 14-methyl-, methylester (pentadecílico)	C ₁₇ H ₃₄ O ₂
14.57	14.49	14.75	1.28E+08	86.77	28964416	80.35	6-Octadecenoic acid, Methyleneester (Z), (Oleico)	C ₁₉ H ₃₆ O ₂

Source [Own elaboration]

Box 8

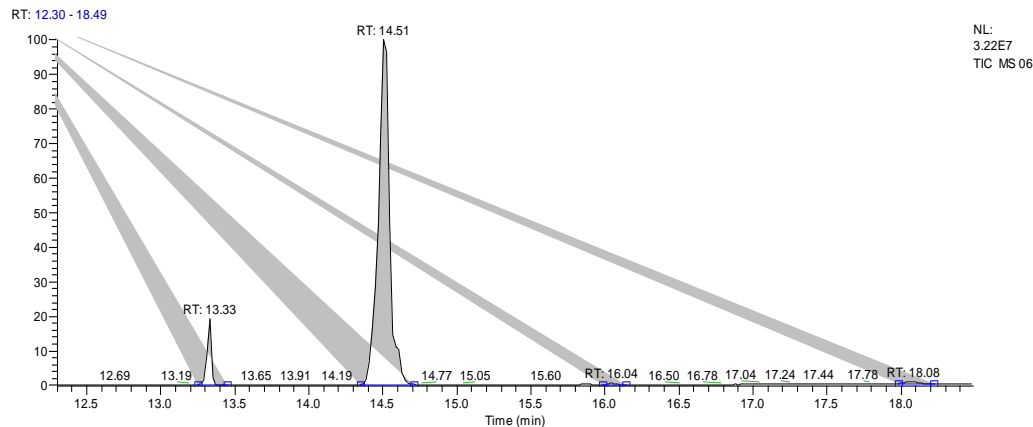


Figure 6

Chromatography of the elements detected in sample 2

Source [Own elaboration]

Box 9

Table 3

Name of elements and percentage of sample 2

02.RAW								
RT: 13.14 - 15.51								
Number of detected peaks: 3								
Apex RT	Start RT	End RT	Area	%Area	Height	%Height	Name	Formula
13.33	13.25	13.45	12798456	6.63	6234587	16.08	Pentadecanoic acid, 14-methyl-, methylester (pentadecílico)	C ₁₇ H ₃₄ O ₂
14.51	14.35	14.71	1.78E+08	92.1	32194767	83.57	6-Octadecenoic acid, methylester, (Z) (oleico)	C ₁₉ H ₃₆ O ₂
16.04	15.98	16.14	577442.1	0.3	137621	0.35	Docosanoic acid, Methyleneester (Behenico)	C ₂₃ H ₄₆ O ₂

Source [Own elaboration]

Box 10

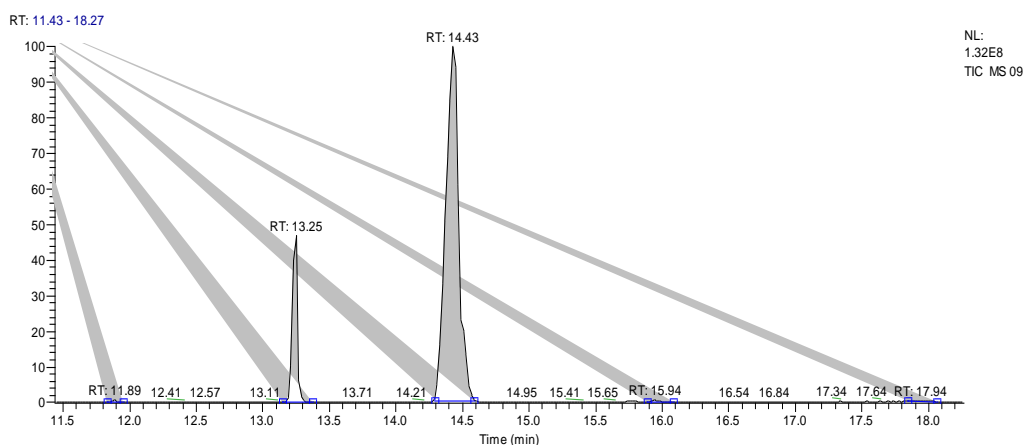


Figure 7

Chromatography of the elements detected in sample 3

Source: [Own elaboration]

Box 11

Table 4

Name of elements and percentage of sample 3

03.RAW								
RT: 11.43 - 18.27								
Number of detected peaks: 5								
Apex RT	Start RT	End RT	Area	%Area	Height	%Height	Name	Formula
11.89	11.83	11.95	1868876	0.17	789925.2	0.4	Tetradecanoic acid, Methyl ester (Miristico)	C15H30O2
13.25	13.15	13.37	1.7E+08	15.64	62086183	31.75	Nonanoic acid, Methyl ester (Pelargonico)	C10H20O2
14.43	14.29	14.59	9.11E+08	83.6	1.32E+08	67.34	6-Octadecenoic acid, methyl ester, (Z) (oleico)	C19H36O2
15.94	15.88	16.08	2787976	0.26	659117.1	0.34	Tetradecanoic acid, Methyl ester (Miristico)	C15H30O2
17.94	17.84	18.06	2044937	0.19	335358	0.17	Cyclopentaneundecanoic acid, methyl ester	C17H32O2

Source: [Own elaboration]

The three analyses show on average more than 99% of different types of methyl ester (biodiesel) and only in the first sample a percentage of 0.19% of glycerine can be seen, therefore, it is assured that these samples easily exceed the ASTM 6751-A standard.

O₂ increase in the blends

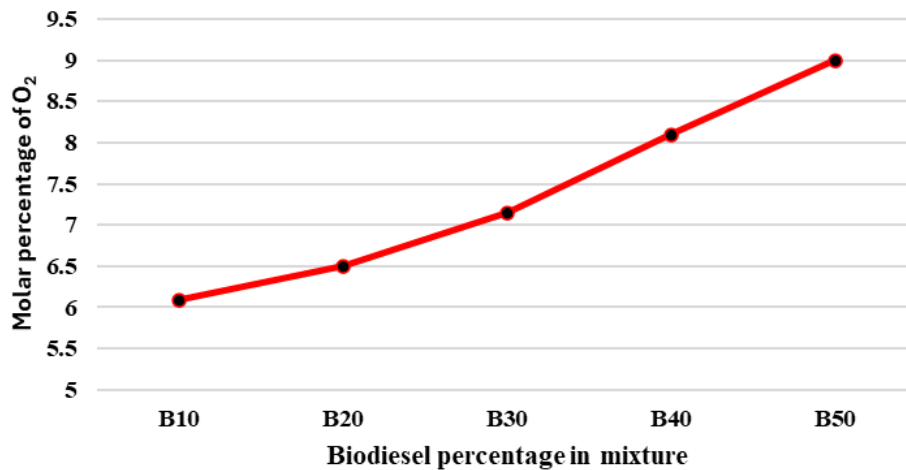
Box 12

Table 5

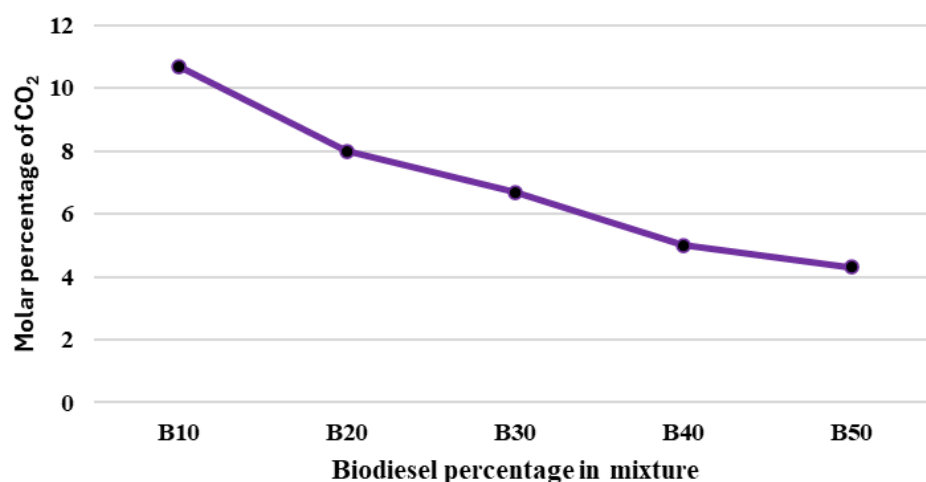
Molar percentage of O₂ at the outlet of the nozzle

% Biodiesel blended with paraffin	% O ₂ molar gases at the nozzle outlet	
	Average	Desv. Standard
B10	6.09	0.23
B20	6.50	0.06
B30	7.15	0.24
B40	8.1	0.10
B50	9.00	0.00

Source: [Own elaboration]

Box 13**Figure 8**Average % molar O₂ of gases at nozzle outletSource [*own elaboration*]*Decrease of CO₂ in the mixtures***Box 14****Table 6**Molar percentage of CO₂ at the nozzle outlet

% Biodiesel blended with paraffin	% CO ₂ molar of gases at the nozzle outlet
	Average
B10	10.7
B20	8
B30	6.7
B40	5
B50	4.3

Source [*own elaboration*]**Box 15****Figure 9**Average % CO₂ molar gases at nozzle outletSource: [*Own elaboration*]

Box 16

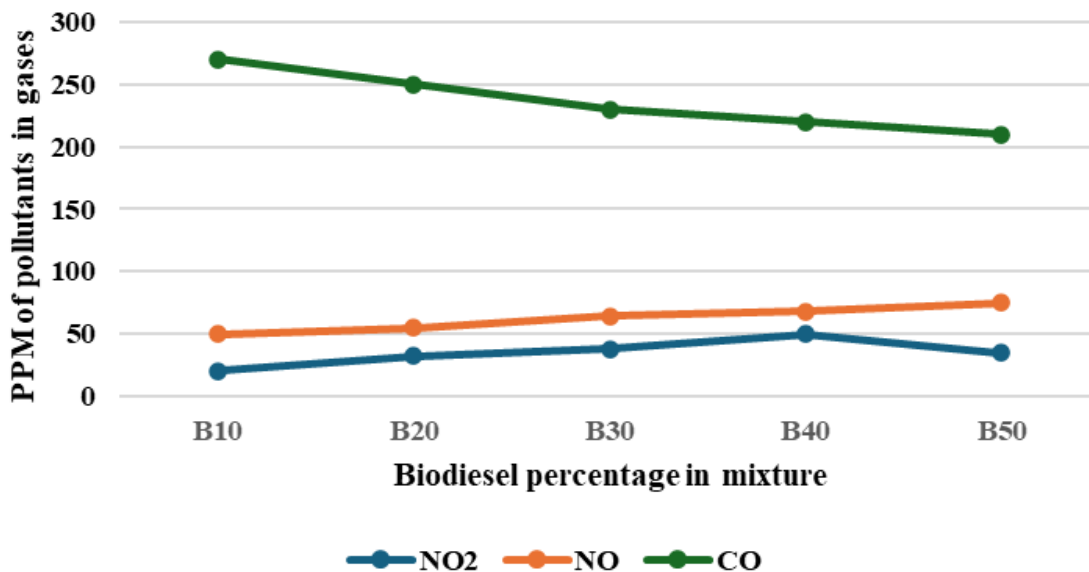
Table 7

PPM of contaminants in mixtures

% Biodiesel in blend with paraffin	Particles per million		
	NO ₂	NO	CO
B10	20	50	270
B20	32	55	250
B30	38	64	230
B40	50	68	220
B50	35	75	210

Source: [Own elaboration]

Box 17

**Figure 10**

Contaminants in PPM by biodiesel/kerosene blend

Source: [Own elaboration]

Conclusions

With the results obtained from the experiments we can observe that the most environmentally friendly blends are the BK20 and BK30 blends, as they show higher levels of O₂ and lower levels of CO₂ and NO₂; we must consider that the higher levels of O₂ could not precisely indicate a bad combustion, but rather that there is good combustion, only that the input increases the proportion of oxygen as the amount of biodiesel in the blend increases. NO_x tends to increase naturally in blends by about 10%, but in contrast to fossil fuels it is about 70% lower. Taking into consideration the power, the consumption of a previous work and the lower amount of pollutant gases in this work we can conclude that the optimal blend for the target is BK20.

Funding

This research work was carried out with own resources.

Acknowledgements

To the Faculty of Engineering of the Autonomous University of Campeche, for the laboratories provided for the experimentation and for the facilities given as an employer to the working group. To the Institute of Renewable Energies (IER-UNAM) for allowing the characterisation of samples in their certified equipment, the facilities provided and the use of the hydrogen and biofuels laboratory.

References

Background

- ASTM. (2023). *Standard Specification for Biodiesel Fuel Blend Stock (B100) for Middle Distillate Fuels.*
- CICSA. (2023). *Analizador de gas E4500.*
- Emilio Rivera Chávez. (2020). *Turbinas a gas.*
- Nuclear power. (2022). *Brayton Cycle – Gas Turbine Engine.*
- Salinas Edmar, & Gasca Víctor. (2009). *Los biocombustibles.*
- Serna, F., Barrera, L., & Montiel, H. (2011). *Impacto Social y Económico en el uso de Biocombustibles.* *Journal of Technology Management & Innovation*, 6(1), 100–114.

Support

- Gallardo, C. (2023). *Implementación de un banco de pruebas monitoreado con Arduino y LabVIEW para la caracterización de mezclas biodiesel-diésel en una microturbina de avión.*

Discussions

- Warawut Tiyapongpattana. (2008). Characterization of biodiesel blends using comprehensive two-dimensional gas. *Journal of Chromatography A.*

- Wilhelm Gabriel, Mandegari Mohsen, Farzad Somayeh, & Gorgens Johann. (2016). Techno-economic comparison of biojet fuel production from lignocellulose, vegetable oil and sugar cane juice. *Bioresource Technology*.

Causes of cracking in the turbine housings of a turbocharger

Causas del agrietamiento en las carcasas de turbina de un turbocompresor

Duffus-Scott, A. B.*^a, Machado-Rodríguez, L. A.^b, Álvarez-García, E. A.^c and Patiño-Carachure, C.^d

^a  Universidad Central "Marta Abreu" de Las Villas •  0000-0001-9959-5697

^b  Universidad Central "Marta Abreu" de Las Villas

^c  Universidad Tecnológica de Campeche •  LRC-9320-2024 •  0000-0002-8046-0124

^d  Universidad Autónoma del Carmen •  AGZ-9935-2022 •  0000-0002-1436-1259 •  226327

CONAHCYT classification

DOI: <https://doi.org/10.35429/H.2024.13.46.55>

Area: Engineering

Field: Engineering and Technology

Discipline: Materials Science and Technology

Sub-discipline: Metallurgy

Key Handbooks

In this chapter, the procedure to determine the failure cause of the cracking of a casing that was exposed during its operation to thermal shock and fatigue conditions is explained. The areas of materials science and mechanical engineering are fundamental to determine the necessary studies according to the conditions and variables to be studied for this type of problem. The fundamental cause of cracking in the casing is due to thermal shock and fatigue which promote cracking. The maximum stress amplitude encountered due to thermal shock exceeds the permissible design limits. This work has been carried out in collaboration with the Centro de Investigaciones de Soldadura (CIS), Facultad de Ingeniería Mecánica e Industrial. Universidad Central "Marta Abreu" de Las Villas, Santa Clara, Villa Clara, Cuba. The Technological University of Campeche, San Antonio, Cardenas, Ciudad Del Carmen, Campeche and the Autonomous University of Carmen, Cd del Carmen, Campeche, Mex.

Citation: Duffus-Scott, A. B., Machado-Rodríguez, L. A., Álvarez-García, E. A. and Patiño-Carachure, C. 2024. Causes of cracking in the turbine housings of a turbocharger. 46-55. ECORFAN.

*  [aduffus@uclv.edu.cu]

Handbook shelf URL: <https://www.ecorfan.org/handbooks.php>



ISBN 978-607-8948-51-2/©2009 The Authors. Published by ECORFAN-Mexico, S.C. for its Holding Mexico on behalf of Handbook HRPG. This is an open access chapter under the CC BY-NC-ND license [<http://creativecommons.org/licenses/by-nc-nd/4.0/>]

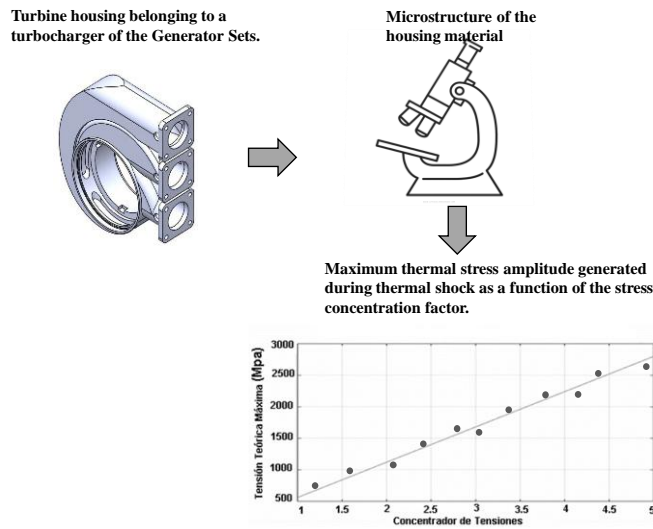
Peer Review under the responsibility of the Scientific Committee MARVID®- in contribution to the scientific, technological and innovation Peer Review Process by training Human Resources for the continuity in the Critical Analysis of International Research.



1702902 CONAHCYT

Abstract

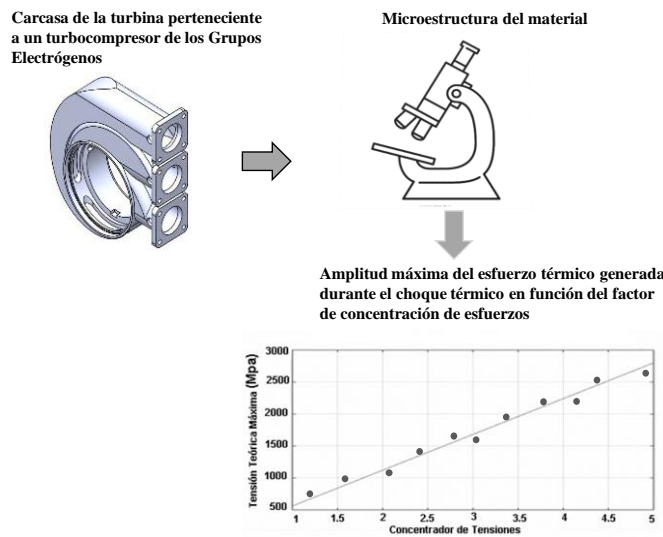
Temperature variation in turbocharger casings of generator sets generates shocks and thermal fatigue that cause cracks in different areas, with permissible limits depending on the direction and location. This study analyzes the microstructure and chemical composition of nodular cast iron castings manufactured under ASTM A 536 and GOST3443-87 standards, using metallographic techniques and emission spectroscopy. With visual inspection and penetrating liquids, the types of cracks and their orientations are examined. The maximum amplitude of the thermal stress generated during the thermal shock was determined using MATLAB software, considering that for a minimum stress concentration factor ($k_f=1$), the thermal stress amplitude is 560 MPa, exceeding the design limit of 210 MPa, which explains the appearance of transverse and longitudinal cracks. Transverse cracks show a higher thermal stress concentration factor than longitudinal cracks.



Turbocharger, Cracking, Thermal shock

Resumen

La variación de temperatura en las carcasas de turbocompresores de grupos electrógenos genera choques y fatiga térmica que provocan grietas en diferentes zonas, con límites permisibles según la dirección y ubicación. Este estudio analiza la microestructura y composición química de las carcasas de hierro fundido nodular fabricadas bajo las normas ASTM A 536 y GOST3443-87, usando técnicas metalográficas y espectroscopía de emisión. Con inspección visual y líquidos penetrantes, se examinan los tipos de grietas y sus orientaciones. La amplitud máxima del esfuerzo térmico generada durante el choque térmico fue determinada con empleo del Software MATLAB, considerando que para un factor de concentración de esfuerzos mínimo ($k_f=1$), la amplitud de tensión térmica es de 560 MPa, superando el límite de diseño de 210 MPa, lo cual explica la aparición de grietas transversales y longitudinales. Las grietas transversales muestran un mayor factor de concentración y esfuerzo térmico que las longitudinales



Turbocompresor; Agrietamiento; Choque térmico

Introduction

The Fuel Generator Maintenance Company ([Planned Preventive Maintenance: EMGEF, 2014](#)) is currently in charge of the operation and maintenance of the Fuel-Oil Power Plants or Generator Sets. It carries out the technological operations for the disassembly, dismantling, inspection, maintenance and assembly of the TPS-57 turbocharger of HYUNDAIHIMSEN 9H 21/32 engines ([Rodríguez, L. A.M., 2019](#)).

According to [Laustela, E. \(2005\)](#), an exhaust gas turbocharger is driven, as the name suggests, by the engine exhaust gas. This gas, at high temperatures, is directed at high speed towards the blades of a turbine that drives a compressor rotor installed on the same shaft. As it rotates, the rotor draws in ambient air through a filter-silencer, compresses it and, through a aftercooler, sends it to the engine air intake, from where it passes into the cylinders. Turbocharging increases engine power by up to four times. Therefore, 75 per cent of the engine's power depends on the turbocharger working efficiently ([Rodríguez, L.A.M., 2019](#)).

The turbine is where the expansion of the gases coming from the engine cylinders takes place. The inlet of these gases is made through an orifice whose layout optimises the incidence of the flow on the blades, with this and the help of the snail-shaped housing (figure 1) the gases are distributed along the turbine losing pressure to make the shaft rotate. ([Rodríguez, L.A.M. 2019](#)).

Box 1



Figure 1

Turbine casing belonging to a turbocharger of the Generator Sets

Source: [Rodríguez L.A.M., 2019](#)

The casing is made of nodular cast iron, according to the ASTM A536 standard, which establishes 5 grades according to its mechanical properties; this standard is in correspondence with the GOST3443-87 standard.

According to Laustela, E. (2005), in Cuba there are cast iron casings with nodular and spheroidal graphite.

Nodular iron is a material currently widely used in the automotive industry and machinery, this is because it has some advantages over steel and grey iron, for example, it has greater resistance to fatigue and wear, although with a higher manufacturing cost than grey iron ([García-Lira J., et al., 2019](#)). Because of its good toughness, nodular iron is being used for the manufacture of parts that experience high fatigue cycles.

Shock often occurs when low temperature fluid hits a hot surface, producing a very high level of stresses close to the exposed surface that can eventually lead to the development of cracks, another less common situation in which thermal shock occurs can occur, particularly where sudden vessel depressurisation occurs (Mellouli, Haddar et al. 2011).

Based on the above, the aim of the present work is to chemically and metallographically characterise the casing material and to explain the causes of cracking in the casings of turbines belonging to turbochargers.

Methodology

Determination of the chemical composition of the casing material.

The chemical composition of the samples extracted from the casing was obtained by the method of Spectral Analysis of Optical Emission, which was carried out in the Chemical Analysis Laboratory of the Planta Mecánica Company, Cuba, with the use of an Optical Emission Spectral Analysis equipment, Belec Vario Lab Spectrograph (Figure 2), which processes the data with the Belec Win 21 software, the equipment's own. Prior to the analysis, the equipment was calibrated with the foundry standards.

Box 2



Figure 2

Optical emission spectral analysis equipment

Source: [Spectrographer's Handbook, 2015](#)

Metallographic observation

The material under study corresponds to a segment of a casing (see figure 1).

To prepare the specimens for metallographic analysis, samples were taken from a section of the carcass, by means of cuts on a metallographic cutting machine (Figure 3) in the Heat Treatment Laboratory of the Welding Research Centre.

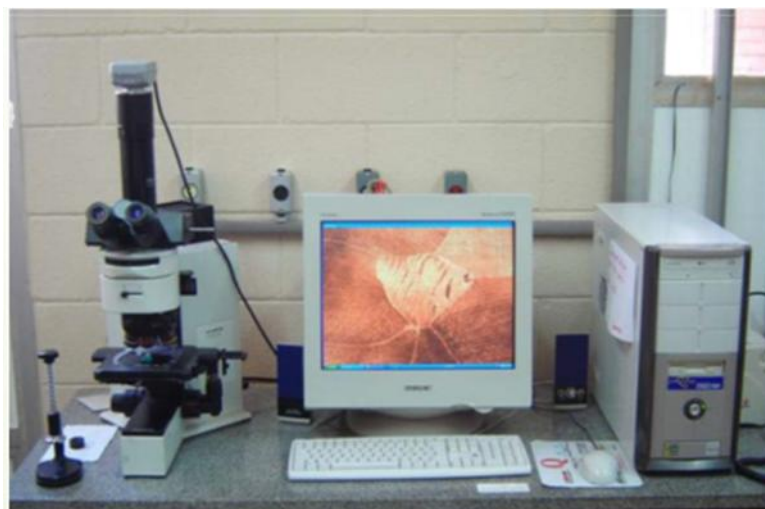
Box 3**Figure 3**

Metal cutting machine with abrasive disc

Source: *Own elaboration*

To facilitate handling during grinding and polishing, two samples were mounted on mechanical supports. The samples were prepared by grinding with sandpaper (from No 100 to No 1200) and polishing with alumina suspension, in accordance with ASTM E3-11 (2011). The grinding and polishing operations were performed on a metallographic polishing machine at the Heat Treatment Laboratory of the Welding Research Centre. After polishing, the samples were attacked with 3 % nital, in correspondence with ASTM E340-15 (2015) and ASTM E407-07(2015)e1 for micro attack.

The metallographic observation of the samples was carried out with the help of a Novel optical metallographic microscope at the Materials Science Laboratory of (CIS-MET-027, 2002). Images of the microstructure were taken with a high sensitivity 1.3 pixel Yuva camera attached to the eyepiece of the microscope and to a computer with specialised software (Image J) for image acquisition, as shown in Figure 4.

Box 4**Figure 4**

Optical metallographic microscope, image acquisition camera and computer

Source: *Own elaboration*

Visual inspection and the application of liquid penetrants

Visual inspection and liquid penetrant testing were used as non-destructive testing methods for the analysis of the types of cracks that appear.

Developing the meaning of the variables in the linear and important writing is the comparison of the criteria used.

Determination of the maximum thermal stress amplitude generated during thermal shock.

The maximum thermal stress amplitude generated during thermal shock was determined using MatLab software. The maximum thermal stress amplitude generated during thermal shock (S_m) was determined by the equation (1) ([ASME 2010](#)):

$$S_m = \frac{E\alpha(\Delta T_m)}{2(1-\nu)} k_f \quad [1]$$

S_m : is the maximum thermal stress amplitude generated during thermal shock.

E: is the modulus of elasticity

α : is the coefficient of thermal expansion.

ΔT_m : is the maximum possible magnitude of the thermal shock

ν : is the Poisson coefficient

k_f : is the stress concentration factor with a value of 1,0 a 5,0.

Results

Chemical analysis

The results obtained from the chemical analysis are shown in table 1..

Box 5

Table 1

Chemical composition of the carcasses (% mass)

Material	C	Si	Mn	P	S	Mg	Cu	Cr	Al
Carcasa	4,4	1,9	0,19	0,018	0,007	0,008	0,017	0,014	--

Source: *Own elaboration*

This composition corresponds to the [ASTM A536-84 \(2019\) e1](#) standard, which establishes 5 grades according to their mechanical properties (table 2).

Box 6

Table 2

Standard ASTM A536

Material	Code	Description	Uses general
ASTM A536	65-45-12	Mostly ferric; decoladaorecognised.	Components subjected to right-hand loads and fatigue.

Source: *Chiaverini, 1985*

The high carbon content in cast irons, both in the inclusion of graphite and the content in the matrix, is a factor that hinders the weldability of these materials (Guliaev, 1987, Aguilar et al ,2000).

The main alloying elements are carbon and silicon. High carbon content increases the amount of graphite or Fe3C and increasing the carbon and silicon content increases the graphitisation potential and fluidity of the cast iron, however, its strength is affected, as ferrite formation and pearlite thickening are promoted.

Analysis of metallographic observation

According to (Guliaev, A.P., 1987) cast irons can be classified as shown in figure 5.

Box 7

Metal matrix	Shape of carbon inclusions		
	Lamellar	Nodular	Spheroidal
Ferrite			
Ferrite + Pearlite			
Pearlite			

Figure 5

Classification of cast iron according to the structure of the metal matrix and the shape of the graphite inclusions.

Source: [Guliaev, 1987](#)

The following figures 6a and 6b at different magnifications show the type of melt and the matrix to which this material corresponds.

Box 8

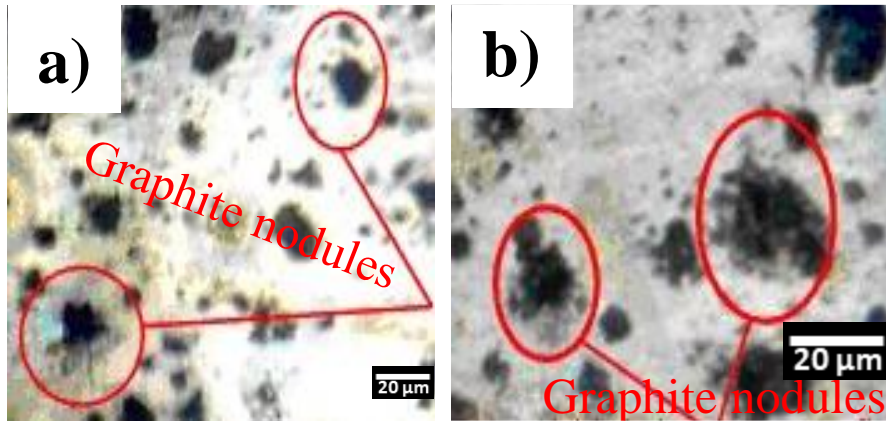


Figure 6

Casing material microstructure (a- 200 X, b-400 X). CIS-MET-027

Source: [Own elaboration](#)

According to figure 6 it can be seen that the type of material present in the casing according to GOST 3443 - 87 is nodular cast iron (non-regular nodular inclusion shape), inclusion size 15-30 μm and uniform distribution of the ferritic matrix. This malleable cast iron, which is obtained by annealing (malleabelling) of white cast iron. In malleable cast iron, all or a large part of the carbon is in the free state in the form of nodules (carbonoderescent).

This compact, almost equiaxial shape of the graphite, but not round, is called nodular or annealed.

Results of the inspection of the casings

The visual inspection was based on detecting the different cracks in the casing, thus determining their length and the areas where they appear most frequently.

Several casings were inspected out of operation due to cracking and it was observed that the cracks appear more frequently in the transversal direction, being these the most dangerous as they cause a rapid breakage of the turbo and leakage of exhaust gases, which gives the lowest permissible value of length, this is explained because in the transverse direction the stress concentration factor (k_f) is much higher. The following figure (figure 7) shows the different cracks that have occurred.

Box 9



Figure 7

Crack in the transverse direction

Source: own elaboration

Results of the determination of the thermal shock produced in the casing by MatLab software

For carbon steels with $\sigma_{última} \leq 552$ MPa, the allowable design stress amplitude (S_a) is considered to be in the order of 210 MPa ([Callister. D.W., 2015](#)).

According to ([Callister D.W., 2015](#)) the value of $\sigma_{última}$ of nodular cast iron casing is of the order of 500MPa, this allows the same value of $S_a = 210$ MPa to be used.

The maximum possible amplitude of the thermal shock $DT_m = T_{cascada} - T_{agua}$, where the

$T_{cascada} = 380^{\circ}\text{C}$ and the $T_{agua} = 30^{\circ}\text{C}$, so that $DT_m = 350^{\circ}\text{C}$.

The stress concentration factor is decided to take values between 1 and 5 ([ASME 2010](#)).

The Poisson's coefficient $n = 0,25$, the coefficient of thermal expansion is $a = 12 \cdot 10^{-6} 1/\text{C}$ and the modulus of elasticity $E = 2 \cdot 10^5 \text{ MPa}$. ([Callister D.W., 2015](#))

The value of the maximum amplitude of the thermal stress generated during thermal shock (S_m) can be seen in the following graph (figure 8).

Box 10

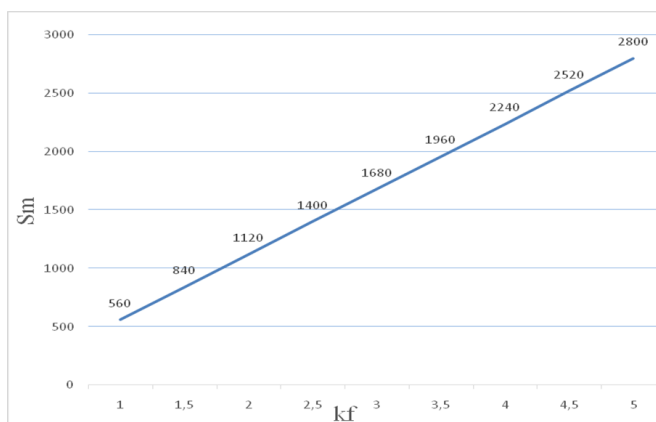


Figure 8

Maximum thermal stress amplitude generated during thermal shock as a function of stress concentration factor

Source: own elaboration

The determination of the value of the maximum amplitude of the thermal stress generated during the thermal shock (Sm), is of great significance to have criteria about the appearance of cracks in the casing, if Sm is greater than Sa it implies that cracks will develop in the casing and due to the fact that the casing is subjected for intervals of time to this periodic stress, the cracks will propagate.

According to figure 5 for a stress concentrating factor (kf) of the order of 1, the value that reaches the maximum amplitude of the thermal stress generated during the thermal shock (Sm), is greater than Sa , therefore, this justifies the appearance of cracks both transversely and longitudinally.

Conclusions

The following conclusions have been drawn from the work:

Through the microstructural and chemical composition characterisation it was determined that the casing material corresponds to a cast iron with inclusion of nodular graphite and ferritic matrix.

The magnitude of the maximum amplitude of the thermal stress produced by the thermal shock generates cracks in the casing and due to the fact that the magnitude of this stress is also periodic, the phenomenon of thermal fatigue appears, bringing as a consequence the propagation of the cracks, i.e. the fundamental cause of the cracking in the casing is due to the thermal shock and thermal fatigue.

The maximum thermal stress amplitude generated during thermal shock (Sm), for the carcass under study, reaches a maximum value of 560 MPa for a stress concentration factor ($kf=1$).

As the magnitude of Sm (560 MPa) is much larger than Sa (210 MPa) and the carcass is periodically stressed, this justifies the crack propagation.

In the section of the shell where there is a higher stress concentration factor (kf), the probability of crack emergence is higher, due to the high stresses created in that area.

Conflict of interest

The authors declare that they have no conflicts of interest. They have no financial interests or personal relationships that could have influenced this book.

Authors' contribution

Patino-Carachure contributed to the writing analysis of the characterisation by optical microscopy,

Alvarez-García contributed to microstructural and metallographic analysis.

Duffus to microstructural and metallographic chemical analysis, PhD Machado to non-destructive testing.

Availability of data and materials

Data are available on request at: aduffus@uclv.edu.cu

Acknowledgements

To the Empresa Planta Mecánica de Santa Clara, Villa Clara, Cuba, to the Centro de Investigación de Soldadura de la UCLV, Santa Clara, Villa Clara, Cuba, to the Tribology and Materials Engineering Laboratory of the Universidad Tecnológica De Campeche (UTCAM), to the Metallurgy and Corrosion Laboratory of the Universidad Tecnológica De Campeche (UTCAM). Metallurgy and Corrosion Laboratory, Faculty of Engineering UNACAR, Welding Research Centre - Metallographic analysis and non-destructive testing.

Abbreviations

s_m : maximum thermal stress amplitude generated during thermal shock.
 E: modulus of elasticity
 α : coefficient of thermal expansion.
 ΔT_m : maximum possible magnitude of thermal shock.
 n: Poisson's coefficient
 kf: stress concentration factor

References

Background

García-Lira J., Castillo Sánchez M. D., Arenas Romero J. J. (2019). [Benefits of austempered nodular iron \(ADI\) in the manufacture of parts.](#) Memorias del Congreso Científico Tecnológico de las carreras de Ingeniería Mecánica Eléctrica, Industrial y Telecomunicaciones, sistemas y electrónica. YEAR 4. No. 4.

GOST3443 -87 (2005). [Cast iron castings with graphite of different form. Methods of structure determination.](#)

Laustela, E. (2005). [The ABB turbocharger for increasing engine power and performance.](#) ABB Magazine (3): 58-62.

Planned Preventive Maintenance. EMGEF. Technical paper, Santa Clara, (2014).

Mellouli, D., et al. (2011). ['Thermal fatigue of cast irons for automotive application.'](#) Materials & Design 32(3): 1508-1514.

Rodriguez, L. A. M. (2019). [Methodology for the reconditioning by welding of turbine casings of turbochargers of Generator Sets.](#) Mechanical Engineering Project III, UCLV, Santa Clara, Villa Clara, Cuba.

Basic and support

Aguilar R. R.A, Celada E.R, Bonilla C. BJ. (2020). [Weldability of grey iron, nodular iron and A304 stainless steel castings.](#) Journal of the School of Graduate Studies, Vol. 11 No. 1.

ASME (2010). ['Rules for construction of Pressure Vessels.'](#) An International Code VIII Division 2: 998.

ASTM E3-11 (2011). [Standard Guide for Preparation of Metallographic Specimens.](#)

ASTM E340-15 (2015). [Standard practice for macroetching metals and alloys.](#)

ASTM E407-07(2015)e1. [Standard Practice for Microetching Metals and Alloys.](#)

ASTM A536-84(2019)e1. [Standard Specification for Ductile Iron Castings1.](#)

CIS- MET-027, (2002). Procedure for observation of specimens by optical microscopy. Welding Research Centre (CIS-UCLV), Santa Clara.

Spectrograph Manual, Mechanical Plant, Santa Clara, Cuba, (2015).

Differences

Callister. D. W. (2015). ['Introduction to Materials Science and Engineering'.](#) Department of Materials Science and Emgineering the University of Utah." Editorial Reverté, S.A.

Guliaev, A.P. (1987). [Metallography Volume 2, Russia Ed. MIR.](#)

Structural modeling of steel profiles to infer preventive maintenance in educational infrastructure

Modelado estructural de perfiles de acero para inferir mantenimiento preventivo en infraestructura educativa

Gutiérrez-Can, Yuriko^a, Palemón-Arcos, Leonardo^b, Naal-Pech, José Wilber^c and Álvarez-Arellano, Juan Antonio^d

^a  Universidad Autónoma del Carmen •  KHW-2340-2024 •  0000-0001-6358-2130 •  798108

^b  Universidad Autónoma del Carmen •  KHW-2160-2024 •  0000-0001-9743-0434 •  49334

^c  Universidad Autónoma del Carmen •  KHW-2538-2024 •  0009-0006-2955-0382 •  1231951

^d  Universidad Autónoma del Carmen •  JRX-8666-2023 •  0000-0001-6341-417X •  273636

CONAHCYT classification:

DOI: <https://doi.org/10.35429/H.2024.13.56.66>

Area: Engineering

Field: Engineering

Discipline Mechanical Engineering

Subdiscipline: Planning

Key Handbooks

The contribution will be in two aspects: engineering and academic. The first will contribute to show the engineering rehabilitation of the entire structure deteriorated by corrosion. In the academic environment, it will contribute to the methodology to infer the behaviour or performance based on the current regulations governing this type of structure. The methodology for the rehabilitation of the entire structure deteriorated by corrosion of all the profiles. According to the current condition with deterioration, the structure does not comply with the two limit states, understanding that a limit state of behaviour is reached in a construction when a combination of forces, displacements, fatigue levels, or several of them, that determines the beginning or the occurrence of an unacceptable behaviour mode of said construction.

Citation: Gutiérrez-Can, Yuriko, Palemón-Arcos, Leonardo, Naal-Pech, José Wilber and Álvarez-Arellano, Juan Antonio. 2024. Structural modeling of steel profiles to infer preventive maintenance in educational infrastructure. 56-66. ECORFAN.

*✉ [doc-034@itsperote.edu.mx]

Handbook shelf URL: <https://www.ecorfan.org/handbooks.php>



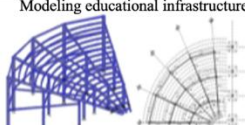
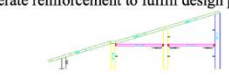
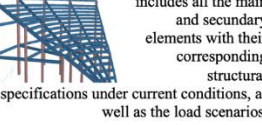
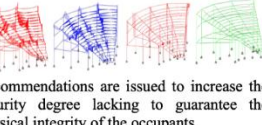
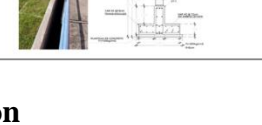
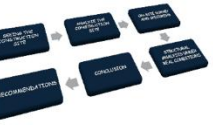
ISBN 978-607-8948-51-2 ©2009 The Authors. Published by ECORFAN-Mexico, S.C. for its Holding Mexico on behalf of Handbook HRPG. This is an open access chapter under the CC BY-NC-ND license [<http://creativecommons.org/licenses/by-nc-nd/4.0/>]

Peer Review under the responsibility of the Scientific Committee MARVID®- in contribution to the scientific, technological and innovation Peer Review Process by training Human Resources for the continuity in the Critical Analysis of International Research.



Abstract

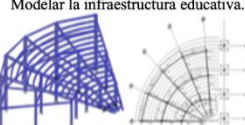
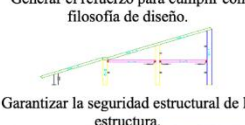
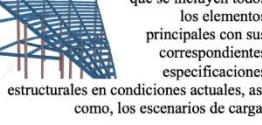
The useful life of an infrastructure depends on the preventive maintenance provided during its use, however, abandonment due to various situations accelerates the deterioration of the elements that comprise it, so it is necessary to rehabilitate them by carrying out mandatory modeling and simulation in the real conditions in which the structure is located. Therefore, this work shows the modeling under real corrosion conditions of structural profiles that make up the support system of the steps of a stadium. It is determined that all the structural elements that make up the educational infrastructure require reinforcements due to the reduction in thickness due to corrosion, this is because the portable capacity of the stadium is reduced.

Structural modeling of steel profiles to infer preventive maintenance in educational infrastructure		
Objectives	Methodology	Contribution
 <p>Modeling educational infrastructure.</p> <p>Obtaining responses at the level of forces and displacements.</p>  <p>Generate reinforcement to fulfill design philosophy.</p>  <p>Guarantees the structural safety of the structure.</p> 	<p>The physical survey is carried out considering deterioration due to corrosion of structural profiles.</p>  <p>The three-dimensional structural model is generated, which includes all the main and secondary elements with their corresponding structural specifications under current conditions, as well as the load scenarios.</p>  <p>The analysis is carried out to understand the structural dynamic behavior of the educational infrastructure.</p>  <p>Recommendations are issued to increase the security degree lacking to guarantee the physical integrity of the occupants.</p> 	<p>The contribution will be in two aspects: engineering and academic.</p> <p>The first will contribute to showing the best option engineering and structural to reinforce the infrastructure and deteriorated with expired useful life.</p> <p>In the academic environment, the methodology to infer behavior is contributed based on the current regulations that govern this type of structures.</p> 

Structural steel, Maintenance, Rehabilitation

Resumen

La vida útil de una infraestructura depende del mantenimiento preventivo que se brinde durante su uso, sin embargo, el abandono por diversas situaciones acelera el deterioro de los elementos que lo conforman, por lo que es necesario rehabilitarlas realizando obligatoriamente una modelación y simulación en las condiciones reales en la que se encuentra la estructura. Por tanto, el presente trabajo, muestra el modelado bajo condiciones reales de corrosión de perfiles estructurales que integran al sistema de soporte de las gradas de un estadio. Se determina que todos los elementos estructurales que integran la infraestructura educativa requieren refuerzos por la reducción de espesor por corrosión, esto debido a que se reduce la capacidad portante del estadio.

Modelado estructural de perfiles de acero para inferir mantenimiento preventivo en infraestructura educativa		
Objetivos	Metodología	Contribución
 <p>Modelar la infraestructura educativa.</p> <p>Obtener respuesta a nivel de fuerzas y desplazamientos.</p>  <p>Generar el refuerzo para cumplir con filosofía de diseño.</p>  <p>Garantizar la seguridad estructural de la estructura.</p> 	<p>Se realiza el levantamiento físico considerando deterioro por corrosión de perfiles estructurales.</p>  <p>Se genera el modelo estructural tridimensional en el que se incluyen todos los elementos principales con sus correspondientes especificaciones estructurales en condiciones actuales, así como los escenarios de carga.</p>  <p>Se realiza el análisis para conocer el comportamiento dinámico estructural de la infraestructura educativa.</p>  <p>Se emiten recomendaciones para incrementar el grado de seguridad faltante para garantizar la integridad física de los ocupantes.</p> 	<p>La aportación será en dos aspectos: ingenieril y académica.</p> <p>La primera contribuirá en mostrar ingenierilmente la rehabilitación de toda la estructura deteriorada.</p> <p>En el ambiente académico se contribuirá en la metodología para inferir el comportamiento o desempeño con base a la normatividad vigente que rigen a este tipo de estructuras.</p> 

Acero estructural, Mantenimiento, Rehabilitación

Introduction

Human beings are constantly looking for comfort, protecting themselves from the harmful conditions generated by nature, and that with engineering this comfort is provided by taking care of the physical integrity of the structure with a reasonable safety factor ranging from 1.5 to 3.0 ensuring that the probability of structural failure is low (Van *et al.*, 2024). In addition, working together with other specialties confirms that the structure is safe, functional, economical and without visual contamination with the trajectory and intervention of professionals according to the phases of the work, as shown in **Figure 1**.

Box 1

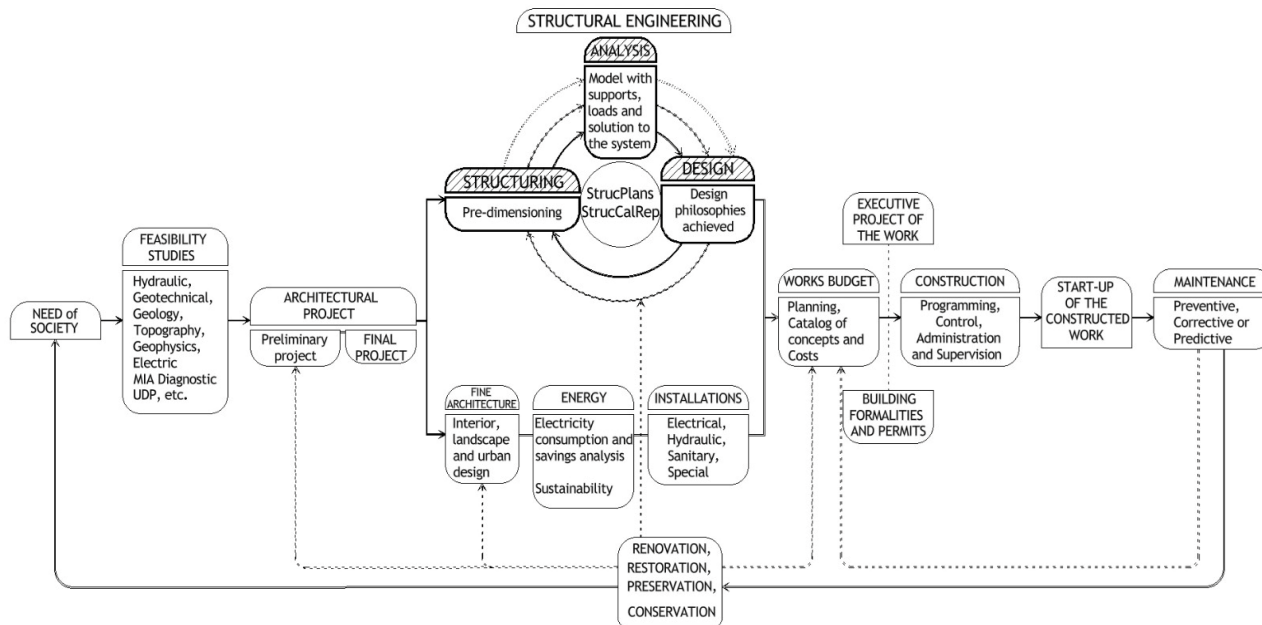


Figure 1

Trajectory of any project

It should be noted that every project is triggered by a need to provide a service to society, carrying out prior studies to assess feasibility. In addition, it is noted that at the end of construction, maintenance is required, where preventive maintenance aims to maintain the normal operation of equipment and assets, avoiding costly downtime due to unexpected failures (Sun *et al.*, 2022).

It is also noted in **Figure 1** that the project cycle includes refurbishment, so it is important to emphasise that refurbishment is an essential part of system resilience, and it is natural to adopt resilience measures in maintenance planning throughout the educational building where financial, human, material and time resources are very limited. In addition, resilience comprises three main capacities: absorption, adaptation and restoration (Sun *et al.*, 2022), however, to maintain the initial load capacity must be rehabilitated by placing reinforcements based on the results obtained, this because the infrastructure is located in Ciudad del Carmen Campeche, which is an island bordering the Gulf of Mexico (Fuentes *et al.*, 2018), so engineers who build, design and provide maintenance to the infrastructure in this area, we must consider the local conditions that prevail in the environment, which is an aggressive environment. That is to say, in this area the corrosion of steel elements is imminent, due to the high concentration of salts in the environment. For this reason, although at a global level steel is an ideal element to accelerate the construction process, the materials degrade gradually and constantly if it does not have the initial corrosive protection during its useful life. In addition to the above, approximately 360 km away is the border where the interaction of two tectonic plates is present: Cocos and North American, where seismic movements are generated and can cause weakened or degraded structures to collapse due to corrosion.

Therefore, this work shows the methodology applied to arrive at the necessary reinforcements by generating the modelling, simulation and analysis with specialised software. Furthermore, once the basic loads have been estimated, as well as the scenarios or combinations of them, the behaviour under real conditions is inferred in order to detect the weak profiles. Subsequently, a conclusion and recommendations are made to guarantee structural safety.

Methodology

Corrosion affects structural profiles including welded joints ([Yelamasetti et al., 2024](#)), especially when these profiles were subjected to high temperatures when welded and were not immediately protected or retouched by anti-corrosion processes, so that over time the element accumulates rust until the core, connections, or the fundamental parts of the structure are calcined. That is, having the elements outdoors, as well as exposed to the accumulation of water or runoff in areas of difficult intervention deteriorates and weakens structurally, however, at first glance you can not infer the decline of the structural capacity, so the following methodology should be used: visit the site in question of educational infrastructure, physical survey of the structure, collation of initial engineering, modelling and simulation in real conditions and finally issue recommendations to ensure the physical integrity of the work. As a fundamental part is the simulation, which [Daou et al., \(2019\)](#) indicates that simulation is one of the most applicable techniques used in cases where it is difficult to solve an equation analytically.

The phases of the project in question described in this section are described in detail. As a first step, a tour of the site is carried out to identify the needs of the project to be rehabilitated, verifying the degree of deterioration in corrosion in which the work is located. Subsequently, the dimensions or characteristics of the current state are taken, removing the paint and loose rust resulting from oxidation.

Next, the work is analysed by comparing the final plans with the existing ones, i.e. the specifications are studied with the data collected on site as a result of the initial execution of the project using as-build plans and, in general, the hidden defects on site, complementing the missing information. It is concluded from this stage that the plans do not coincide with what was built.

The structural model is elaborated considering joints, boundary conditions, basic loads and their combinations to infer the behaviour in the worst case scenarios.

In this work, three categories of loads will be considered according to the duration in which they act on the structures with their maximum intensity: permanent, variable and accidental.

Permanent actions are defined as those that act continuously on the structure and whose intensity varies little over time ([NTC, 2023](#)). The main actions that belong to this category are: dead load, static thrust of soils, liquids, deformations and displacements imposed on the structure that vary little over time, such as those due to prestressing or permanent differential movements of the supports. **Table 1** shows the loads of this item in which the weight of all the construction systems and finishes are considered, while the self-weight of the beams and columns will be generated within the specialised software through the ‘selfweight’ command.

Box 2

Table 1

Dead loads of education infrastructure

No.	Construction system	Magnitude (kg/m ²)
1	Galvadeck 25 gauge 22 with 6cm compression layer.	220
2	Finished floor finish	120
3	Installations, ducts and soffits	45
4	Regulatory additional weight	40
Total		425 kg/m²

Variable actions are those that act on the structure with an intensity that varies significantly with time ([NTC, 2023](#)). The main actions that fall into this category are: live load; temperature effects; imposed deformations and differential subsidence that have a time-varying intensity; and actions due to the operation of machinery and equipment, including dynamic effects that may occur due to vibration, impact or braking. **Table 2** shows the loads of this item in which three types are considered: maximum (W_m), instantaneous (W_a) and average (W).

Box 3

Table 2

Live loads of education infrastructure in kg/m²

Destination of floor or roof	W	Wa	Wm
Stadiums and venues without individual seating	40	350	450

Source: NTC, 2023

The maximum live load **Wm** should be used for structural design for gravity forces and for calculation of immediate settlements in soils, as well as for structural design of foundations for gravity loads; the instantaneous load **Wa** should be used for design for accidental loads, such as earthquake or wind, and when checking load distributions more unfavourable than uniformly distributed over the whole area, and the mean load **W** should be used in the calculation of deferred settlements and for the calculation of deferred deflections.

Accidental actions are those which are not due to the normal operation of the building and which can reach significant intensities only for short periods of time. This category includes: seismic actions; wind effects; hail loads; effects of explosions, fires and other phenomena that may occur in extraordinary cases. It will be necessary to take precautions in the structures, in their foundations and in the construction details, to avoid catastrophic behaviour of the structure in the event of these actions occurring. In the case of the present work, the load generated by earthquakes (CFE, 2015) will be estimated using the prodisis using the site location described in the introduction section, while the wind load will be estimated using the wind system software (CFE, 2020) of the National Institute of Electricity and Clean Energy (ntc).

When the description of the behaviour of a structural system is required, the formulation of a mathematical model is used (Sarah *et al.*, 2020). This formulation is done by means of equations that reflect the properties, geometry, materials and the interaction between the elements. Different sets of equations then appear that can be related to each other to achieve the final formulation. The model with basic loads and load scenarios, from which results of the behaviour of the structure under real conditions will be obtained, and recommendations will be issued to address the findings.

The physical and mechanical characteristics of the existing profiles in the project are shown in **Table 3**, in which the safety assessment and reliability analysis of a structure as a function of time depends mainly on the corrosion model, which directly affects the accuracy of the calculation (Wu *et al.*, 2021). Destructive testing yielded an $f_y = 3,314.08 \text{ kg/cm}^2$ and $E = 2,039.432 \text{ kg/cm}^2$, the magnitude of which was reliably generated (Kostic *et al.*, 2022).

Box 4

Table 3

Specifying the profiles that make up the infrastructure

ID	Structural profile	Specification
C-1	OC-508 mm x 12.7 mm	A-500 Gr. B
C-2	OC-406 mm x 12.7 mm	A-500 Gr. B
TR-1	IR-356 mm x 50.7 kg/m	A-572 Gr. 50
L-1	IR-254 mm x 32.8 kg/m	A-572 Gr. 50

Results

As shown in **Figure 1**, it can be observed that the analysis includes three phases, which consists of a numerical procedure or mathematical formulation whose fundamental objective is the determination of forces or stresses, displacements or deformations of a structure subjected to loads and their combinations, while the structural design involves the selection of the material, the dimensioning of the components of the structural system that allows it to adequately and rationally support the acting forces, in order to fulfil the function for which it was conceived. Although these two aspects of structural engineering are often studied in separate courses, in professional practice they are strongly linked and are carried out through iteration until a project that complies with the design philosophy is achieved.

The structural analysis and design of this project covers a section of the stadium, from the foundations to the stands. All the elements that make up the stadium system such as the footings, steel slab system and stands including the beams and columns will be designed in accordance with AISC-ASD ([AISC, 1989](#)). The strength will be obtained by means of the computer aided linear analysis, Staad-Pro, and therefore the value judgement regarding the structural behaviour of the elements that make up the stadium required to fulfil the objective entrusted by the client will be obtained from the result obtained.

In its initial stage, the analysis of a structure is detonated from the knowledge of the preliminary dimensions of all its elements ([Tahir & Ghafoor, 2023](#)). This preliminary design is often based on a more or less crude or simple analysis, and is influenced by the engineer's experience and judgement. Having determined an initial set of member sizes, a more detailed analysis can be made to determine forces and displacements using equilibrium, kinematic, constitutive and compatibility equations. Equilibrium equations establish relationships between the forces acting on the system and can be classified into static and dynamic. Kinematic equations relate displacements to deformations, constitutive equations relate stresses to deformations and compatibility equations relate deformations to displacements ([Chen et al., 2005](#)). **Figure 2** shows the axial load resulting from the loading scenarios, where the red lines represent compression and the blue lines represent tension.

Box 5

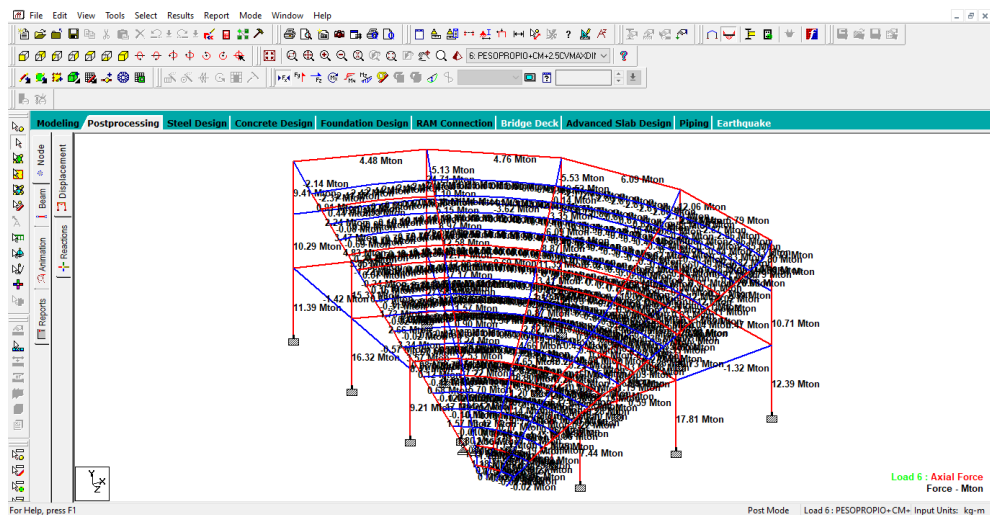


Figure 2

Maximum axial load, 47.6 ton

Figure 3 shows the shear force diagram produced by the load scenarios, which is a graph that shows the behaviour of the internal force of the beams produced by the effects of the external forces over their entire length ([Hibbeler, 2012](#)). When modelling a structure, the geometry, the type of material and the acting loads with their critical scenarios are defined a priori. The definition of the geometry includes specifying at which points and in which degrees of freedom the value of the displacement is known, in this case referring to the supports, this being defined as everything in which the value taken by one or more of its degrees of freedom is known, i.e. every point of known displacement is called a support. This value may be zero or non-zero.

Box 6

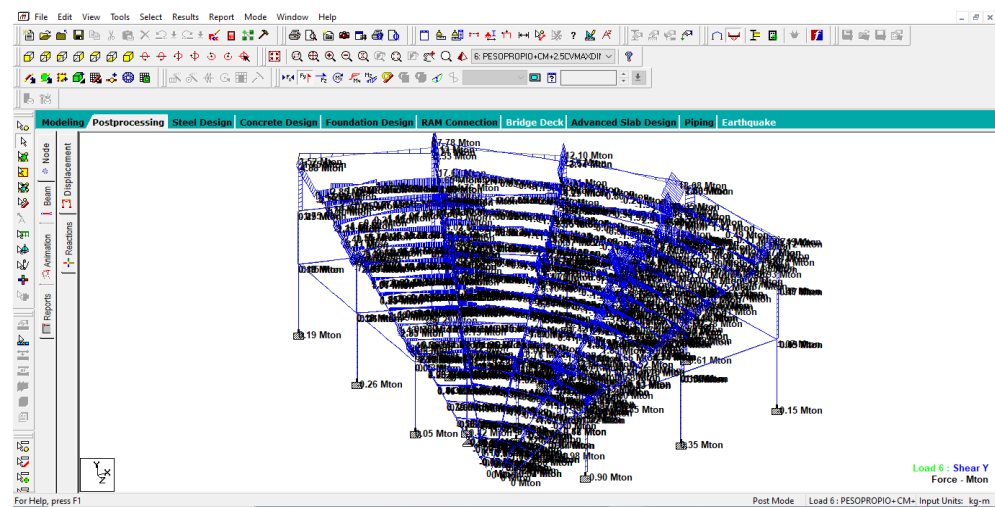


Figure 3

Maximum shear, 24.30 ton

Figure 4 shows the bending moment diagram resulting from the loading scenarios. This graph represents the moment produced due to external loads (Kassimali et al., 2015).

Box 7

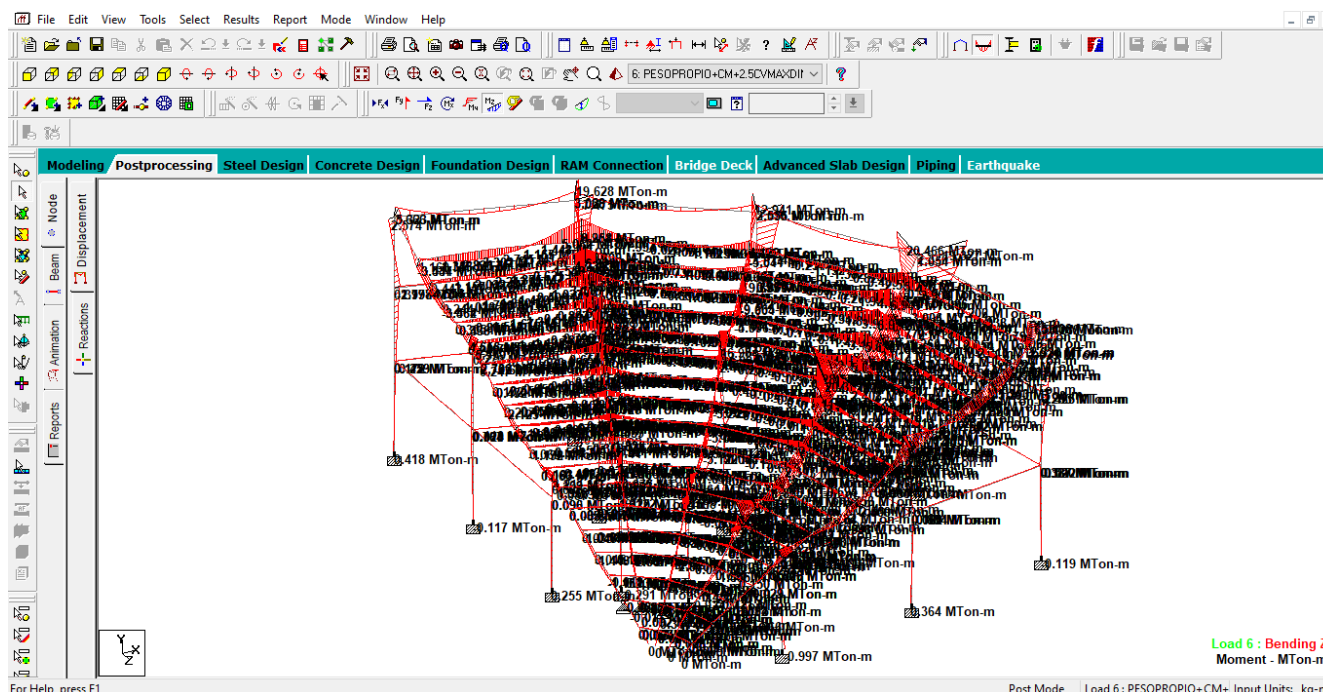
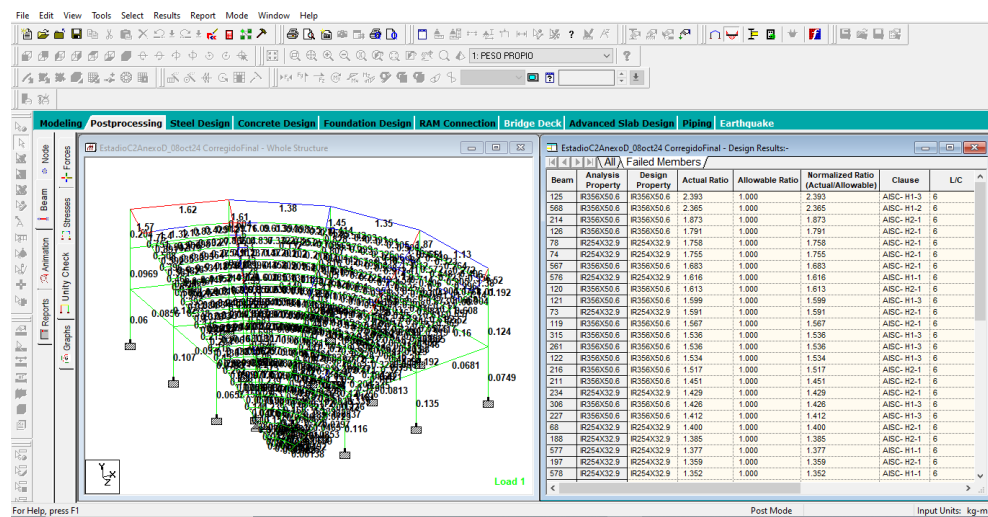


Figure 4

Maximum bending moment, 24.90 ton-m

Figure 5 shows the interaction ratio in which the ultimate acting magnitude is divided by the resistance. Note that it exceeds the optimum magnitude of 0.8, which implies that in a deteriorated state it needs to be strengthened.

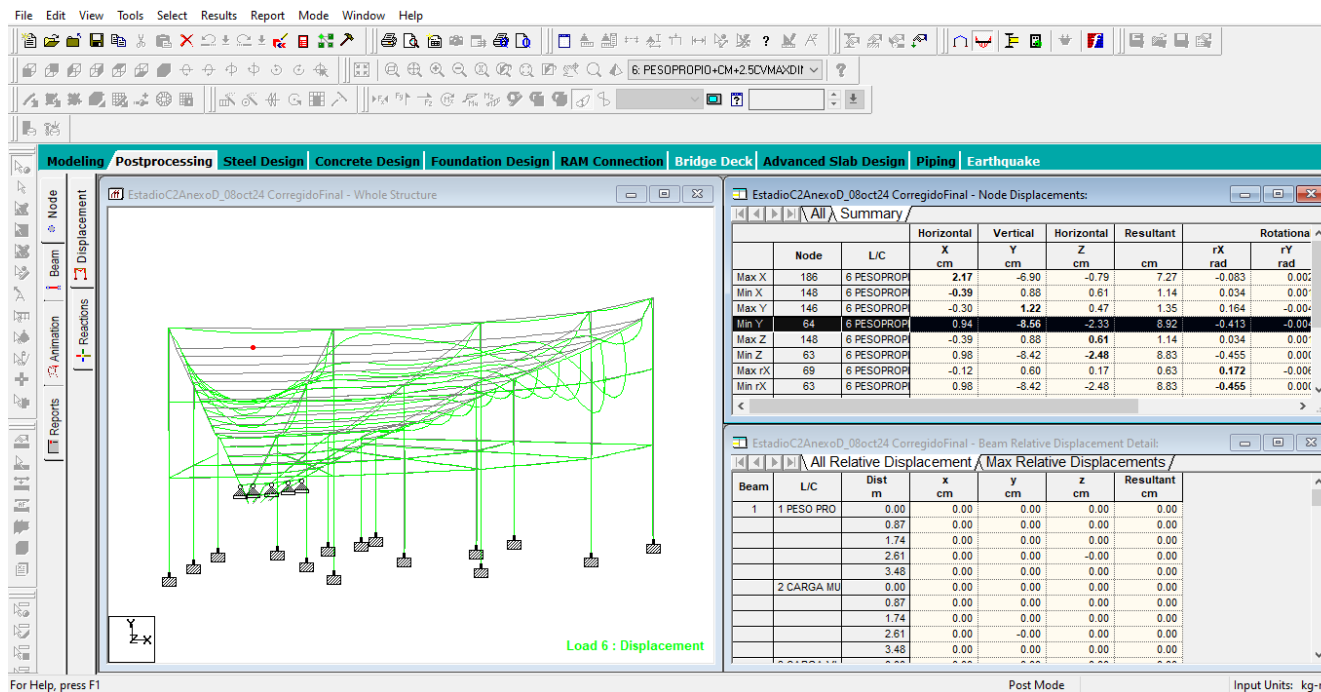
Box 8

**Figure 5**

Failure limit state, 2.93

Figure 6 shows the maximum deformation in the structure. It is observed that a maximum magnitude of 8.92cm is present, which exceeds the tolerance, which should be reinforced to ensure structural safety.

Box 9

**Figure 6**

Serviceability limit state, 8.92 cm

Conclusions

When generating results, it is concluded that the structure does not comply with the limit states, understanding that a limit state of behaviour is reached in a construction when a combination of forces, displacements, fatigue levels, or several of them, which determines the onset or occurrence of an unacceptable behaviour mode of such construction, is present (NTC, 2023). According to the Regulation, such limit states are classified into two groups: failure limit states and serviceability limit states. The former involve the occurrence of behavioural modes that endanger the stability of the construction or part of it, or its ability to resist new load applications. The latter include economic damage or the occurrence of conditions that prevent the proper performance of the functions for which the construction was designed, resulting in a result shown in equation [1]:

$$\Delta_{\max} = \frac{L}{240} = \frac{551 \text{ cm}}{240} = 2.30 \text{ cm} \quad [1]$$

It is recommended to reinforce the structure at the points shown in Figure 7.

Box 10

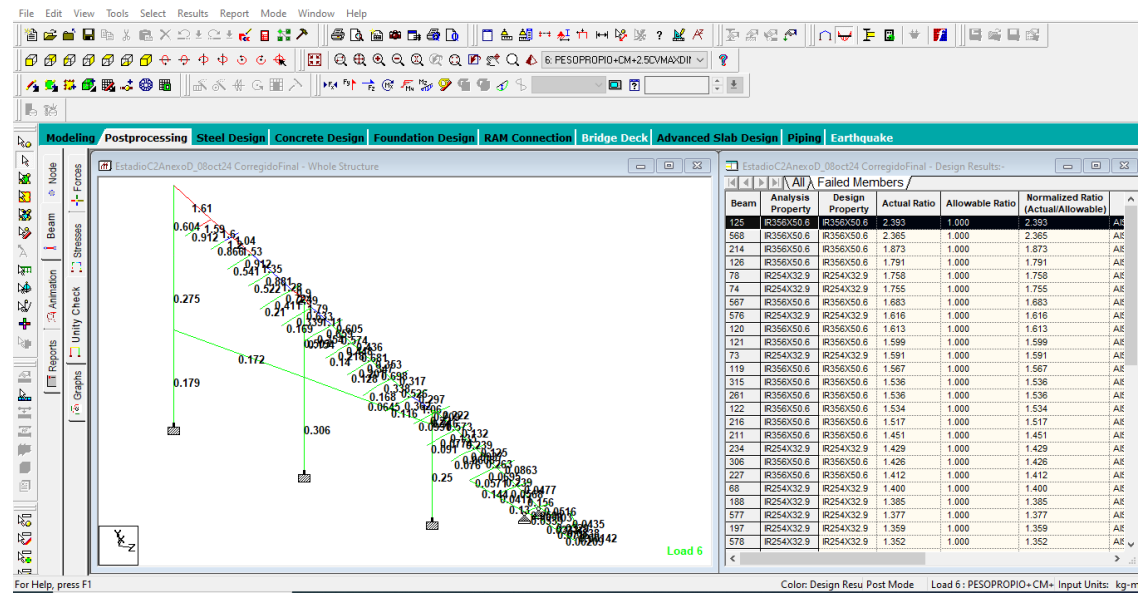


Figure 7

Recommended reinforcement

Annexes

Declarations

Conflict of interest

The authors declare that they have no conflicts of interest. They have no financial interests or personal relationships that could have influenced this book.

Authors' contribution

The contribution of each researcher to each of the points developed in this research is:

Gutierrez-Can, Yuriko: Contributed to the data collection and as-built drawings analysis.

Palemón-Arcos, Leonardo: Carried out the modelling, simulation, analysis and structural design.

Naal-Pech, José Wilber: Contributed to the determination of thicknesses of profiles damaged by corrosion.

Álvarez-Arellano, Juan Antonio: Contributed in data processing and application technique.

Availability of data and materials

The data obtained in this research is available at any time it is required.

Funding

This research did not receive any funding.

Acknowledgements

The authors, Yuriko Gutiérrez-Can, Leonardo Palemón-Arcos, José W. Naal-Pech and Juan Antonio Álvarez Arellano, gratefully acknowledge the support of the Consejo Nacional de Humanidades, Ciencias y Tecnologías (CONAHCYT), as well as the Programa para el Desarrollo Profesional Docente (PRODEP) through the Grupo Disciplinar Ingeniería Estructural Aplicada e Ingeniería de la Construcción y sus Procesos Sustentables provided through the Universidad Autónoma del Carmen (UNACAR).

Abbreviations

CFE	Federal Electricity Commission
INEEL	National Institute of Electricity and Clean Energies (Instituto Nacional de Electricidad y Energías Limpias)
NTC	Complementary Technical Standards
W	Average load
Wa	Instantaneous load
Wm	Maximum gravitational load

References

Background

AISC Manual Committee, & American Institute of Steel Construction (1989). *Manual of Steel Construction: Allowable Stress Design*. American Institute of Steel Construction.

Fuentes, J. C. N., Granados, P. A., & Martins, F. C. (2018). Integrated coastal management in Campeche, Mexico; a review after the Mexican marine and coastal national policy. *Ocean & coastal management*, 154, 34-45.

Tahir, F., & Ghafoor, L. (2023). *Structural Engineering as a Modern Tool of Design and Construction* (No. 10051). EasyChair.

Chen, W. F., & Lui, E. M. (2005). *Handbook of structural engineering*. CRC press.

Basics

Sun, H., Yang, M., & Wang, H. (2022). *Resilience-based approach to maintenance asset and operational cost planning*. Process Safety and Environmental Protection, 162, 987-997.

Hibbeler, R. C. (2012). *Structural analysis*. Pearson Mexico.

Kassimali, A., Galán, A. A. A. A., & Mellado, J. F. H. (2015). *Análisis estructural*. Cengage Learning.

Support

Van Coile, R., Jovanović, B., Put, F., (2024). Reliability-based safety format for structural fire engineering - Derivation based on the most likely failure point, Journal of Infrastructure Intelligence and Resilience.

NTC, D. (2023). Complementary technical standards on criteria and actions for the structural design of buildings. *Official Gazette of Mexico City, CDMX*.

CFE. (2020). **Manual de Obras Civiles de Comisión Federal de Electricidad, Diseño por Viento.** (MOC-CFE-DV-2020), Instituto de Investigaciones Eléctricas, Cuernavaca, Morelos; Mexico.

CFE. (2015). **Manual de Obras Civiles de Comisión Federal de Electricidad, Diseño por Sismo.** (MOC-CFE-DS-2015), Instituto de Investigaciones Eléctricas, Cuernavaca, Morelos; Mexico.

Wu, H., Lei, H., & Frank, C. Y. (2021). Study on corrosion models of structural steel exposed in urban industrial atmospheric and laboratory simulated environments based on the 3D profile. *Thin-Walled Structures*, 168, 108286.

Sarath, C. V. K., Kumar, K. A., Lingeshwaran, N., VigneshKannan, S., & Pratheba, S. (2020). Study on analysis and design of a multi-storey building with a single column using STAAD. Pro. *Materials Today: Proceedings*, 33, 728-731.

Kostic, S., Milojkovic, J., Simunovic, G., Vukelic, D., & Tadic, B. (2022). Uncertainty in the determination of elastic modulus by tensile testing. *Engineering science and technology, an international journal*, 25, 100998.

Differences

Yelamasetti, B., Sonia, P., Aslesha, C. L., Vardhan, V., Ahmed, F., Kumar, A., ... & Alnaser, I. (2024). Investigations on corrosion rate, mechanical properties and structural homogeneity of interpulse TIG dissimilar weldments. *Journal of Materials Research and Technology*, 32, 2537-2546.

Discussion

Daou, H., Raphael, W., Chateauneuf, A., & Geara, F. (2019). Probabilistic Assessment of Structural Safety of Complex Structures-Application to Terminal 2E at Roissy, CDG Airport. *Procedia Structural Integrity*, 22, 17-24.

Thermal analysis of a single-cell PEM-type fuel cell with a coil as flow field architecture and its impact on cathode water formation

Análisis térmico de una monocelda de combustible tipo PEM con un serpentín como arquitectura de campo de flujo y su impacto en la formación de agua en el cátodo

Ceballos-Pérez, José^a, Ordóñez-López, Luis^{b*} and Sierra-Grajeda, Juan^c

^a ROR Centro de Investigación Científica de Yucatán • AFR-9015-2022 • 0000-0001-7529-0346 • 928198

^b ROR Centro de Investigación Científica de Yucatán • GRX-9836-2022 • 0000-0003-1110-1934 • 43804

^c ROR Universidad Autónoma del Carmen • LSK-8588-2024 • 0000-0002-0565-6450 • 219284

CONAHCYT classification:

DOI: <https://doi.org/10.35429/H.2024.13.67.75>

Area: Physics-Mathematics and Earth Sciences

Field: Physics

Discipline: Physical chemistry

Subdiscipline: Theory of fuel cells

Key Handbooks

The research carried out presents crucial contributions in the field of PEM fuel cells. The analysis of the thermal effects, especially on the formation of liquid water inside the cathode, is further explored, considering variables such as temperature and tortuosity. Increasing the operating temperature in a PEM cell significantly increases the water saturation in the cathode, which can negatively impact its electrochemical performance. Cells with lower tortuosity (1.5) are more efficient in water evacuation, which reduces saturation and improves performance, especially at higher temperatures. Conversely, higher tortuosity (2.5) results in higher water accumulation, which affects reagent diffusion and overall efficiency. As temperature increases, the difference in saturation between tortuosities is amplified, highlighting the importance of optimising the porous structure to avoid water blockages that compromise cell performance.

Citation: Ceballos-Pérez, José, Ordóñez-López, Luis and Sierra-Grajeda, Juan. 2024. Thermal analysis of a single-cell PEM-type fuel cell with a coil as flow field architecture and its impact on cathode water formation. 67-5. ECORFAN.

*✉ [lcol@cicy.mx]

Handbook shelf URL: <https://www.ecorfan.org/handbooks.php>



ISBN 978-607-8948-51-2 ©2009 The Authors. Published by ECORFAN-Mexico, S.C. for its Holding Mexico on behalf of Handbook HRPG. This is an open access chapter under the CC BY-NC-ND license [<http://creativecommons.org/licenses/by-nc-nd/4.0/>]

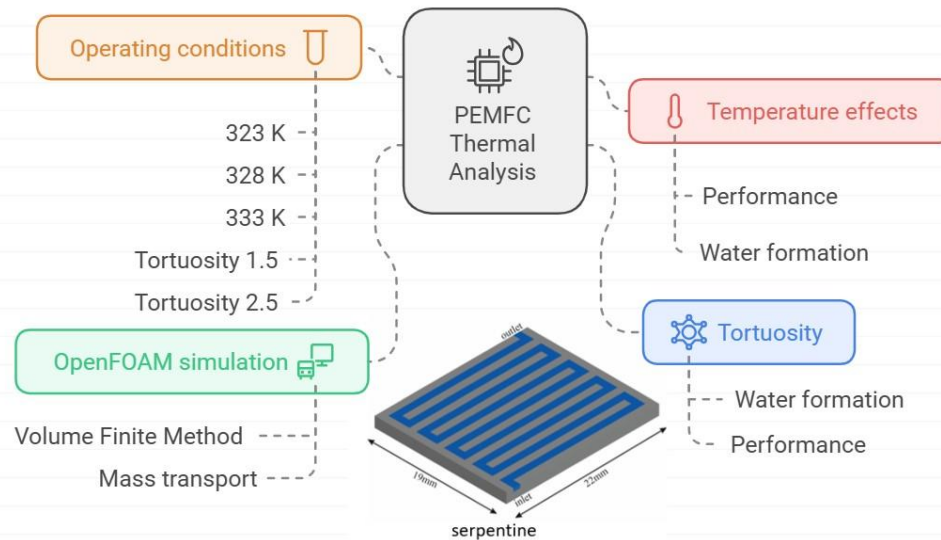
Peer Review under the responsibility of the Scientific Committee MARVID®- in contribution to the scientific, technological and innovation Peer Review Process by training Human Resources for the continuity in the Critical Analysis of International Research.



1702902 CONAHICYT

Abstract

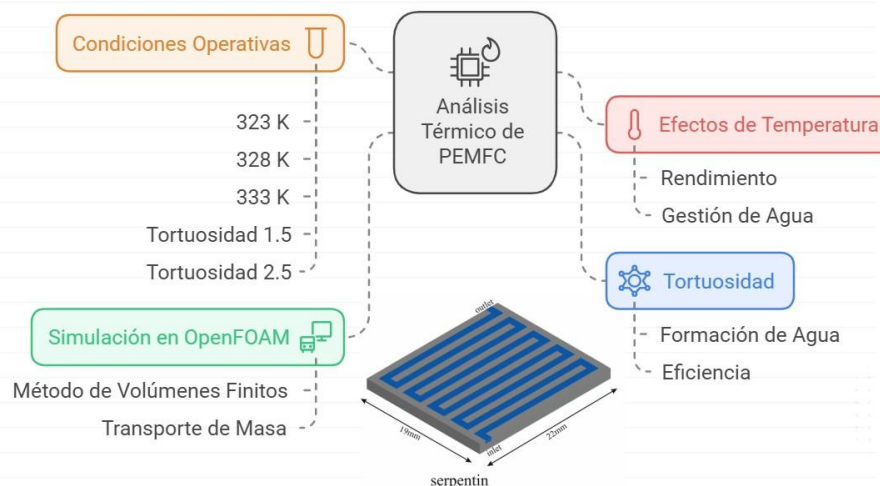
The thermal analysis of Proton Exchange Membrane Fuel Cells (PEMFC) is crucial for understanding how temperature impacts both electrochemical performance and water management, key aspects of their operation. This study focuses on evaluating the effect of thermal variations and tortuosity on liquid water formation in the cathode and its influence on overall efficiency. The thermal analysis considers the interaction between heat transfer, tortuosity due to porosity, and the presence of liquid water. To solve the governing equations of the system, the open-source software OpenFOAM, based on C++, is used with the Finite Volume Method (FVM). This approach allows for accurate modeling of thermal behavior and mass transport in the PEMFC. The study examines performance through polarization curves at three operational temperatures: 323, 328, and 333 K, combined with tortuosity values of 1.5 and 2.5. These variations help understand how tortuosity affects reactant and product transport, as well as water management and overall cell performance.



PEMFC, OpenFOAM, Tortuosity

Resumen

El análisis térmico en celdas de combustible tipo PEM (PEMFC) es crucial para entender cómo la temperatura afecta tanto el rendimiento electroquímico y la gestión de agua, un aspecto clave en su operación. Este estudio se enfoca en evaluar el impacto de las variaciones térmicas y la tortuosidad en la formación de agua líquida dentro del cátodo de la PEMFC y su efecto en su eficiencia global. Este análisis térmico considera la interacción entre la transferencia de calor, la tortuosidad debido a la porosidad y la presencia de agua líquida por su formación en el cátodo. Para resolver las ecuaciones gobernantes del sistema, se utiliza OpenFOAM (Open Field Operation and Manipulation), un software de código abierto basado en C++, empleando el Método de Volúmenes Finitos (FVM, por sus siglas en inglés). Este enfoque permite modelar con precisión el comportamiento térmico y el transporte de masa dentro de la PEMFC. El estudio analiza rendimiento de una PEMFC descrito por las curvas de polarización obtenidas bajo tres temperaturas operativas: 323, 328 y 333 K, combinadas con valores de tortuosidades de 1.5 y 2.5. Estas variaciones permiten entender cómo la tortuosidad afecta el transporte de reactivos y productos, así como el manejo del agua dentro de la celda, y su rendimiento global.



PEMFC, OpenFOAM, Tortuosidad

Introduction

The search for sustainable and clean energy sources has led to a growing interest in proton exchange membrane fuel cells (PEMFCs). These cells represent one of the most promising technologies for the highly efficient conversion of chemical energy from fuel into electrical energy, with low pollutant emissions and the ability to operate at relatively low temperatures. However, to maximise the performance of a PEMFC, it is crucial to thoroughly understand the factors that affect its operation, including thermal management and water dynamics within the system ([Shiva Kumar & Himabindu, 2019](#)).

Thermal analysis in PEMFCs is critical, as temperature has a significant impact on electrochemical performance. Improper temperature control can lead to problems such as decreased system efficiency, water accumulation in unwanted locations and, in extreme cases, damage to cell components. It is therefore critical to analyse how thermal variations affect not only the electrochemical reaction itself, but also water management, which is a crucial aspect for the optimal operation of these cells ([Yu et al., 2009](#)).

One of the key characteristics influencing the performance of PEMFCs is the tortuosity of the porous medium of the catalyst and diffuser layers. Tortuosity refers to the complexity of the path that the reactants and products must follow through the pores of the material, which affects the diffusion and, consequently, the efficiency of the electrochemical reactions. In this study, we seek to assess the impact of different levels of tortuosity on liquid water formation and overall cell efficiency. Understanding how tortuosity affects the transport of reactants and products is vital to improve water management, which in turn influences overall system performance ([Ceballos et al., 2022](#)).

The present study focuses on the use of OpenFOAM, an open source simulation software based on C++. This program is widely used in the scientific community to solve complex fluid and heat transfer problems through the Finite Volume Method (FVM). The choice of OpenFOAM allows accurate modelling of thermal behaviour and mass transport within the PEMFC. Using this approach, different scenarios considering both thermal variations and different tortuosity levels can be simulated, thus providing a robust framework for the analysis of cell performance.

In the research, simulations are carried out at three operating temperatures: 323 K, 328 K and 333 K. These temperatures represent a typical operating range for PEM fuel cells. The choice of these temperatures allows us to observe how the performance of the cell is affected by thermal changes, as well as by variations in tortuosity, which is analysed at two levels: 1.5 and 2.5. This work is based on a previous study ([Ceballos et al., 2024](#)), from which key information has been extracted for the methodology used in this analysis. In the previous work, the quality of the mesh was verified, all governing equations and their variables were defined, as well as the numerical method used.

Methodology

Domain

The study domain consists of a PEM-type single fuel cell with a serpentine flow channel design. This geometry was chosen because of its ability to improve reagent distribution and water management.

The study domain includes several key regions. The gas flow channel is the region where gaseous reagents, such as oxygen and hydrogen, are transported. The gas diffusion layer (GDL) consists of a porous material that facilitates the transport of these reactants to the catalytic layers, as well as allowing the evacuation of water produced during the reaction. The catalytic layer is the area where the electrochemical reaction that converts chemical energy into electrical energy takes place, while the membrane is responsible for transporting the protons from the anode to the cathode. The dimensions of the cell are as follows: the channel is 1 mm wide and 1 mm high. The thickness of the GDL is 200 μm , the thickness of the catalytic layer is 10 μm , and the thickness of the membrane is 50 μm .

The domain was discretised using the Finite Volume Method (FVM) in OpenFOAM, due to its ability to solve complex fluid dynamics and heat transfer problems. The meshing was performed with a structured approach, paying special attention to the refinement at the interfaces between the catalytic layer, the membrane and the GDL, where the highest concentration and thermal gradients occur. The quality of the meshing was verified in a previous work (Ceballos et al., 2024) where a mesh independence study was performed.

Governing equations

The governing equations (Table 1) describe the fundamental physical and chemical phenomena occurring inside a PEMFC. These equations allow representing the flow of reactants, heat transfer and species transport inside the cell, key elements to understand and predict its behaviour. The correct implementation of these equations is essential to determine the dynamics of the system, from the distribution of reactants and products in the flow channels and porous media, to the impact of temperature on the electrochemical performance. In addition, these equations help to model water formation and management, which is critical to avoid problems such as excessive accumulation at the cathode and to ensure efficient operation. Together, the governing equations provide the basis for accurately simulating cell performance under different operating conditions, facilitating the analysis of key variables for optimisation.

Box 1

Table 1

Main governing equations

Ecuación	Number
Continuity $\nabla \cdot (\rho_g \vec{U}_g) = -S_l$	[1]
Moment $\nabla \cdot (\rho_g \vec{U}_g \vec{U}_g) = -\nabla p_g + \nabla \cdot (\mu_g \nabla \vec{U}_g) + S_M$	[2]
Chemical species $\nabla \cdot (\rho_g \vec{U}_g y_i) = (\nabla \cdot \rho_g D_g^{eff} \nabla y_i)$	[3]
Energy $\nabla \cdot (\rho_{mix} C_{p_{mix}} \vec{U}_g T) = \nabla \cdot (k_{mix} \nabla T) + S_E^{reac} + S_E^{PC}$	[4]
Liquid water transport $\nabla \cdot (\rho_l D_l \nabla S) - \nabla \cdot (\rho_g \vec{U}_g S) = S_l$	[5]

Source: Own elaboration

In equation 5, the effective diffusion coefficient is defined as

$$D_g^{eff} = D_i^{bulk} f(\varepsilon) f(S) \quad [6]$$

Where the overall diffusion coefficient through the flow channel is expressed as binary diffusion for each component of the gas mixture is obtained by

$$D_i^{bulk} = 10^{-4} \times \frac{10^{-3} \times T^{1.75} \left(\frac{1}{M_j} + \frac{1}{M_i} \right)^{0.5}}{p \left[(v_j)^{\frac{1}{3}} + (v_i)^{\frac{1}{3}} \right]^2} \quad [7]$$

where M_i , M_j the molar masses and v_i , v_j species diffusion volumes. $f(\varepsilon)$ and $f(S)$ are the normalised porosity and saturation functions, respectively. These functions account for the tortuosity due to porous media and the presence of liquid water.

$$f(\varepsilon) = \left(\frac{\varepsilon - 0.037}{1 - 0.037} \right)^{0.661} \quad [8]$$

$$f(S) = (1 - S)^\tau \quad [9]$$

The term represents the tortuosity due to the presence of water in the porous medium. In this study, it is analysed with values of 1.5 and 2.5, by varying the initial simulation temperatures of 323, 328 and 333 K, to observe the impact of this parameter on the overall performance of the cell.

Numerical method.

OpenFOAM is used, solves the incompressible laminar Navier-Stokes equations using the Pressure Implicit with Splitting of Operator (PISO) algorithm and discretises the equations based on the finite volume method. The Preconditioned Bi-Conjugate Gradient Gradient (PBiCG) method was used to find convergence in the energy equation, and the Preconditioned Bi-Conjugate Gradient Stabilised Gradient (PBiCGStab) for other variables (continuity, momentum, species transport, energy and liquid water transport). For all variables, the convergence criterion was a residual of 1×10^{-9} .

Results

Data validation.

The validation of the simulation data was carried out in the previous study (Ceballos et al., 2024) where the independence of results was verified with the mesh and the construction of the polarisation curve of the coil-type geometry. The study was performed from 12,159 to 96,141 hexahedral elements analysing the values of maximum current densities, reaching mesh independence with 45,170 elements.

Impact of tortuosity on the maximum temperatures on the cathode side.

Figure 1 presents the initial operating temperatures of the cell, corresponding to 323 K, 328 K and 333 K; and the maximum temperatures reached at the cathode during operation. The two sets of data correspond to tortuosities of 1.5 and 2.5.

The results show that as the initial temperature increases, so does the maximum temperature at the cathode, reflecting an expected trend due to heat accumulation inside the cell during the electrochemical reaction. However, the tortuosity is observed to have a significant impact on the magnitude of the maximum temperature reached.

For a tortuosity of 1.5, the maximum cathode temperatures are lower compared to the values obtained for a tortuosity of 2.5. This can be explained by the fact that a higher tortuosity value increases the resistance to gas flow in the porous medium, which can lead to higher heat accumulation due to the difficulty in evacuating water and reaction products. In turn, the reduced efficiency of heat transfer to the surrounding regions contributes to a higher temperature rise at the cathode.

It is noticeable that the difference in the maximum temperatures between the two tortuosities widens as the initial temperature increases. For example, at 323 K, the difference between the maximum temperatures for tortuosities of 1.5 and 2.5 is relatively small; however, at 333 K, the difference is considerably larger. This suggests that the effect of tortuosity becomes more relevant as extreme thermal conditions increase within the cell, exacerbating the effects of thermal and water mismanagement in more tortuous media.

Impact of tortuosity on peak current density on the cathode side.

Figure 2 shows the relationship between the initial operating temperature of the cell and the maximum current density obtained at the cathode, with two data sets representing tortuosities of 1.5 and 2.5. The analysis reveals that, as the initial cell temperature increases, the maximum current density also increases, which is consistent with the general trend that higher temperatures favour electrochemical reactions by increasing the mobility of protons in the membrane and enhancing catalytic activity.

However, the tortuosity of the porous medium has a noticeable impact on the magnitude of the current density achieved. For the tortuosity of 1.5, it is observed that the cell achieves higher peak current densities compared to the tortuosity of 2.5. This is because a lower tortuosity favours the transport of reagents towards the catalytic layer, reducing the resistance to oxygen flow and improving the access of the reagents to the active site where the oxygen reduction reaction occurs at the cathode.

On the other hand, when the tortuosity is 2.5, a significant decrease in the peak current density is observed, which can be attributed to the fact that a more tortuous porous medium generates a higher resistance to the transport of reactants and products, limiting the efficiency of the electrochemical reaction. In addition, the accumulation of water in more tortuous media can clog porosity and gas channels, further affecting the availability of oxygen for the reaction.

Importantly, the effect of tortuosity is amplified at higher temperatures. At 333 K, the difference in peak current density between the 1.5 and 2.5 tortuosities is much more pronounced than at 323 K. This suggests that, at higher temperatures, the tortuosity effect is amplified. This suggests that, at higher temperatures, the transport capacity of the reagents becomes even more critical for electrochemical performance, highlighting the importance of optimising the structure of the porous medium to ensure efficient transport of oxygen and water within the cell

Box 2

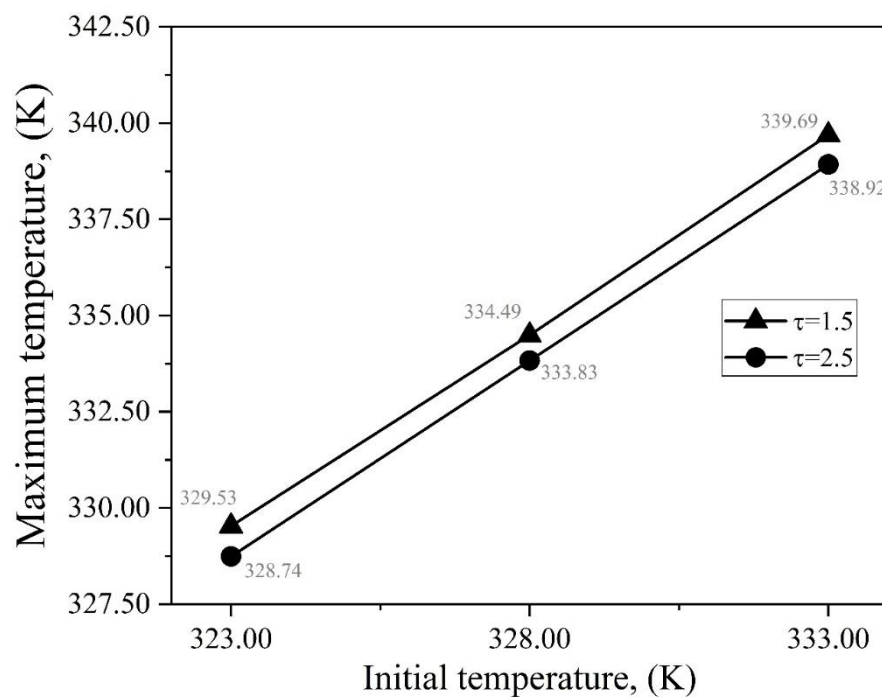


Figure 1

Effect of tortuosity on the maximum temperature gradients on the cathode side

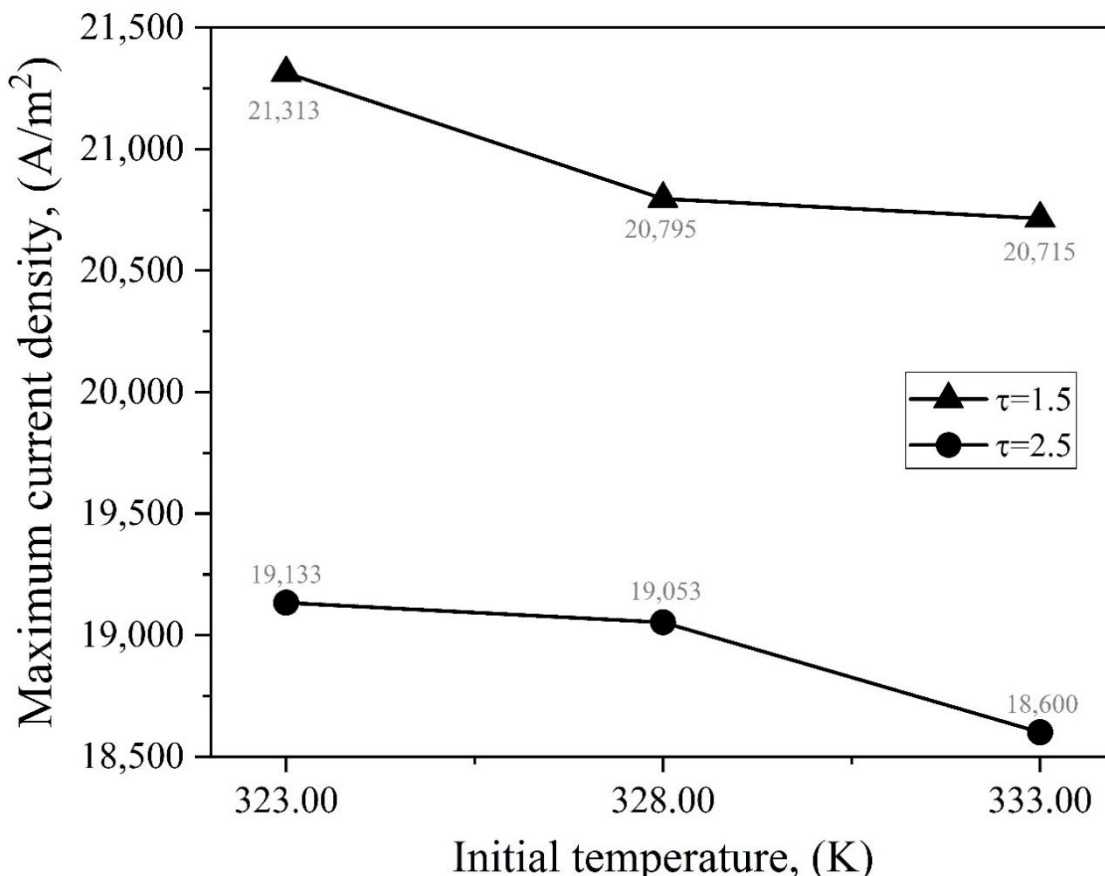
Source: Own elaboration

Impact of saturation on cathode side peak current density

The water saturation contours for the 1.5 and 2.5 tortuosities show how the water accumulation within the cell varies as both the operating temperature and the structure of the porous medium changes. As the temperature increases, a significant increase in saturation values is observed for both tortuosities, although this increase is more pronounced in the 2.5 tortuosity cell.

For the 1.5 tortuosity, the saturation values go from 0.34 at 323 K, to 0.38 at 328 K, and finally reach 0.71 at 333 K. This indicates that, although there is an increase in water accumulation at higher temperatures, the porous medium with lower tortuosity still allows a relatively efficient evacuation of the water generated during the electrochemical reaction.

On the other hand, the cell with a tortuosity of 2.5 shows slightly higher saturation values than the 1.5 tortuosity at all temperatures tested. At 323 K, the saturation is 0.36, increasing to 0.40 at 328 K and reaching a remarkable value of 0.79 at 333 K. This steeper increase in saturation as temperature increases highlights the limitations of a more tortuous porous medium to handle water transport. A tortuosity of 2.5 imposes greater resistance to water flow, leading to greater accumulation at the cathode, especially at elevated temperatures.

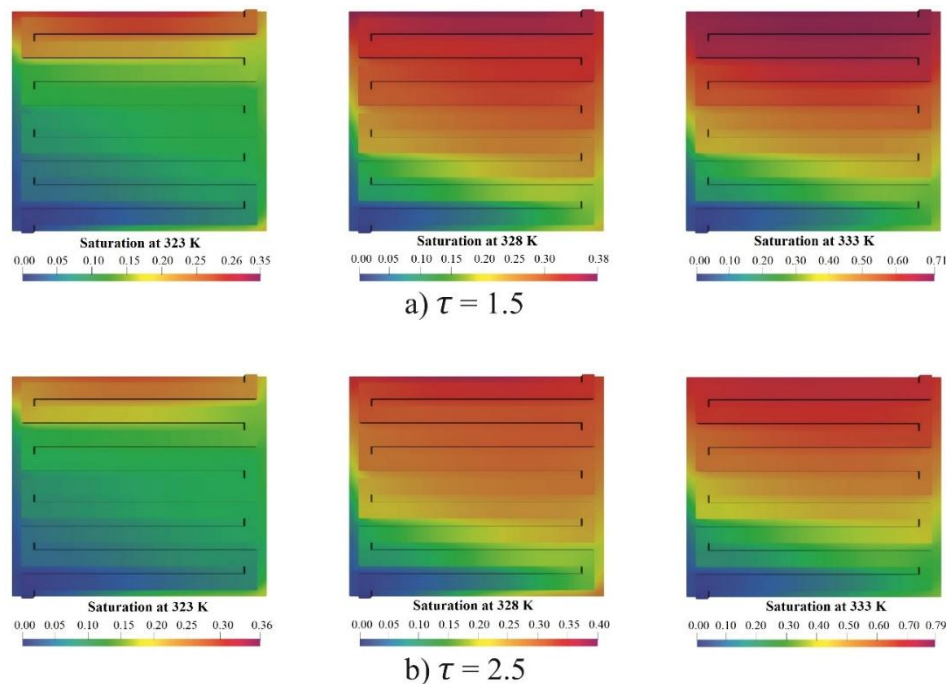
Box 3**Figure 2**

Effect of tortuosity on the values of peak current densities on the cathode side

Source: Own elaboration

On the other hand, the cell with a tortuosity of 2.5 shows slightly higher saturation values than the 1.5 tortuosity at all temperatures analysed. At 323 K, the saturation is 0.36, increasing to 0.40 at 328 K and reaching a remarkable value of 0.79 at 333 K. This steeper increase in saturation as temperature increases highlights the limitations of a more tortuous porous medium to handle water transport. A tortuosity of 2.5 imposes greater resistance to water flow, leading to greater accumulation at the cathode, especially at elevated temperatures.

Comparative analysis between the two tortuosities reveals that, although the difference in saturation is minimal at low temperatures (with differences of 0.02 at 323 K and 328 K), the disparity is amplified considerably at 333 K, where the 2.5 tortuosity has a saturation value 0.08 points higher than the 1.5 tortuosity. This suggests that, as thermal conditions become more severe, the ability of the porous medium to evacuate water is more compromised in cells with higher tortuosities, which could negatively affect cell performance due to pore clogging and reduced reagent transpor.

Box 4**Figure 2**

Saturation contours on the cathode side

Source: Own elaboration

Conclusions

From the results obtained, it is concluded that increasing the operating temperature of the PEM cell causes a significant increase in water saturation in both 1.5 and 2.5 tortuosity cells. At 333 K, saturation levels are considerably higher compared to 323 K and 328 K, highlighting the importance of proper thermal control to avoid excessive water accumulation at the cathode, which could negatively affect the electrochemical performance of the cell. Cells with a tortuosity of 1.5 present a more effective capacity to handle the generated water, showing relatively lower saturation values at all temperatures analysed. This behaviour suggests that a porous medium with lower tortuosity facilitates water evacuation, which reduces the risk of flooding at the cathode and improves the overall performance of the cell. In contrast, cells with a tortuosity of 2.5 tend to accumulate more water, which could clog the gas channels and limit oxygen diffusion towards the catalytic layer. As the temperature increases, the difference in saturation between the 1.5 and 2.5 tortuosities becomes more noticeable. At 333 K, the saturation in the 2.5 tortuosity cell is considerably higher than in the 1.5 tortuosity cell, highlighting the limitations of a more complex porous structure for water transport at elevated thermal conditions. This behaviour highlights the importance of optimising tortuosity to avoid water blockages that impair electrochemical performance.

Statements**Conflict of interest**

The authors declare that they have no conflicts of interest. They have no financial interests or personal relationships that could have influenced this book.

Authors' contribution

Ceballos-Pérez, José: Contributed to the project idea, research method and technique.

Ordóñez-López, Leadership in the planning and execution of the research activity.

Sierra-Grajeda, Juan: Development or design of methodology; creation of models.

Acknowledgements

We are grateful to the Fondo Sectorial CONACYT-Sustentabilidad Energética 254667, PhD grant No. 789267, and to the CEISSPA laboratory for supporting the doctoral stay for the development of this research project.

References

Background

Ceballos, J. O., Ordoñez, L. C., & Sierra, J. M. (2022). [Numerical simulation of a PEM fuel cell: Effect of tortuosity parameters on the construction of polarization curves](#). *International Journal of Hydrogen Energy*, 47(70), 30291-30302.

Ceballos, J. O., Sierra, J. M., & Ordoñez, L. C. (2024). [Numerical analysis on the liquid saturation at the cathode side of a PEM fuel cell with different flow paths](#). *Ionics*, 0123456789.

Basic

Shiva Kumar, S., & Himabindu, V. (2019). [Hydrogen production by PEM water electrolysis - A review](#). *Materials Science for Energy Technologies*, 2(3), 442-454.

Support

Yu, L. jun, Ren, G. po, Qin, M. jun, & Jiang, X. min. (2009). [Transport mechanisms and performance simulations of a PEM fuel cell with interdigitated flow field](#). *Renewable Energy*, 34(3), 530-543.

Comparison of the effect on electricity production in benthic microbial fuel cells using plasma-treated anodes

Comparación del efecto en la producción de electricidad en celdas de combustible microbianas béticas empleando ánodos tratados con plasma

Flores-Martínez, Jordy Alexis^a, Fuentes-Albarrán, María del Carmen*^b, Alarcón-Hernández, Fidel Benjamín^c and Gadea-Pacheco, José Luis^d

^a Universidad Autónoma del Estado de Morelos • LPP-8245-2024 • 0009-0009-8356-6328

^b Universidad Autónoma del Estado de Morelos • LFS-3039-2024 • 0000-0003-1308-1332 • 171814

^c Universidad Autónoma del Estado de Morelos • AEO-9146-2022 • 0000-0002-2465-0898 • 131028

^d Universidad Autónoma del Estado de Morelos • LEM-8262-2024 • 0000-0001-9341-9289 • 160429

CONAHCYT classification:

DOI: <https://doi.org/10.35429/H.2024.13.76.84>

Area: Engineering

Campo: Technological sciences

Discipline: Energy technology

Subdiscipline: Energy generation

Key Handbooks

The main contributions to the generation of science and technology in this research are based on the use of non-thermal plasma treatment technology on anodes that can be used in microbial fuel cells, with the purpose of improving their performance to produce electricity. Key aspects that must be understood to apply to the generation of universal knowledge consist of the changes that take place on the surface of plasma-treated electrodes and that can influence the optimization of the performance of a microbial fuel cell. In conclusion, in this research the effect of anodes treated with plasma was analyzed in comparison to an untreated anode, obtaining greater power production with the anode that had less exposure to plasma. The authors of this chapter do not have a CONAHCYT, PRODEP or external scholarship), they come from state public institutions (Autonomous University of the State of Morelos). The most used keywords are benthic microbial fuel cells, anodes, air plasma and power production.

Citation: Flores-Martínez, Jordy Alexis, Fuentes-Albarrán, María del Carmen, Alarcón-Hernández, Fidel Benjamín and Gadea-Pacheco, José Luis. 2024. Comparison of the effect on electricity production in benthic microbial fuel cells using plasma-treated anodes. 76-84. ECORFAN.

* ✉ [carmen.fuentes@uaem.mx]

Handbook shelf URL: <https://www.ecorfan.org/handbooks.php>



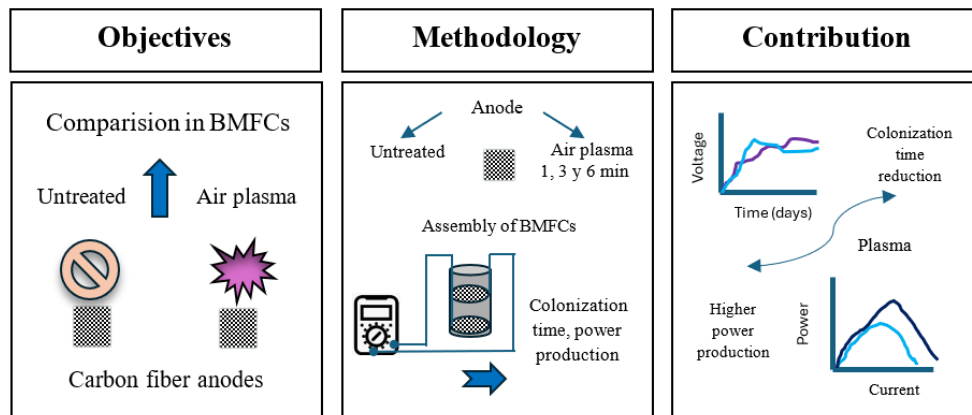
ISBN 978-607-8948-51-2/©2009 The Authors. Published by ECORFAN-Mexico, S.C. for its Holding Mexico on behalf of Handbook HRPG. This is an open access chapter under the CC BY-NC-ND license [<http://creativecommons.org/licenses/by-nc-nd/4.0/>]

Peer Review under the responsibility of the Scientific Committee MARVID®- in contribution to the scientific, technological and innovation Peer Review Process by training Human Resources for the continuity in the Critical Analysis of International Research.



Abstract

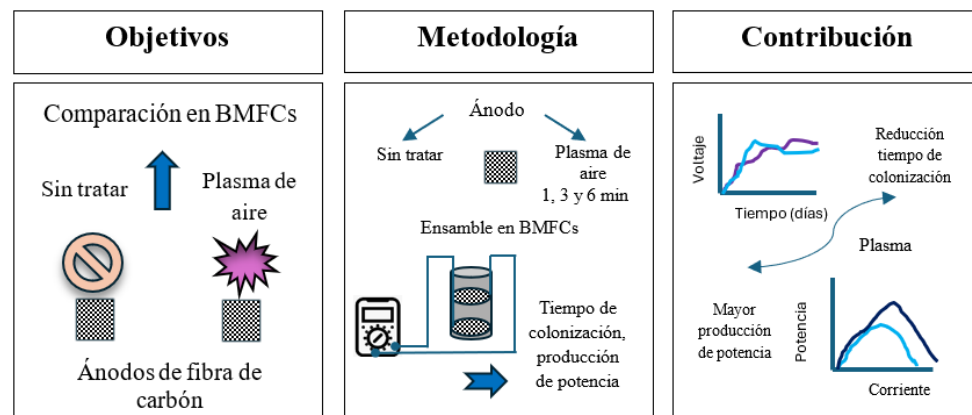
In this study, the effect on electricity production in four benthic microbial fuel cell (BCMB) devices was compared. The CCMBs used carbon fiber anodes subjected to different exposure times to a non-thermal plasma at low pressure, with exposure times of 1, 3 and 6 minutes respectively, in addition to a control (untreated anode). The lowest power production was obtained with the anode treated for 6 minutes, recording a power density of 1.33 mW/m^2 with a current density of 22.22 mA/m^2 , while the highest power production was achieved with the CCMB using the anode treated for 1 minute, obtaining a maximum peak power of 2.02 mW/m^2 with a current density of 27.40 mA/m^2 . The results showed that a shorter exposure time of the anode to plasma treatment has a favorable effect on power production.



Benthic microbial fuel cell, Anode, Air plasma

Resumen

En este estudio se comparó el efecto en la producción de electricidad en cuatro dispositivos de celdas de combustible microbianas béticas (CCMBs). Las CCMBs emplearon ánodos de fibra de carbón sometidos a diferentes tiempos de exposición a un plasma no térmico a baja presión, con tiempos de exposición de 1, 3 y 6 minutos respectivamente, además de un testigo (ánodo sin tratar). La menor producción de potencia se obtuvo con el ánodo tratado 6 minutos, registrando una densidad de potencia de 1.33 mW/m^2 con una densidad de corriente de 22.22 mA/m^2 , mientras que la mayor producción de potencia se alcanzó con la CCMB empleando el ánodo tratado 1 minuto, obteniendo un máximo pico de potencia de 2.02 mW/m^2 con una densidad de corriente de 27.40 mA/m^2 . Los resultados mostraron que un menor tiempo de exposición del ánodo al tratamiento con plasma tiene un efecto favorable en la producción de potencia.



Celda de combustible microbiana bética, Ánodo, Plasma de aire

Introduction

Benthic microbial fuel cells (BMFCs) are bioelectrochemical systems that use the metabolism of microorganisms to produce electricity (Tavakolian et al., 2020). BMFCs can use sediments from different aquatic bodies such as; rivers, lagoons and seas (Feregrino et al., 2023), also have the advantage of not requiring the use of a membrane for their operation. In a BMFC the anode is buried in the sediments, while the cathode remains floating or submerged in the overlying water. Electroactive bacteria (EAB) that colonize the anode oxidize the organic matter in the sediment using an electrode as an electron acceptor. Electrons and protons released by the oxidation of organic compounds at the anode are transferred to the cathode, where they react with oxygen (electron acceptor) to form water (Wang et al., 2023).

BMFCs constitute an alternative to generate bioelectricity while degrading pollutants. These systems can be used to power submersible ultrasound receivers, wireless temperature and oxygen sensors, as well as wireless telecommunications systems and low-power sensors for remote monitoring (Sun et al., 2024), in addition to being used in bioremediation processes, removing polychlorinated biphenyls (PBCs), polycyclic aromatic hydrocarbons (PAHs) and antibiotics and immobilizing heavy metals and phosphorus from sediments (Danhassan et al., 2023). However, its performance still faces several challenges for large-scale applications. Despite their advantages, the power output of BMFCs is low, several factors related to the configuration of these devices affect their performance, such as the electrode material, distance between the electrodes, depth of the anode, height of the anode embedded in the sediments, cathode configuration and type of aquatic body used (Gupta et al., 2023). Recent advances in BMFCs have focused on modifications of the anode as a key element to improve the performance of these systems, with the purpose of increasing the exposed surface, decreasing the internal resistance and having high electrochemical activity (Prakash et al., 2018).

These modification methods include surface treatments with physical or chemical methods, addition of highly conductive or electroactive coatings and the use of electrodes composed of metal and graphite (Wei et al., 2011). In this context, non-thermal plasma or cold plasma technology has attracted attention in many areas of study because it is environmentally sustainable. Non-thermal plasma is generated by subjecting a gas to an electric field in a low-temperature reactor, resulting in the production of an ionized gas. The free electrons of ionic species react with substances, oxidizing them (Abdalameer et al., 2024). This technology has various applications and has allowed the investigation of surface treatments of multiple types of materials, such as surfaces that will be coated with nanomaterials (Walden et al., 2024) and emerges as a highly efficient and controllable approach for the surface treatment of materials of electrodes, which allows improving their electrochemical performance (Zhang et al., 2017).

From this perspective, in this study, carbon fiber electrodes were subjected to different exposure times to low-pressure non-thermal plasma (1, 3 and 6 minutes), to be used as anodes in three Benthic Microbial Fuel Cell devices. (BMFC-1, BMFC-3 and BMFC-6). Thus, the electricity production performance of fuel cells that used plasma-treated anodes was compared to a BMFC-U that used an untreated anode (control). It is suggested that plasma treatment modifies the surface of the anodes, improving their performance for electricity production in a BMFC.

This research was developed in the following stages: exposure of three anodes to a non-thermal plasma at low pressure, assembly of four BMFCs using the treated anodes and one BMFC-U with an untreated anode (control). Monitoring the microbial colonization time in the cells, and finally the performance of the cells was characterized using polarization and power curves.

Methodology

Microbial fuel cell benthics configuration

Four glass vessels were used to construct each of the BMFCs. The vessels had a lower diameter of 4.5 cm, an upper diameter of 8 cm and a height of 14 cm, having a total volume of 140.28 cm³. Sediments from a jagüey from a town in the state of Morelos, Mexico were used. The electrodes used were carbon fiber (Fibreglast®) with an area of 0.0009 m². To build the BMFCs, an untreated anode (Control) was used, and three anodes subjected to different exposure times to a non-thermal plasma.

For plasma treatment, each electrode was placed in a reaction chamber at different exposure times (1, 3, and 6 minutes). To generate the plasma, a high voltage source (SPELLAN SL600) was used, applying a voltage of 5 kV with a current of 70 mA, a vacuum pump (LABCONCO 117) was used to generate vacuum in the reaction chamber (24 Torr).

Assembly of benthic microbial fuel cells

To assemble the cells, the anode was placed at the base of each cell, then a 3 cm layer of sediment, and then a layer of water was added at a height of 3 cm from the container. The cathode was placed on the surface of the water supported by a plastic base, and finally it was covered with water to a height of 3 cm. The electrodes were connected to the outside using copper wire to carry out the measurements. The cells were kept in operation for 18 days at room temperature. A schematic of the assembly is shown in Figure 2.1.

Box 1

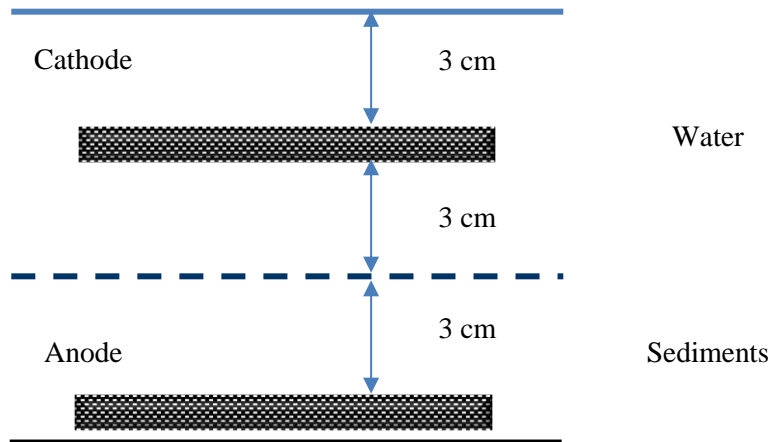


Figure 1

Scheme of the BMFCs

Source: Own Elaboration

Data acquisition and characterization of the BMFCs

During the startup stage of each of the BMFCs, the open circuit voltage (OCV) was monitored using a multimeter (Steren Professional Deluxe Multimeter with PC interface, Model: MUL-600). During this period microorganisms colonized the anode of each system. Once the BMFCs reached a stable voltage, the characterization of each cell was carried out using polarization curves and power curves, using a variable external resistance (R_{ext}) in a range of 500Ω and $10 \text{ k}\Omega$. For each resistance, the voltage obtained in each cell (E_{BMFC}) was recorded. For each pair of values (Ω - V) obtained experimentally, the current was determined using Ohm's law:

$$I = \frac{E_{BMFC}}{R_{ext}} \quad [1]$$

To obtain the polarization curves, cell voltage was plotted against the current. The cell power (P_{BMFC}) was obtained using the following equation:

$$P_{BMFC} = \frac{E^2_{BMFC}}{R_{ext}} \quad [2]$$

The obtained power density was normalized to the anode area (mW/m^2).

Results

Microbial colonization time

Figure 2 shows the microbial colonization time in the four BMFCs devices. In BMFC-U the voltage was slowly increasing during the first 4 days, while the voltage in BMFCs-1, 3 and 6 was slightly higher during the same period of time. The BMFC-U reached a maximum voltage of 0.35 V after 11 hours of operation, the BMFC-1 and the BMFCs-3 and 6 in a period of 7 and 9 days respectively, that is, the microbial colonization time was reduced by a in the cells that used the plasma-treated anodes by up to 36%. Finally, all systems maintained a relatively stable voltage during the last days of operation.

Box 2

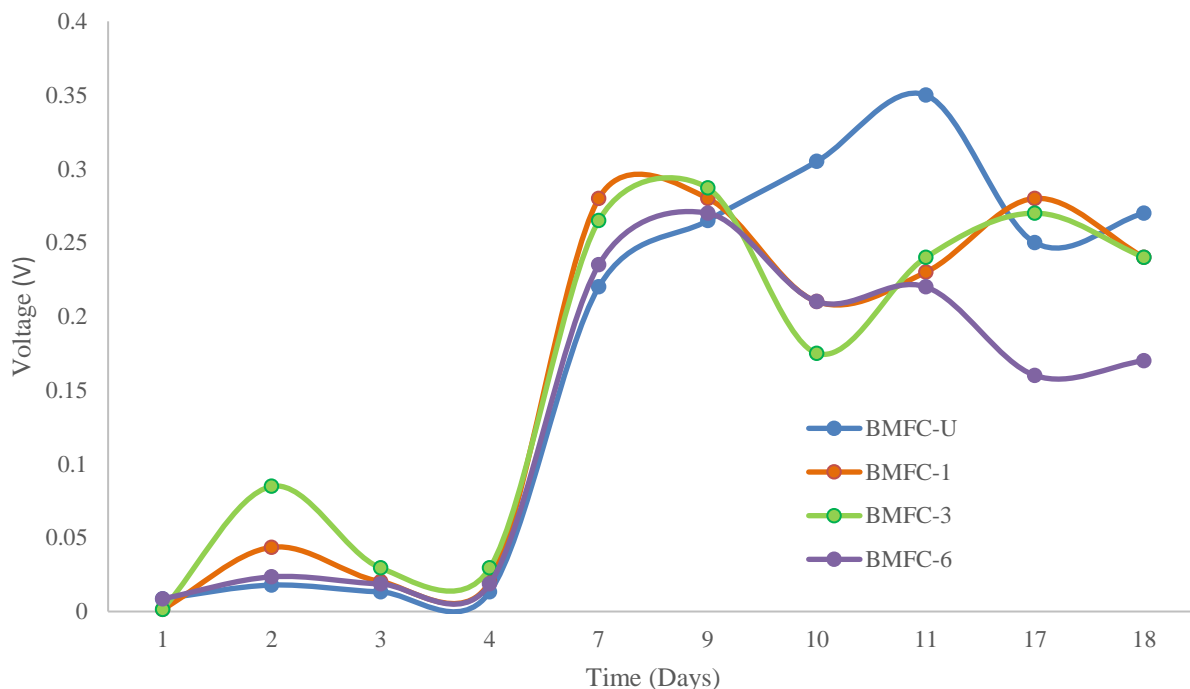


Figure 2

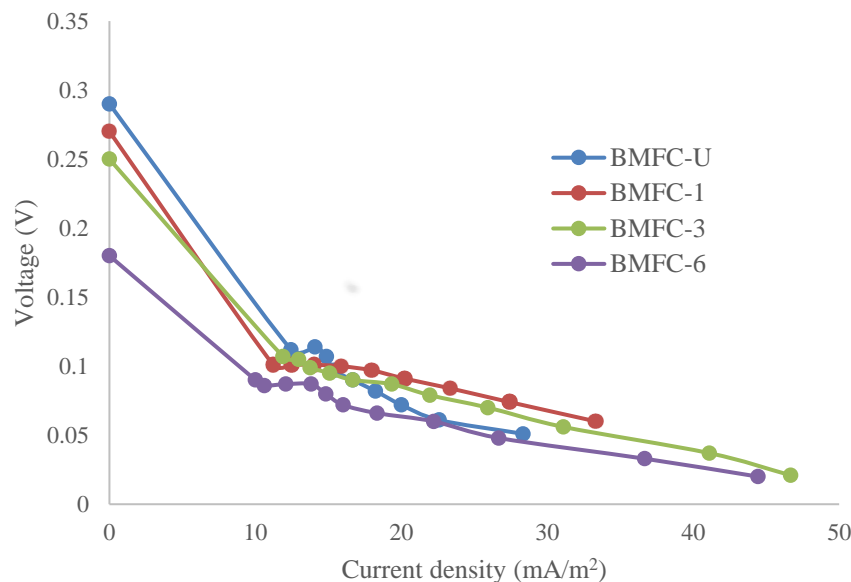
Microbial colonization time in CCMBs

Source: Own Elaboration

The reduction in microbial colonization time in BMFCs that used plasma-treated anodes suggests that changes occur on the anode surface when the treatment is applied, which allow greater microbial colonization in less time. In a study (Gholami et al., 2024) they used a nitrogen plasma modified nickel foam as an anode to improve the electrochemical performance in an MFC. They observed that the Ni foam exhibited an open cell structure and rough surface morphology, which provided a large contact area between bacteria and anodes in microbial fuel cells (MFCs) improving their performance.

Comparison of polarization curves

Figure 3 shows the polarization curves obtained for the four microbial fuel cell systems. BMFC-U reached the highest open circuit voltage (OCV) of 0.29 V, followed by BMFCs-1, 3 and 6 with an OCV of 0.27, 0.25 and 0.18 V respectively. Obtaining a lower OCV for the cell that used the anode treated with plasma for a longer time (6 minutes).

Box 3**Figure 3**

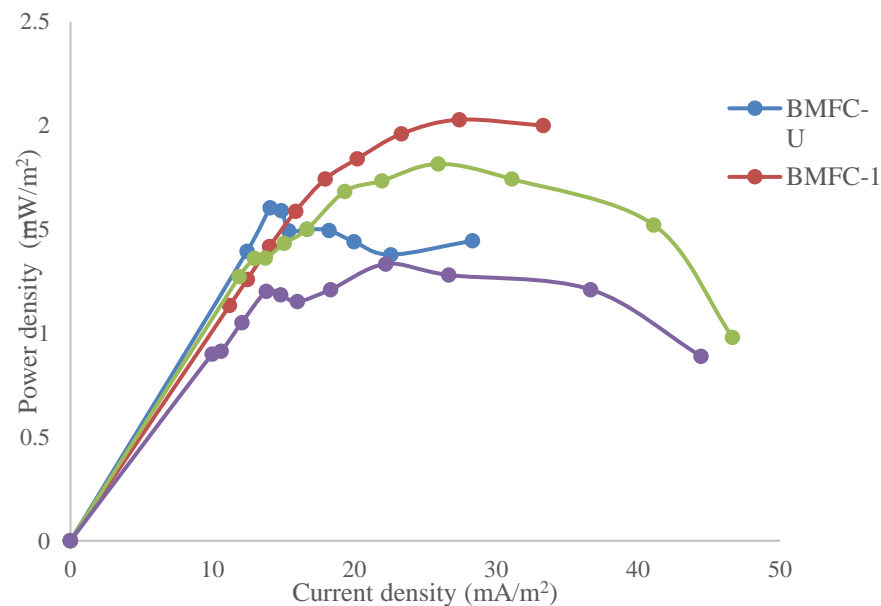
Polarization curves for BMFCs with different anodes

Source: *Own Elaboration*

In the four BMFCs devices, a rapid drop in potential is observed at low current densities, attributed to the activation losses of each system. As the current density increases, the BMFC-U shows a rapid loss of potential, while the BMFC-1 shows slower losses of potential.

Power production in benthic microbial fuel cells

The performance of the BMFCs in power production was examined. Figure 4 shows the results obtained. The BMFC-U achieved a maximum power density of 1.60 mW/m² with a current density of 14.07 mA/m². While the BMFC-1 reached the maximum peak power of 2.02 mW/m² with a current density of 27.40 mA/m², that is, in this system power production increased by 26% and the current density was reduced. doubled. However, with the BMFC-6 the lowest peak power was obtained, reaching 1.33 mW/m². Table 3.1 summarizes the results obtained for each BMFC.

Box 4**Figure 4**

Power production in BMFCs

Source: *Own Elaboration*

It has been reported that pure carbon materials have a lower number of active sites, so they exhibit a lower electrochemical performance, which could be attributed to the lower power density obtained in the BMFC-U. Different levels of topological defects could be obtained by varying the duration of the plasma on the anode, which could improve the electrochemical performance of the material, influencing the power production, as observed in BMFC-1 ([Ouyang et al., 2018](#)).

Box 5

Table 2

OCV and power production for BMFCs

BMFC	OCV (V)	Maximum power density (mW/m ²)	Current density (mA/m ²)
BMFC-U	0.29	1.60	14.86
BMFC-1	0.27	2.02	27.40
BMFC-3	0.25	1.81	25.92
BMFC-4	0.18	1.28	26.66

Source: Own elaboration

Some studies have explored the use of plasma to treat electrodes for MFC applications. ([Chang et al., 2016](#)) used flow plasma at atmospheric pressure to treat carbon cloth electrodes for use in an MFC. They obtained a maximum power density of 7.56 mW/m², finding that the plasma treatment improved the electrochemical performance of the system by tripling the power density with respect to the MFC that used untreated electrodes. The plasma treatment allowed the carbon fabric to be highly hydrophilic, and the internal resistance of the MFC was significantly lower than the MFC with untreated electrodes, which influenced the increase in power. In another study, ([Gholami et al., 2024](#)), they used nickel foam modified with nitrogen plasma as an anode in an MFC, applying a treatment for 60 minutes, the MFC reached a maximum power density of 247.1 mW/m². In this work, a high hydrophilicity of the plasma-modified Ni foam electrodes was obtained, which facilitated the adhesion of bacteria and the formation of biofilms.

Conclusions

In this study, it was observed that plasma treatment reduces the microbial colonization time at the anode of BMFC-1 by up to 36%, compared to BMFC-U.

Greater power production was achieved in BMFC-1, obtaining a peak power of 2.01 mW/m², increasing up to 26% compared to the cell that used an untreated anode. This can be attributed to changes that occurred on the surface of the plasma-treated anode, which favored the adhesion of microorganisms and the transfer of electrons to the anode of the cell.

In this work, the morphology of the anode before and after plasma treatment was not examined, which can be done for future work.

Conflict of interest

The authors declare that they have no conflict of interest. They have no financial interests or personal relationships that could have influenced this book.

Authors' contribution

Flores Martínez, Jordy Alexis: Supported in carrying out the experiments and applying the research methods and techniques. Contributed to laboratory analysis.

Fuentes-Albarrán, María del Carmen: Design and implementation of the project idea, methods and applied research techniques. He supported the development of the experimentation, carried out the data analysis and wrote the work.

Alarcón-Hernández, Fidel Benjamín: Contributed to the research design, type of research, laboratory analysis, analysis of collected data and writing of the article.

Gadea-Pacheco, José Luis: Supported in the laboratory analysis. He worked on writing the article.

Availability of data and materials

All data used to support the findings of this study are included in the work.

Financing

This work was funded by PRODEP [DSA/103.5/14/10703]

Acknowledgments

The authors thank the Xalostoc School of Higher Studies of the Autonomous University of the State of Morelos, for the facilities provided to carry out this research.

Abbreviations

BMFC	Benthic microbial fuel cell
MFC	Microbial fuel cell
OCV	Open circuit voltage

References

Background

Danhassan, U.A., Lin, H., Lawan, I., Zhang, X., Ali, M. H., Muhammad, A. I., y Sheng, K. (2023). [Critical insight into sediment microbial fuel cell: Fundamentals, challenges, and perspectives as a barrier to black-odor water formation](#). *Journal of Environmental Chemical Engineering*, 11, (1), 109098.

Feregrino, M., Ramírez, B., Estrada, F., Cuesta, L.F., Rochin, J. J., Bustos, Y. A., y Gonzalez, V. A. (2023). [Performance of a sediment microbial fuel cell for bioenergy production: Comparison of fluvial and marine sediments](#). *Biomass and Bioenergy*, 168, 106657.

Gupta, S., Patro, A., Mittal, Y., Dwivedi, S., Saket, P., Panja, R., Saeed, T., Martínez, F., y Yadav, A. K. (2023). [The race between classical microbial fuel cells, sediment-microbial fuel cells, plant-microbial fuel cells, and constructed wetlands-microbial fuel cells: Applications and technology readiness level](#). *Science of the Total Environment*, 879, 162757.

Sun, F., Chen, J., Tang, M., y Yang, Y. (2024). [Recent research progress, challenges and future directions of sediment microbial fuel cell: A comprehensive review](#). *International Journal of Hydrogen Energy* 50, (Part C), 870-886.

Tavakolian, M., Taleghani, H. G., y Khorshidian, M. (2020). [New design of benthic microbial fuel cell for bioelectricity generation: Comparative study](#). *International Journal of Hydrogen Energy*, 45, 23533-23542.

Wang, H., Ye, Y., Zhang, J., Ning, H., Xiang, Y., Song, X., Zhao, W., y Guo, F. (2023). [Power performance improvement in sediment microbial fuel cells: Recent advances and future challenges](#). *International Journal of Hydrogen Energy*, 48(63), 24426-24446.

Basic

Abdalameer, N. kh., Ali, H.M.J., y Majed, M. D. (2024). [The effect of cold plasma generated from argon gas on the optical band gap of nanostructures](#). *Kuwait Journal of Science*, 51, (2), 100195.

Prakash, O., Mungray, A., Kailasa, S. K., Chongdar, S., y Mungray, A. K. (2018). [Comparison of different electrode materials and modification for power enhancement in benthic microbial fuel cells \(BMFCs\)](#). *Process Safety and Environment Protection*, 117, 11-21.

Walden, R., Goswami, A., Scally , L., McGranaghan, G., Cullen, P. J., y Pillai, S. C. (2024), [Nonthermal plasma technologies for advanced functional material processing and current applications: Opportunities and challenges](#). *Journal of Environmental Chemical Engineering* 12, (5), 11354.

Wei, J., Liang, P., y Huang, X. (2011). [Recent progress in electrodes for microbial fuel cells](#). *Bioresource Technology*, 102, 9335-9334.

Zhang, Y., Rawat, R.S., y Fan, H. F. (2017). [Plasma for Rapid Conversion Reactions and Surface Modification of Electrode Materials](#). *Small Methods*, 1700164.

Discussions

Chang, S., H., Liou, J., S., Liu, J., L., Chiu, Y., F., Xu, C., H., Chen, B., Y., y Chen, J. Z. (2016). [Feasibility study of surface-modified carbon cloth electrodes using atmospheric pressure plasma jets for microbial fuel cells](#). *Journal of Power Sources*. 336, 99-106.

Gholami, M., Cheng, M., Lange, G., y Chang, S. H. (2024). [Effects of N₂ plasma modification on the surface properties and electrochemical performance of Ni foam electrodes for double-chamber microbial fuel cells](#). *Materials Advances*, 5, 5554-5560.

Ouyang, B., Zhang, Y., Xia, X., Rawat, R. S., y Fan, H. J. (2018), [A brief review on plasma for synthesis and processing of electrode materials](#). *Materials Today Nano* 3, 28e47.

Evaluation of an aqueous solution degradation of textile dye Permalon Rhodamine B by non-thermal plasma treatments

Evaluación de la degradación de una solución acuosa de colorante textil Permalon Rhodamine B mediante tratamientos de plasma no térmico

Gómez-Anzures, Uriel Yosimar^a, Alarcón-Hernández, Fidel Benjamín*^b, Fuentes-Albarrán, María del Carmen^c and Gadea-Pacheco, José Luis^d

^a Universidad Autónoma del Estado de Morelos • LPP-8245-2024 • 0009-0002-0241-9916 • 2074659

^b Universidad Autónoma del Estado de Morelos • AEO-9146-2022 • 0000-0002-2465-0898 • 131028

^c Universidad Autónoma del Estado de Morelos • LFS-3039-2024 • 0000-0003-1308-1332 • 171814

^d Universidad Autónoma del Estado de Morelos • LEM-8262-2024 • 0000-0001-9341-9289 • 160429

CONAHCYT classification:

DOI: <https://doi.org/10.35429/H.2024.13.85.95>

Area: Engineering

Field: Engineering

Discipline: Chemical engineering

Subdiscipline: Water contamination

Key Handbooks

The main contributions to the generation of science and technology in this research are mainly reflected in obtaining knowledge for wastewater treatment through non-conventional technologies, such as plasma treatments. In particular, it seeks to establish a methodology that allows more efficient treatments. The key aspects that must be understood to apply to the generation of universal knowledge are the chemical and physical changes generated under this methodology, as they are key to adequate wastewater treatment and optimization of the results obtained. From this perspective, the conclusion derived from this research can be summarized in the adequate degradation of the pollutant under study, which other methodologies have not achieved. The authors of this chapter do not have any scholarship (CONAHCYT, PRODEP or external) and come from State Public Institutions (Autonomous University of the State of Morelos). The keywords most commonly used are plasma, degradation, rhodamine, wastewater, electrical conductivity, total dissolved solids, chemical oxygen demand, and organic carbon.

Citation: Gómez-Anzures, Uriel Yosimara, Alarcón-Hernández, Fidel Benjamín*^b, Fuentes-Albarrán, María del Carmen and Gadea-Pacheco, José Luis. 2024. Evaluation of an aqueous solution degradation of textile dye Permalon Rhodamine B by non-thermal plasma treatments. 85-95. ECORFAN.

*✉ [honorato@uaem.mx]

Handbook shelf URL: <https://www.ecorfan.org/handbooks.php>

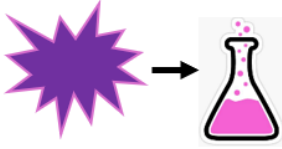
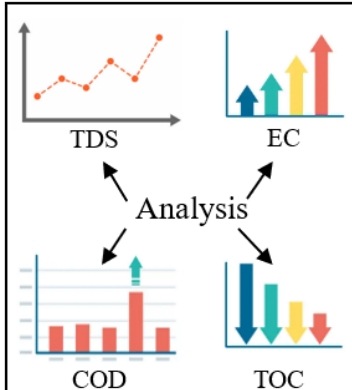
 ISBN 978-607-8948-51-2 ©2009 The Authors. Published by ECORFAN-Mexico, S.C. for its Holding Mexico on behalf of Handbook HRPC. This is an open access chapter under the CC BY-NC-ND license [<http://creativecommons.org/licenses/by-nc-nd/4.0/>]

Peer Review under the responsibility of the Scientific Committee MARVID®- in contribution to the scientific, technological and innovation Peer Review Process by training Human Resources for the continuity in the Critical Analysis of International Research.



Abstract

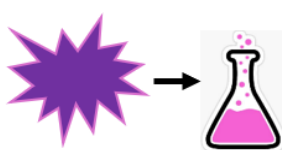
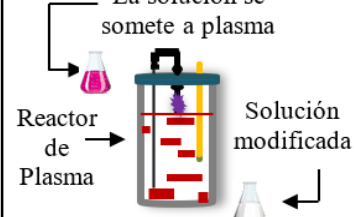
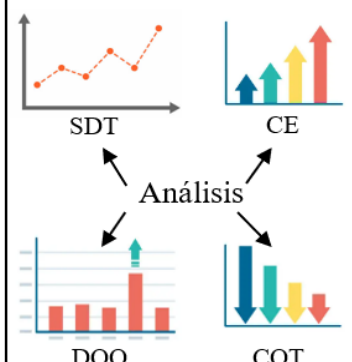
The degradation generated by plasma treatments of the dye Permalon Rhodamine B in aqueous solution (123 mg/L) was evaluated. The degradation was quantified as a function of the exposure time (240 min) and the plasma generation current (20.0, 30.0, 40.0 and 50 mA) at a voltage of 2000 V. The changes (degradation) were monitored by Chemical Oxygen Demand (COD) and Total Organic Carbon (TOC). Total dissolved solids (TDS) and electrical conductivity (EC) were also measured. The degradation of the dye in terms of TOC in the solution was maximum (97 %) for the 50 mA plasma treatment. As the current increases, the COD in the solution also increases. For the 50 mA treatment, the COD increased by 27%. The TDS and EC increased as the exposure time increased. The higher the current and exposure time, the greater the degradation of the dye

Objectives	Methodology	Contribution
<p>Air plasma degrading</p>  <p>Evaluate physical and chemical changes</p>	<p>The solution is subjected to plasma</p>  <p>Plasma reactor → Treated solution</p> <p>Measured: TDS, EC, COD and TOC</p>	 <p>TDS</p> <p>EC</p> <p>Analysis</p> <p>COD</p> <p>TOC</p>

Plasma, degradation, rhodamine B

Resumen

Se evaluó la degradación generada mediante tratamientos de plasma del colorante Permalon Rhodamine B en solución acuosa (123 mg/L). Se cuantificó la degradación como función del tiempo de exposición (240 min) y de la corriente de generación del plasma (20.0, 30.0, 40.0 y 50 mA) a un voltaje de 2000 V. Los cambios (degradación) se monitorearon mediante Demanda Química de Oxígeno (DQO) y Carbono Orgánico Total (COT). También se midieron sólidos disueltos totales (SDT) y conductividad eléctrica (CE). La degradación del colorante en términos del COT en la solución fue máxima (97 %) para el tratamiento de plasma de 50 mA. Conforme la corriente incrementa, la DQO en la solución también aumenta; para el tratamiento de 50 mA la DQO incrementó un 27 %. Los SDT y la CE aumentaron conforme el tiempo de exposición sucede. A mayor corriente y tiempo de exposición, mayor degradación del colorante.

Objetivos	Metodología	Contribución
<p>Degradar por plasma de aire</p>  <p>Evaluar cambios físicos y químicos</p>	<p>La solución se somete a plasma</p>  <p>Reactor de Plasma → Solución modificada</p> <p>Se mide: SDT, CE, DQO y COT</p>	 <p>SDT</p> <p>CE</p> <p>Análisis</p> <p>DQO</p> <p>COT</p>

Plasma, degradación, rhodamine B

Introduction

The dye Rhodamine B is one of the most widely used substances in the industry. It is mainly used in the textile industry, paints, manufacturing pens, dyes, explosives, carbon sheets, stamp inks, and even biscuits (Imam & Babamale, 2020; Hamdaoui, 2011).

This dye is one of the most toxic due to its high stability and non-biodegradability, which is why it is present in textile industrial wastewater. On the other hand, since it prevents the passage of light and inhibits the bioprocesses of aquatic plants and microorganisms that cohabit in water bodies, generating anoxic conditions (Sharma *et al.*, 2022), as well as inducing inflammation of the organs of living beings (Seerangaraj *et al.*, 2021; Nasr *et al.*, 2023), it becomes a highly harmful compound (Sharma *et al.*, 2022). In general, apart from the Rhodamine B dye, a large amount of toxic and dangerous organic or inorganic compounds are dumped into bodies and water currents, destroying the ecological system and human health because they have not been previously treated or degraded by some wastewater treatment methodology (Nasr *et al.*, 2023).

Alternative procedures are currently being developed and researched to address the problem of water body pollution. In particular, advanced oxidation processes (AOP) are studied, representing a promising option of techniques and an active field of research for removing dyes. These processes include atmospheric pressure air plasmas, where degradation occurs when reactive molecules, ions and/or radical species created during the plasma discharge in the gaseous or liquid phase attack organic molecules and oxidize them (Ma *et al.*, 2021; Aggelopoulos *et al.*, 2024; García *et al.*, 2017; Aggelopoulos., 2022; Pandiyaraj *et al.*, 2021; Ghezzar *et al.*, 2009).

In general, these non-thermal plasma degradation processes have the advantages of high efficiency, no secondary pollution and low energy consumption (Petrović *et al.*, 2024; Hentit *et al.*, 2014). Considering the degradation characteristics of atmospheric pressure air plasmas and the multiple advantages of this methodology, the present experimental research aims to evaluate the degradation percentage generated by this methodology in a solution of the dye Permalon Rhodamine B at an initial concentration of 123 mg/L. The degradation is evaluated by measuring Chemical Oxygen Demand (COD) and Total Organic Carbon (TOC). The behaviour of total dissolved solids (TDS) and electrical conductivity (EC) is also determined; all of this is a function of the time of exposure of the solution to the treatments and the plasma generation parameters.

The analysis and observation of the degradation behaviour of the dye of interest in aqueous solutions through this research provide a solid basis for developing effective methodologies in treating industrial wastewater with similar characteristics. This experiment uses atmospheric pressure air plasma, which can offer an innovative and efficient alternative to removing contaminants. In the methodology section, the experimental device's particularities, the dye's chemical properties, and the techniques selected to evaluate the variables of interest are detailed and presented. The results section presents graphs illustrating the evolution of chemical oxygen demand (COD), total organic carbon (TOC), total dissolved solids (TDS) and electrical conductivity (EC) of the solution over the exposure time and as a function of the power of the plasma used. These data allow a precise analysis of the effectiveness of the treatment. Finally, in the conclusions section, the most significant observations are highlighted, which could guide future research and applications in wastewater treatment.

This approach not only underlines the importance of understanding the dynamics of dye degradation but also highlights the potential of using advanced technologies, such as plasma, to improve the quality of treated water.

Methodology

The experiment was carried out considering an initial concentration of 123 mg/L. To obtain this value (123 mg/L), 246 mg of Permalon Rhodamine B dye powder was added to 2.0 L of distilled water. The dye was weighed using an ADAM brand analytical balance, model PW 254. This concentration was chosen for all the experiments performed. The Permalon Rhodamine B dye is identified with C.I: 45170. It was used without any purification or physical or chemical changes. Its formula and molecular weight are $C_{28}H_{31}ClN_2O_3$ and 479.01 g/mol, respectively.

The plasma treatment process is carried out as follows. It begins by exposing 500 ml of the solution of interest at a concentration of 123 mg/L to the air plasma. The plasma is generated with specific determined values (voltage and current) in a high-voltage source (**SPELLMAN SL600**), as shown in Figure 1 ([Ávila et al., 2023](#)).

Box 1

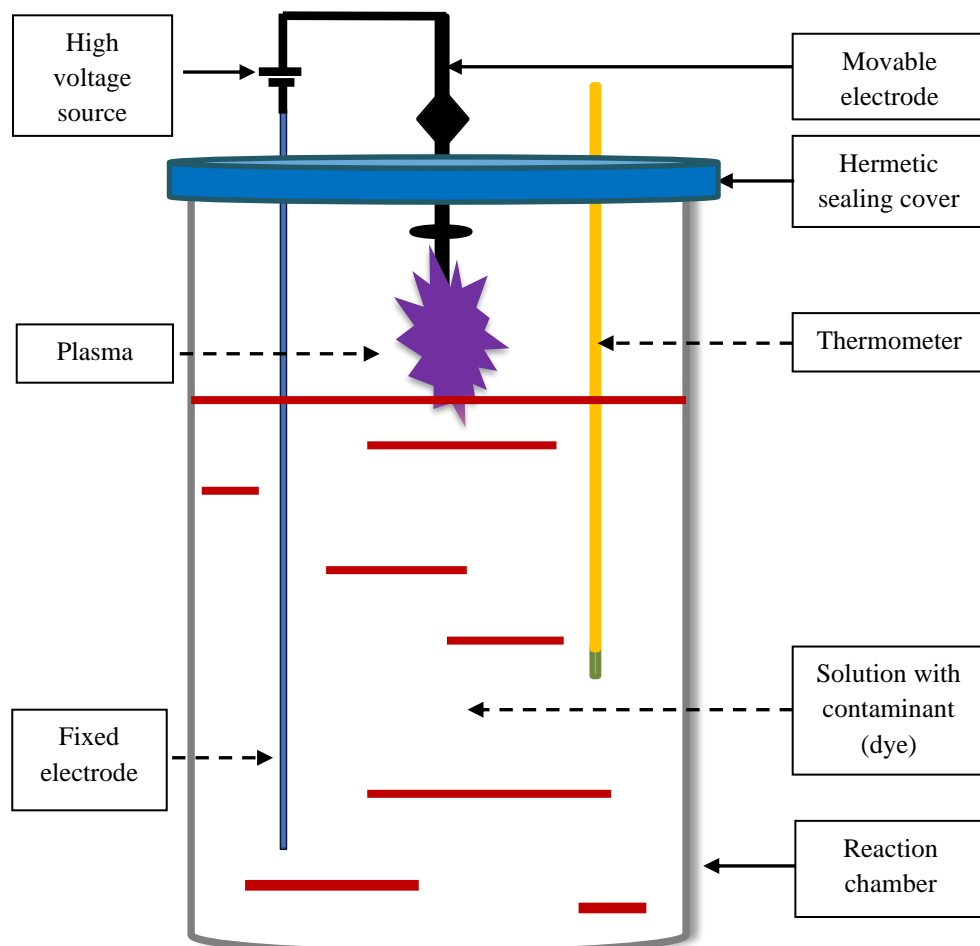


Figure 1

Diagram of the solution exposure to plasma and components of the experimental device

Source: Own elaboration

The device consists of a hermetically sealed glass chamber with a capacity of 1.0 L, two tungsten electrodes, a mercury thermometer, and a high-voltage source. In this device, one electrode is immersed in the solution of interest. At the same time, the other, which is movable, is placed at a distance of approximately 2 mm to facilitate plasma generation. This plasma is formed at the interface between the air in the reaction chamber and the solution, as illustrated in the diagram. The thermometer remains immersed in the solution, allowing the temperature to be measured at all times. Four treatments were carried out with different electric currents and the same voltage (2000 V). Likewise, the values of exposure time (240 minutes), concentration (123 mg/L), and volume of solution treated (500 mL) were kept constant. All treatments started with a temperature value of 28 °C. The electric current values used to generate the plasma are specified in Table 1.

Box 2

Table 1

Electric current parameters used to generate the air plasma in the present experiment

Treatment	Electric current (mA)
T1	20
T2	30
T3	40
T4	50

Source: Own elaboration

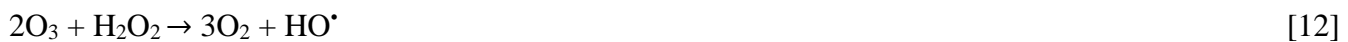
The parameters of interest were measured every 20 minutes for electrical conductivity (EC) and total dissolved solids (TDS) (HI 9813-6N potentiometer). In these cases, the plasma treatment is interrupted to perform the measurement. Once the necessary measurements have been taken, the sample solution is added to the reaction chamber and the treatment is continued. This procedure is repeated until the 240 minutes have elapsed. On the other hand, the measurement of chemical oxygen demand (COD) and total organic carbon (TOC) (Hach DRB 200 digester, Hach DR 3900 spectrophotometer) was carried out before starting the respective treatment and at the end of the experiment.

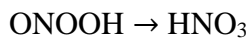
The values of chemical oxygen demand and total organic carbon were determined according to the procedure established by the Hach method. Vials ranging between 3 - 150 mg O₂/L and 15 - 150 mg C/L were used. All testing was performed with analytical-grade chemicals.

Results and discussion

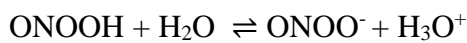
The changes generated in the degradation of the dye in an aqueous solution are presented after exposure to air plasma generated by different electric currents and atmospheric pressure. The changes concerning electrical conductivity, total dissolved solids, chemical oxygen demand, and total organic carbon of the solution are analyzed over time.

In this treatment, the chemically active species that may be present and explain the mechanisms of dye degradation when subjected to plasma are the following (Safenraider *et al.*, 2020; Alarcón *et al.*, 2022). Reactions [1] – [20].





[19]



[20]

Reactions [1] – [8] (primary species) are favoured and stabilized in water, given the experimental system (Lukes *et al.*, 2014; Cadorin *et al.*, 2015). These have the possibility of forming secondary species (Reactions [9] – [20]) that are capable of inducing chemical degradation reactions of organic compounds in the medium. On the other hand, the interaction of high-energy electrons resulting from the generation of non-thermal plasma in the study solution induces different processes, such as hydrolysis and electron impact ionization, that favour recombination processes and the appearance of different species (Bruggeman *et al.*, 2016).

Electrical conductivity and total dissolved solids

Given the conditions under which this experiment was carried out (atmospheric pressure, ambient temperature, electric current for generating the plasma, treated volume, solution concentration and exposure time), it can be observed in Figures 2 and 3, respectively, that both the electrical conductivity and the total dissolved solids of the solution increase. The electrical conductivity of a solution increases as the amount of dissolved ions increases. Total dissolved solids include substances that dissociate into ions (such as salts, acids and bases) and those that do not, but in general, the direct relationship between CE and TDS is clearer when the dissolved solids generated are ions.

Mainly, an increase in electrical conductivity and total dissolved solids for all treatments as a function of exposure time is observed in Figures 2 and 3. The longer the exposure time, the greater the generation of ions (electrical conductivity and total dissolved solids). The above expression suggests that plasma exposure influences the solution, possibly generating ionic species or radicals that increase electrical conductivity (More *et al.*, 2020; Ávila *et al.*, 2023).

Box 3

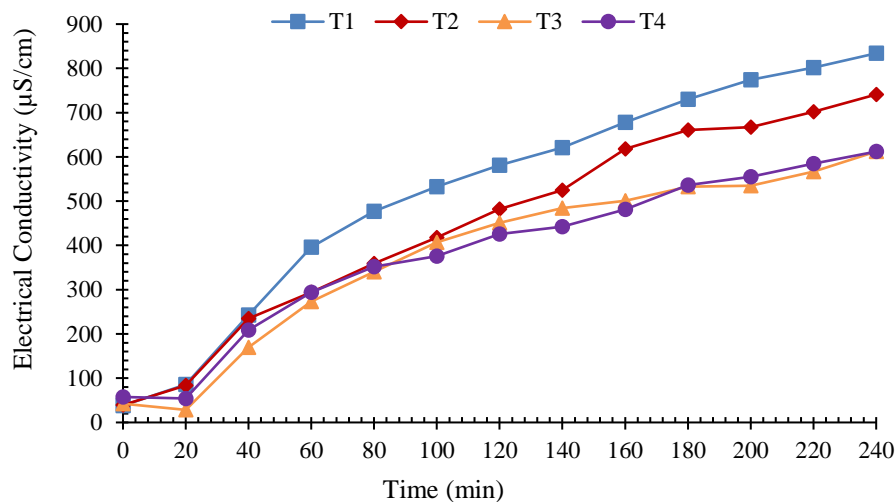
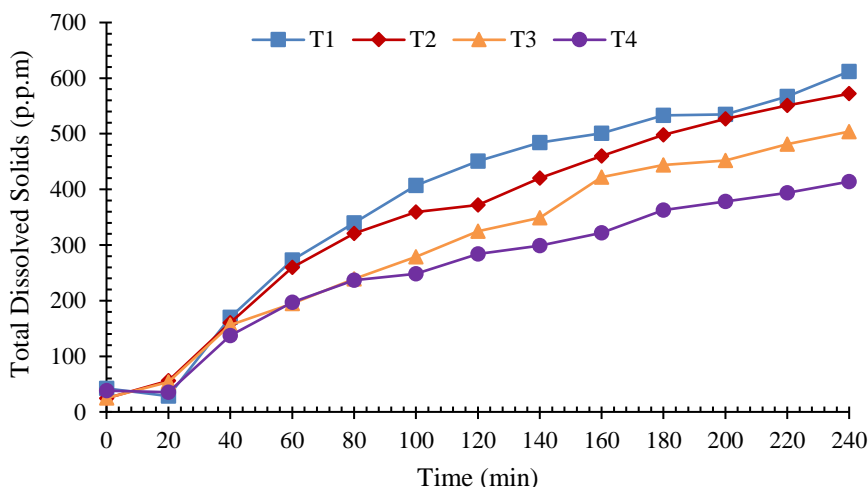


Figure 2

Behaviour of electrical conductivity as a function of time and electric current

Source: Own elaboration

The most significant increase (~94.6%) was observed for treatment T1, with the initial value changing from 38.1 to 834 $\mu\text{S}/\text{cm}$. Treatments T3 and T4 saw a minor change, reaching only 612 $\mu\text{S}/\text{cm}$ and below treatment T2 (741 $\mu\text{S}/\text{cm}$). This behaviour indicates that the electric current used to generate the plasma during the treatment has a particular effect on generating ionic species in the Rhodamine B solution (Chen *et al.*, 2015).

Box 4**Figure 3**

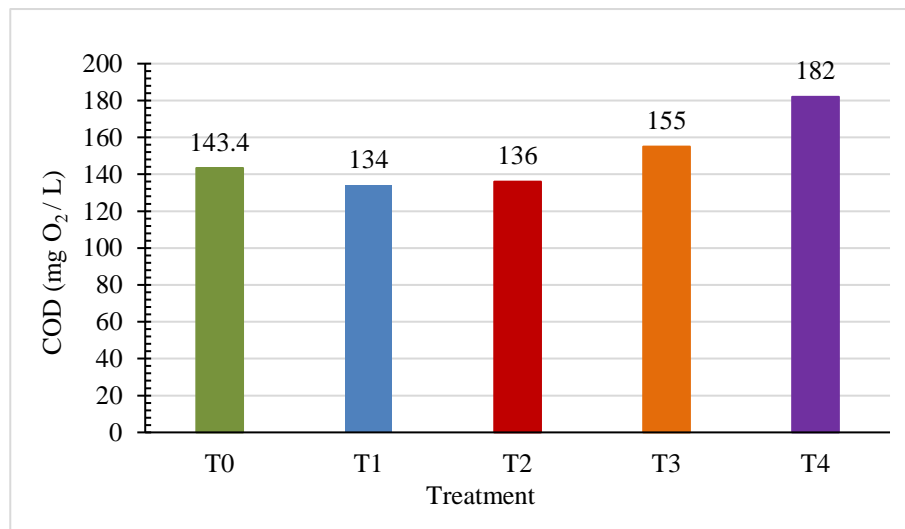
Change in total dissolved solids in the solution

Source: Own elaboration

As the current increases, a decrease in electrical conductivity and total dissolved solids is observed; these phenomena are more prominent at minute 240 of exposure for all treatments. Such behaviour is due to a more significant generation of ions or secondary products at a low plasma generation current. This type of transformation could be related to oxidation processes or dye degradation by the plasma (Komarov *et al.*, 2020). In particular, for total dissolved solids, a significant difference (32.3%) is observed between the final value reached by treatment T1 (20 mA) and the final value of treatment T4 (50 mA). In general, both electrical conductivity and total dissolved solids show an increasing behaviour as the exposure time increases and a decreasing one as the current of the treatments increases.

Chemical oxygen demand

The COD was determined for the final samples of the treatments (240 min) (Figure 3.3). For treatments T1 and T2, the COD decreases concerning the value of the untreated sample (6.5 and 5.1 %, respectively); however, it is observed that for all treatments, the COD value increases as a function of the electric current of plasma generation; which allows inferring an increase of products and byproducts generated by the interaction of the solution of interest with the plasma that requires more oxygen to oxidize.

Box 5**Figure 3**

Behavior of the change in the chemical oxygen demand of the solution at the end of the treatments, as a function of the plasma generation current

Source: Own elaboration

Overall, the percentage increase between the COD values of treatment T1 and T4 is 35.8%. The values depend on the treatment's physical variables. The higher the plasma generation current, the greater the change in COD. This increase in COD may be due to the decomposition of Rhodamine B under the influence of plasma, giving rise to a variety of organic by-products, such as phenolic compounds, organic acids or smaller molecular fragments, as well as new functional groups that can be more easily oxidized. The formation of carbonyl groups (C=O), carboxyls (COOH) or even smaller nitrogen-containing structures increases the oxygen demand (Chen *et al.*, 2015; Le Thi *et al.*, 2021). These by-products can be more difficult to oxidize than the original Rhodamine B molecule.

In general, the interaction of air plasma with the Rhodamine B solution not only decomposes the dye but also generates a variety of organic and inorganic by-products due to the oxidizing action of the reactive species generated in the plasma. This shows the complexity of the process and its potential to modify the original chemical structure of Rhodamine B significantly.

Total organic carbon

Figure 4 shows the change in the solution's TOC values for the four treatments after 240 minutes of exposure. In this case, a decrease in the values is observed depending on the electric current used to generate the plasma.

Box 5

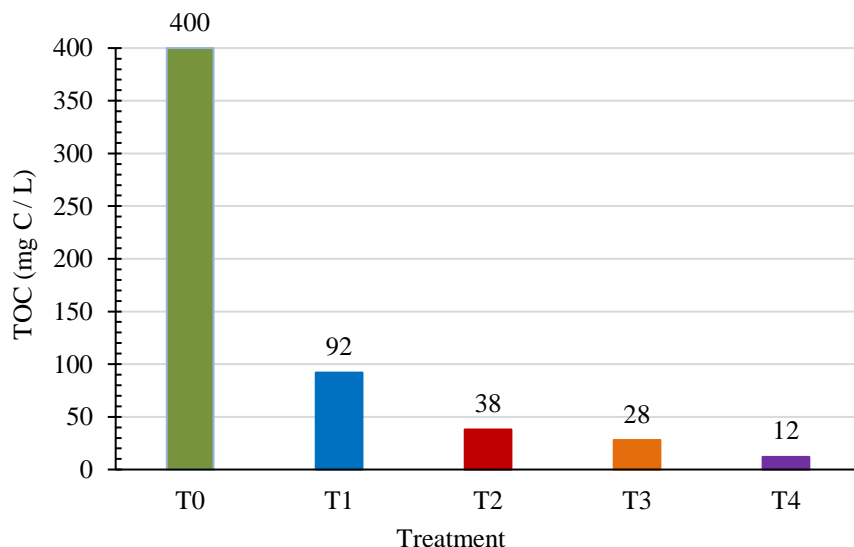


Figure 4

Change in total organic carbon values in solution as a function of electric current

Source: Own elaboration

At 240 minutes of exposure to plasma generated with an electric current of 50 mA, the TOC value decreased from 400.0 mg C/L to 12.0 mg C/L, which corresponds to a dye removal of 97.0 %, while for the minimum electric current value (20 mA) it decreased to 92 mg C/L, which corresponds to a removal value of 77.0 %.

Table 3.1 shows the measured and percentage values of COD and TOC for each treatment at 240 minutes of exposure. These data show that increasing the plasma electric current generates a more significant change in the TOC removal values.

Box 6

Table 2

Percentage change of dye in solution as a function of plasma generation current

Electric current (mA)	COD (mg O ₂ / L)	Change (%)	TOC (mg C / L)	Change (%)
00	143.4	Initial value	400.0	Initial value
20	134.0	06.5 ↓	92.0	77.0 ↓
30	136.0	05.1 ↓	38.0	90.5 ↓
40	155.0	08.0 ↑	28.0	93.0 ↓
50	182.0	26.9 ↑	12.0	97.0 ↓

Source: Own elaboration

The results obtained from TOC suggest that plasma treatment mineralizes organic matter. In particular, it has been reported that mainly intermediate products are generated, such as benzoic acid, paradioxybenzene, benzoquinone, and benzene, among others, as well as some carboxylic acids, such as formic, oxalic, and malonic acids. All carboxylic acids can be decomposed into inorganic carbon (Gai *et al.*, 2014).

Conclusions

Given the specific characteristics of this type of treatment and the chemically active species that may be present, the degradation of the dye, when subjected to plasma, had a particular behaviour. In general, both the electrical conductivity and the total dissolved solids showed an increase in behaviour as the exposure time increased and a decrease in behaviour as the treatment current increased. The chemical oxygen demand changed concerning the initial value of the solution, which indicates modifications to the original molecule and its decomposition into byproducts that require more oxygen for higher values of plasma generating current. On the other hand, the total organic carbon of the solution decreased as the treatment current increased, thus achieving the mineralization of the dye. This type of plasma-based treatment offers a potentially efficient approach for the removal of organic contaminants, such as Rhodamine B, in an aqueous solution since it not only degrades the original compound but can also contribute to the reduction of the organic load by generating simpler and possibly less contaminating products. However, the variability in the products formed and the possible formation of toxic or difficult-to-remove byproducts must be carefully evaluated in large-scale applications to ensure the safety and effectiveness of the process.

Conflict of interest

The authors declare that they have no conflict of interest. They have no financial interests or personal relationships that could have influenced this book.

Authors' contribution

Gómez-Anzures, Uriel Yosimar: Supported the execution of the experiments and application of the research methods and techniques. He contributed to the laboratory analysis.

Alarcón-Hernández, Fidel Benjamín: Design and implementation of the project idea, the research methods and techniques applied. Supported the development of the experimentation, performed the data analysis and wrote the work.

Fuentes-Albarrán, María del Carmen: Contributed to the design of the research, type of research, laboratory analysis, analysis of collected data and writing the article.

Gadea-Pacheco, José Luis: Supported the laboratory analysis. Worked on writing the article.

Availability of data and materials

All data used to support the findings of this study are included in the work.

Funding

This work was funded by PRODEP [DSA/103.5/14/10703]

Acknowledgements

The authors would like to thank the Escuela de Estudios Superiores Xalostoc of the Universidad Autónoma del Estado de Morelos for the facilities provided for this research.

Abbreviations

COD	Chemical Oxygen Demand
TOC	Total Organic Carbon
TDS	Total Dissolved Solids
EC	Electrical Conductivity
AOP	Advanced Oxidation Processes

References

Background

Aggelopoulos, C. A. (2022). [Recent advances of cold plasma technology for water and soil remediation: A critical review](#). *Chemical Engineering Journal*, 442, 136235.

Aggelopoulos, C. A., Foutch, G., & Tsioptsias, C. (2024). [A comprehensive insight on plasma-catalytic degradation of organic pollutants in water: Comparison between ZnO and TiO₂](#). *Chemosphere*.

Ávila-Mares, I. M., Alarcón Hernández, F. B., Fuentes-Albarrán, M. D. C., & Gadea-Pacheco, J. L. (2023). [The behavior of the pigment discoloration Permalon Rhodamine B 400% red in a liquid medium after exposure to a non-thermal plasma of different electrical power at atmospheric pressure](#). *Engineering and Applied Sciences*, 6, 50-59.

García, M. C., Tello, G., & Cañete, S. (2017). [Microwave atmospheric pressure plasma jets for wastewater treatment: Degradation of methylene blue as a model dye](#). *Chemosphere*, 181, 561-568.

Ghezzar, M. R., Khamassi, K., & Bouguerra, A. (2009). [Enhancement of the bleaching and degradation of textile wastewaters by Gliding arc discharge plasma in the presence of TiO₂ catalyst](#). *Journal of Hazardous Materials*, 168(2-3), 1363-1369.

Hamdaoui, O. (2011). [Intensification of the sorption of Rhodamine B from aqueous phase by loquat seeds using ultrasound](#). *Desalination* 271, 279–286.

Hentit, H., Baghour, M., & Amara, A. B. (2014). [Plasma-catalytic degradation of anthraquinonic acid green 25 in solution by gliding arc discharge plasma in the presence of tin containing aluminophosphate molecular sieves](#). *Journal of Molecular Catalysis A: Chemical*, 395, 134-144.

Imam, S.S., Babamale, H.F. (2020). [A short review on the removal of Rhodamine B dye using agricultural waste-based adsorbents](#). *Asian J. Chem. Sci.* 7, 25–37.

Ma, D., Wang, W., Zhang, L., & Xu, W. (2021). [Critical review of advanced oxidation processes in organic wastewater treatment](#). *Chemosphere*, 263, 128266.

Nasr, R. A., & AboBakr Ali, E. (2023). [Polyethersulfone/gelatin nano-membranes for the Rhodamine B dye removal and textile industry effluents treatment under cost effective condition](#). *Journal of Environmental Chemical Engineering*, 11(2), 108543.

Pandiyaraj, K. N., Karthik, R., & Annamalai, K. (2021). [Dye wastewater degradation by the synergetic effect of an atmospheric pressure plasma treatment and the photocatalytic activity of plasma-functionalized Cu-TiO₂ nanoparticles](#). *Journal of Hazardous Materials*, 416, 126267.

Petrović, M., Kostić, M., Rančev, S., Radivojević, D., Vučić, M. R., Hurt, A., & Bojić, A. (2024). Co-doped ZnO catalyst for non-thermal atmospheric pressure pulsating corona plasma degradation of reactive dye. *Materials Chemistry and Physics*, 325, 129733.

Seerangaraj, V., Kannan, S., & Sundaram, M. (2021). Cytotoxic effects of silver nanoparticles on Ruellia tuberosa: Photocatalytic degradation properties against crystal violet and coomassie brilliant blue. *Journal of Environmental Chemical Engineering*, 9(3), 105451.

Sharma, J.; Sharma, S.; Bhatt, U.; Soni, V. (2022). Toxic effects of Rhodamine B on antioxidant system and photosynthesis of *Hydrilla verticillata*. *J. Hazard. Mater.* 3, 100069.

Basics

Ávila-Mares, I. M., Alarcón Hernández, F. B., Fuentes-Albarrán, M. D. C., & Gadea-Pacheco, J. L. (2023). The behavior of the pigment discoloration Permalon Rhodamine B 400% red in a liquid medium after exposure to a non-thermal plasma of different electrical power at atmospheric pressure. *Engineering and Applied Sciences*, 6, 50-59.

Alarcón Hernández, F. B., Fuentes Albarrán, M. D. C., Gadea Pacheco, J. L., Tlatelpa Becerro, Á., & Cañete Cabrera, V. A. (2022). Evaluation of the Degradation Process of Diethyl (3H-1-Ethoxy-3-phenoxazinylidene) Ammonium Chloride in Water, after Exposure to Nonthermal Plasma at Atmospheric Pressure. *Journal of Chemistry*, 2022(1), 4486227.

Discussions

Bruggeman, P.J., Kushner, M.J., Locke, B.R., Gardeniers, J.E., Graham, W.G., Graves, D.B., et al., (2016). Plasma-liquid interactions: a review and roadmap. *Plasma Sources Sci. Technol.* 25, 053002-053059.

Cadorin, B.M., Tralli, V.D., Ceriani, E.E., Benetoli, L.O.B., Marotta, E., Ceretta, C., Debacher, N.A., Paradisi, C., (2015). Treatment of methyl orange by nitrogen nonthermal plasma in a corona reactor: the role of reactive nitrogen species. *J. Hazard Mater.* 300, 754-764.

Chen, Y., Li, Y., Zhang, X., Zhu, A., Huang, Y., Liu, Z. y Yan, K. (2015). Degradation of Aqueous Rhodamine B with Gaseous Streamer Corona Plasma. *IEEE Transactions on Plasma Science*, 43 (3), 828-835.

Gai, K., Qi, H. L., Ma, D. P., & Zhang, Y. Q. (2014). Liquid phase Rhodamine Boxidation induced by plasma with glow discharge electrolysis. *Advanced Materials Research*, 989, 60-64.

Komarov, S., Yamamoto, T., Fang, Y., y Hariu, D. (2020). Combined effect of acoustic cavitation and pulsed discharge plasma on wastewater treatment efficiency in a circulating reactor: A case study of Rhodamine B. *Ultrasonics Sonochemistry*, 68 , 105236.

Le Thi, Q., Tran, H. Q., Trinh, T. H., & Dao, N. T. (2021). Removal of rhodamine B dye by plasma jet oxidation process. *Communications in Physics*, 31(1), 95-102.

Lukes, P., Dolezalova, E., Sisrova, I., Clupek, M., (2014). Aqueous-phase chemistry and bactericidal effects from an air discharge plasma in contact with water: evidence for the formation of peroxynitrite through a pseudo-second-order postdischarge reaction of H₂O₂ and HNO₂. *Plasma Sources Sci. Technol.* 23, 015019-1-015019-15.

More, SE, Dwivedi, N., Sable, S., Mane, DS, Tapase, SR, Kodam, KM, Bhoraskar, SV y Mathe, VL (2020). Highly efficient degradation of concentrated Rhodamine-B effluent using environment friendly needle-plate non-thermal plasma probe. *Journal of Environmental Chemical Engineering*, 8 (3).

Safenraider, A. P., Piazza, L. D., Amadeu, G., Angelo, N., (2020). Degradation of indigo carmine in water induced by non-thermal plasma, ozone and hydrogen peroxide: A comparative study and by-product identification. *Chemosphere*, Volume 244,125502, ISSN 0045-6535.

Instructions for Scientific, Technological and Innovation Publication

[Title in TNRoman and Bold No. 14 in English and Spanish]

Surname, Name 1st Author^{*a}, Surname, Name 1st Co-author^b, Surname, Name 2nd Co-author^c and Surname, Name 3rd Co-author^d [No.12 TNRoman]

a  [Affiliation institution](#),  [Researcher ID](#),  [ORC ID](#),  [SNI-CONAHCYT ID](#) or CVU PNPC [No.10 TNRoman]

b  Affiliation institution,  Researcher ID,  ORC ID,  SNI-CONAHCYT ID or CVU PNPC [No.10 TNRoman]

c  Affiliation institution,  Researcher ID,  ORC ID,  SNI-CONAHCYT ID or CVU PNPC [No.10 TNRoman]

d  Affiliation institution,  Researcher ID,  ORC ID,  SNI-CONAHCYT ID or CVU PNPC [No.10 TNRoman]

All ROR-Clarivate-ORCID and CONAHCYT profiles must be hyperlinked to your website.

Prot-  [University of South Australia](#) •  [7038-2013](#) •  [0000-0001-6442-4409](#) •  416112

CONAHCYT classification: <https://marvid.org/area-i.php> [No.10 TNRoman]

Area:

Field:

Discipline:

Subdiscipline:

DOI: <https://doi.org/>

Key Handbooks

(Explain the following aspects:)

- What are the main contributions to generating Science and Technology written in this research?
- What are the key aspects to be understood in order to apply to the generation of universal knowledge?
- Outline the main conclusions of the research.
- How many citations did the authors of the work generate in the last year?
- From which institutions do they originate?

Citation: Surname, Name 1st Author, Surname, Name 1st Co-author, Surname, Name 2nd Co-author and Surname, Name 3rd Co-author. Year. Book title. [Pages]. ECORFAN.

Contact e-mail address:

*  [example@example.org]

Handbook shelf URL: <https://www.ecorfan.org/handbooks.php>



ISBN XXX-XX-XXXXXX-XX-X/© 2009 The Author[s]. Published by ECORFAN-Mexico, S.C. for its Holding X on behalf of Book X. This is an open access chapter under the CC BY-NC-ND license [<http://creativecommons.org/licenses/by-nc-nd/4.0/>]

Peer Review under the responsibility of the Scientific Committee **MARVID®** - in contribution to the scientific, technological and innovation Peer Review Process by training Human Resources for the continuity in the Critical Analysis of International Research.



Instructions for Scientific, Technological and Innovation Publication

Abstract [In English]

Must contain up to 150 words

Graphical abstract [In English]

Your title goes here		
Objectives	Methodology	Contribution

Authors must provide an original image that clearly represents the work described in the chapter. Graphical abstracts should be submitted as a separate file. Please note that, as well as each article must be unique. File type: the file types are MS Office files. No additional text, outline or synopsis should be included. Any text or captions must be part of the image file. Do not use unnecessary white space or a "graphic abstract" header within the image file.

Keywords [In English]

Indicate 3 keywords in TNRoman and Bold No. 12

Abstract [In Spanish].

Must contain up to 150 words

Graphical abstract [In Spanish]

Your title goes here		
Objectives	Methodology	Contribution

Authors must provide an original image that clearly represents the work described in the book. Graphical abstracts should be submitted as a separate file. Please note that, as well as each article must be unique. File type: the file types are MS Office files. No additional text, outline or synopsis should be included. Any text or captions must be part of the image file. Do not use unnecessary white space or a "graphic abstract" header within the image file.

Keywords [In Spanish]

Indicate 3 keywords in TNRoman and Bold No. 12

Instructions for Scientific, Technological and Innovation Publication

Introduction

Text in TNRoman No.12, single space.

General explanation of the subject and explain why it is important.

What is your added value with respect to other techniques?

Clearly focus each of its features

Clearly explain the problem to be solved and the central hypothesis.

Explanation of sections Chapter.

Development of headings and subheadings of the chapter with subsequent numbers

Products in development No.12 TNRoman, single spaced.

Including figures and tables-Editable

In the Chapter content any figure and table should be editable formats that can change size, type and number of letters, for the purposes of edition, these must be high quality, not pixelated and should be noticeable even reducing image scale.

[Indicating the title at the top with No.12 and TNRoman Bold]

Box

Table 1

Title [Should not be images-everything must be editable]

Source [in italic]

Box

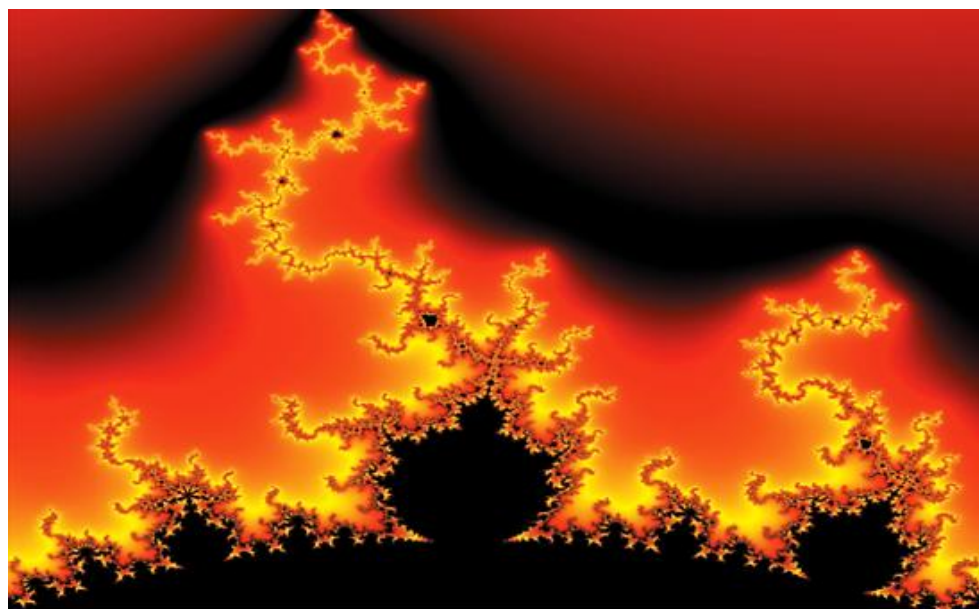


Figure 1

Title [Should not be images-everything must be editable]

Source [in italic]

The maximum number of Boxes is 10 items

For the use of equations, noted as follows:

$$\int_{lim^{-1}}^{lim^1} = \int \frac{lim^1}{lim^{-1}} = \left[\frac{1(-1)}{lim} \right]^2 = \frac{(0)^2}{lim} = \sqrt{lim} = 0 = 0 \rightarrow \infty \quad [1]$$

Must be editable and number aligned on the right side.

Methodology

Develop give the meaning of the variables in linear writing and important is the comparison of the used criteria.

Results

The results shall be by section of the chapter.

Conclusions

Clearly explain the results and possibilities of improvement.

Annexes

Tables and adequate sources.

The international standard is 7 pages minimum and 14 pages maximum.

Declarations

Conflict of interest

The authors declare no interest conflict. They have no known competing financial interests or personal relationships that could have appeared to influence in this chapter.

Instructions for Scientific, Technological and Innovation Publication

Author contribution

Specify the contribution of each researcher in each of the points developed in this research.

Prot-

Benoit-Pauleter, Gerard: Contributed to the project idea, research method and technique.

Availability of data and materials

Indicate the availability of the data obtained in this research.

Funding

Indicate if the research received some financing.

Acknowledgements

Indicate if they were financed by any institution, University or company.

Abbreviations

List abbreviations in alphabetical order.

ANN Artificial Neural Network

References

Use APA system. Should not be numbered, nor with bullets, however if necessary numbering will be because reference or mention is made somewhere in the chapter.

Use the Roman alphabet, all references you have used should be in Roman alphabet, even if you have cited a chapter, book in any of the official languages of the United Nations [English, French, German, Chinese, Russian, Portuguese, Italian, Spanish, Arabic], you should write the reference in Roman alphabet and not in any of the official languages.

Citations are classified the following categories:

Antecedents. The citation is due to previously published research and orients the citing document within a particular scholarly area.

Basics. The citation is intended to report data sets, methods, concepts and ideas on which the authors of the citing document base their work.

Supports. The citing article reports similar results. It may also refer to similarities in methodology or, in some cases, to the reproduction of results.

Differences. The citing document reports by means of a citation that it has obtained different results to those obtained in the cited document. This may also refer to differences in methodology or differences in sample sizes that affect the results.

Discussions. The citing article cites another study because it is providing a more detailed discussion of the subject matter.

The URL of the resource is activated in the DOI or in the title of the resource.

Prot-

Mandelbrot, B. B. [2020]. [Negative dimensions and Hölders, multifractals and their Hölder spectra, and the role of lateral preasymptotics in science](#). Journal of Fourier Analysis and Applications Special. 409-432.

Instructions for Scientific, Technological and Innovation Publication

Intellectual Property Requirements for editing:

- Authentic Signature in Color of [Originality Format](#) Author and Coauthors.
- Authentic Signature in Color of the [Acceptance Format](#) of Author and Coauthors.
- Authentic Signature in blue color of the [Conflict of Interest Format](#) of Author and Co-authors.

Reservation to the Editorial Policy

ECORFAN Handbooks reserves the right to make any editorial changes required to bring the Scientific Work into compliance with the ECORFAN Handbooks Editorial Policy. Once the Scientific Work has been accepted in its final version, ECORFAN Handbooks will send the author the proofs for review. ECORFAN® will only accept the correction of errata and errors or omissions arising from the editing process of the journal, reserving in its entirety the rights of authorship and dissemination of content. Deletions, substitutions or additions that alter the formation of the Scientific Work will not be accepted.

Code of Ethics - Good Practices and Statement of Solution to Editorial Conflicts

Declaration of Originality and unpublished character of the Scientific Work, of Authorship, on the obtaining of data and interpretation of results, Acknowledgements, Conflict of interests, Assignment of rights and distribution.

The Management of ECORFAN-Mexico, S.C. claims to the Authors of the Scientific Work that its content must be original, unpublished and of Scientific, Technological and Innovation content in order to submit it for evaluation.

The Authors signing the Scientific Work must be the same who have contributed to its conception, realization and development, as well as to the obtaining of the data, the interpretation of the results, its writing and revision. The Corresponding Author of the proposed Scientific Work should fill in the following form.

Title of the Scientific Work:

- The submission of a Scientific Paper to ECORFAN Handbooks implies the author's commitment not to submit it simultaneously to the consideration of other serial publications. To do so, he/she must complete the Originality Form for his/her Scientific Paper, unless it is rejected by the Referee Committee, it may be withdrawn.
- None of the data presented in this Scientific Work has been plagiarized or invented. The original data are clearly distinguishable from those already published. And we are aware of the PLAGSCAN test, if a positive plagiarism level is detected, we will not proceed to refereeing.
- The references on which the information contained in the Scientific Work is based are cited, as well as theories and data from other previously published Scientific Works.
- The authors sign the Authorization Form for their Scientific Work to be disseminated by the means that ECORFAN-Mexico, S.C. in its Holding Mexico considers pertinent for the dissemination and diffusion of their Scientific Work, ceding their Scientific Work Rights.
- Consent has been obtained from those who have provided unpublished data obtained through verbal or written communication, and such communication and authorship are properly identified.
- The Author and Co-Authors signing this work have participated in its planning, design and execution, as well as in the interpretation of the results. Likewise, they critically reviewed the work, approved its final version and agree with its publication.
- No signature responsible for the work has been omitted and the criteria for Scientific Authorship have been met.
- The results of this Scientific Work have been interpreted objectively. Any results contrary to the views of the signatories are stated and discussed in the Scientific Work

Copyright and Access

The publication of this Scientific Work implies the assignment of the copyright to ECORFAN-Mexico, S.C. in its Holding Mexico for its ECORFAN Handbooks, which reserves the right to distribute on the Web the published version of the Scientific Work and the availability of the Scientific Work in this format implies for its Authors the compliance with the provisions of the Law of Science and Technology of the United Mexican States, regarding the obligation to allow access to the results of Scientific Research.

Title of the Scientific Work:

Name and surname(s) of Contact Author and Co-authors	Signature
1.	
2.	
3.	
4.	

Principles of Ethics and Editorial Conflict Resolution Statement

Editor's Responsibilities

The Editor undertakes to guarantee the confidentiality of the evaluation process, and may not reveal the identity of the Authors to the Referees, nor may he/she reveal the identity of the Referees at any time.

The Editor assumes the responsibility of duly informing the Author of the stage of the editorial process in which the submitted text is, as well as of the resolutions of the Double Blind Arbitration.

The Editor must evaluate manuscripts and their intellectual content without distinction of race, gender, sexual orientation, religious beliefs, ethnic origin, nationality, or political philosophy of the Authors.

The Editor and its editorial staff of ECORFAN® Holdings will not disclose any information about the submitted Scientific Work to anyone other than the corresponding Author.

The Editor must make fair and impartial decisions and ensure a fair peer review process.

Responsibilities of the Editorial Board

The description of the peer review process is made known by the Editorial Board so that the Authors are aware of the evaluation criteria and will always be ready to justify any controversy in the evaluation process. In case of Plagiarism Detection to the Scientific Work, the Committee notifies the Authors for Violation of the Right of Scientific, Technological and Innovation Authorship.

Responsibilities of the Referee Committee

The Referees undertake to notify any unethical conduct on the part of the Authors and to point out any information that may be a reason to reject the publication of the Scientific Work. In addition, they must undertake to keep confidential the information related to the Scientific Work they evaluate.

Any manuscript received for refereeing must be treated as a confidential document, not to be shown or discussed with other experts, except with the permission of the Editor.

Referees should conduct themselves in an objective manner; any personal criticism of the Author is inappropriate.

Referees should express their views clearly and with valid arguments that contribute to the Scientific, Technological and Innovation achievements of the Author.

Referees should not evaluate manuscripts in which they have conflicts of interest and which have been notified to the Editor before submitting the Scientific Work for evaluation.

Responsibilities of Authors

Authors must guarantee that their Scientific Works are the product of their original work and that the data have been obtained in an ethical manner.

Authors must guarantee that they have not been previously published or that they are not being considered in another serial publication.

Authors must strictly follow the rules for the publication of Scientific Works defined by the Editorial Board.

Authors should consider that plagiarism in all its forms constitutes unethical editorial conduct and is unacceptable; consequently, any manuscript that incurs in plagiarism will be eliminated and will not be considered for publication.

Authors should cite publications that have been influential in the nature of the Scientific Work submitted for refereeing.

Information Services

Indexing - Bases and Repositories

V|LEX (Global Legal Intelligence Platform)

RESEARCH GATE (Germany)

MENDELEY (Bibliographic Reference Manager)

GOOGLE SCHOLAR (Citation Indexes-Google)

REDIB (Ibero-American Network of Innovation and Scientific Knowledge- CSIC)

Editorial Services

Citation Identification and H Index

Originality and Authorization Format Management

Handbooks Testing with PLAGSCAN

Evaluation of Scientific Work

Issuance of Referee Certificate

Scientific Work Editing

Web Layout

Indexing and Repository

Publication of Scientific Work

Scientific Work Certificate

Invoicing for Publishing Services

Editorial Policy and Administration

Park Pedregal Business 3580 – Adolfo Ruiz Cortines Boulevard, CP-01900. San Jeronimo Aculco Álvaro Obregón - Mexico City. Tel: +52 1 55 6159 2296, +52 1 55 1260 0355, +52 1 55 6034 9181; E-mail: contact@ecorfan.org www.ecorfan.org

ECORFAN®

Editor in Chief

Vargas-Delgado, Oscar. PhD

Executive Director

Ramos-Escamilla, María. PhD

Editorial Director

Peralta-Castro, Enrique. MsC

Web Designer

Escamilla-Bouchan, Imelda. PhD

Web Diagrammer

Luna-Soto, Vladimir. PhD

Editorial Assistant

Trejo-Ramos, Iván. BsC

Philologist

Ramos-Arancibia, Alejandra. BsC

Advertising and Sponsorship

(ECORFAN® - Mexico – Bolivia – Spain – Ecuador – Cameroon – Colombia - El Salvador – Guatemala – Nicaragua – Peru – Paraguay - Democratic Republic of The Congo - Taiwan),
sponsorships@ecorfan.org

Site Licenses

03-2010-032610094200-01-For printed material, 03-2010-031613323600-01-For electronic material, 03-2010-032610105200-01-For photographic material, 03-2010-032610115700-14-For Compilation of Data, 04 -2010-031613323600-01-For its Web page, 19502-For Ibero-American and Caribbean Indexing, 20-281 HB9-For Latin American Indexing in the Social Sciences and Humanities, 671-For Indexing in Electronic Scientific Journals in Spain and Latin America, 7045008-For dissemination and publication in the Ministry of Education and Culture-Spain, 25409-For its repository in the University Library-Madrid, 16258-For its indexing in Dialnet, 20589-For Indexing in the Directory in the countries of Iberoamerica and the Caribbean, 15048-For the international registration of Congresses and Colloquia.
financingprograms@ecorfan.org

Management Offices

Park Pedregal Business 3580 - Adolfo Ruiz Cortines Boulevard, CP-01900. San Jeronimo Aculco Álvaro Obregón - Mexico City.

21 Santa Lucia, CP-5220. Libertadores -Sucre - Bolivia.

38 Matacerquillas, CP-28411. Moralzarzal -Madrid-Spain.

18 Marcial Romero, CP-241550. Avenue, Salinas I - Santa Elena-Ecuador.

1047 Avenida La Raza - Santa Ana, Cusco-Peru.

Boulevard de la Liberté, Immeuble Kassap, CP-5963.Akwa- Douala-Cameroon.

Avenida Suroeste, San Sebastian - León-Nicaragua.

31 Kinshasa 6593- Republique Démocratique du Congo.

Avenida San Quentin, R 1-17 Miralvalle - San Salvador-El Salvador.

16 kilometers, U.S. highway, Terra Alta house, D7 Mixco Zone 1-Guatemala.

105 Alberdi Rivarola Capitán, CP-2060. Luque City- Paraguay.

69 Street YongHe District, Zhongxin. Taipei-Taiwan.

43 Street # 30 -90 B. El Triunfo CP.50001. Bogotá-Colombia.



ISBN: 978-607-8948-51-2

